

REPORT NO.  
EERC 2003-06

EARTHQUAKE ENGINEERING RESEARCH CENTER

# RECENT ADVANCES IN SOIL LIQUEFACTION ENGINEERING: A UNIFIED AND CONSISTENT FRAMEWORK

By

R.B. Seed	M.F. Riemer
K.O. Cetin	R.B. Sancio
R.E.S. Moss	J.D. Bray
A.M. Kammerer	R.E. Kayen
J. Wu	A. Faris
J.M. Pestana	



COLLEGE OF ENGINEERING

UNIVERSITY OF CALIFORNIA, BERKELEY

## RECENT ADVANCES IN SOIL LIQUEFACTION ENGINEERING: A UNIFIED AND CONSISTENT FRAMEWORK

by

R. B. Seed<sup>1</sup>, K. O. Cetin<sup>2</sup>, R. E. S. Moss<sup>3</sup>, A. M. Kammerer<sup>4</sup>, J. Wu<sup>5</sup>, J. M. Pestana<sup>1</sup>,  
M. F. Riemer<sup>1</sup>, R.B. Sancio<sup>1</sup>, J.D. Bray<sup>1</sup>, R. E. Kayen<sup>6</sup>, and A. Faris<sup>1</sup>

### ABSTRACT

Over the past decade, major advances have occurred in both understanding and practice with regard to assessment and mitigation of hazard associated with seismically induced soil liquefaction. Soil liquefaction engineering has evolved into a sub-field in its own right, and engineering assessment and mitigation of seismic soil liquefaction hazard is increasingly well addressed in both research and practice. This rapid evolution in the treatment of liquefaction has been pushed largely by a confluence of lessons and data provided by a series of major earthquakes over the past dozen years, as well as by the research and professional/political will engendered by these major seismic events. The overall field of soil liquefaction engineering is now beginning to coalesce into an internally consistent and comprehensive framework, and one in which the various elements are increasingly mutually supportive of each other. Although the rate of progress has been laudable, further advances are occurring, and more remains to be done. As we enter a “new millenium”, engineers are increasingly well able to deal with important aspects of soil liquefaction engineering. This paper will highlight a number of important recent and ongoing developments in soil liquefaction engineering, and will offer insights regarding research in progress, as well as suggestions regarding further advances needed.

### 1.0 INTRODUCTION

Soil liquefaction is a major cause of damage during earthquakes. “Modern” engineering treatment of liquefaction-related issues evolved initially in the wake of the two devastating earthquakes of 1964; the 1964 Niigata (Japan) and 1964 Great Alaskan Earthquakes. Seismically-induced soil liquefaction produced spectacular and devastating effects in both of these events, thrusting the issue forcefully to the attention of engineers and researchers.

Over the nearly four decades that have followed, significant progress has occurred. Initially, this progress was largely confined to improved ability to assess the likelihood of initiation (or “triggering”) of liquefaction in clean, sandy soils. As the years passed, and earthquakes continued to provide lessons and data, researchers and practitioners became increasingly aware of the additional potential problems associated with both silty and gravelly soils, and the important

additional issues of post-liquefaction strength and stress-deformation behavior also began to attract increased attention.

Today, the area of “soil liquefaction engineering” is emerging as a semi-mature field of practice in its own right. This area now involves a number of discernable sub-issues or sub-topics, as illustrated schematically in Figure 1. As shown in Figure 1, the first step in most engineering treatments of soil liquefaction continues to be (1) assessment of “liquefaction potential”, or the risk of “triggering” (initiation) of liquefaction. There have been major advances here in recent years, and some of these will be discussed.

Once it is determined that occurrence of liquefaction is a potentially serious risk/hazard, the process next proceeds to assessment of the consequences of the potential liquefaction. This, now, increasingly involves (2) assessment of available post-liquefaction strength, and resulting post-liquefaction overall stability (of a site, and/or of a structure or other built facilities, etc.). There has been considerable progress in

<sup>1</sup> Dept. of Civil and Environmental Engineering, University of California, Berkeley.

<sup>2</sup> Dept. of Civil Engineering, Middle East Technical University, Ankara, Turkey.

<sup>3</sup> Fugro Engineering, Santa Barbara, California.

<sup>4</sup> Arup, San Francisco, California.

<sup>5</sup> URS Corporation, Oakland, California.

<sup>6</sup> U.S. Geological Survey, Menlo Park, California.

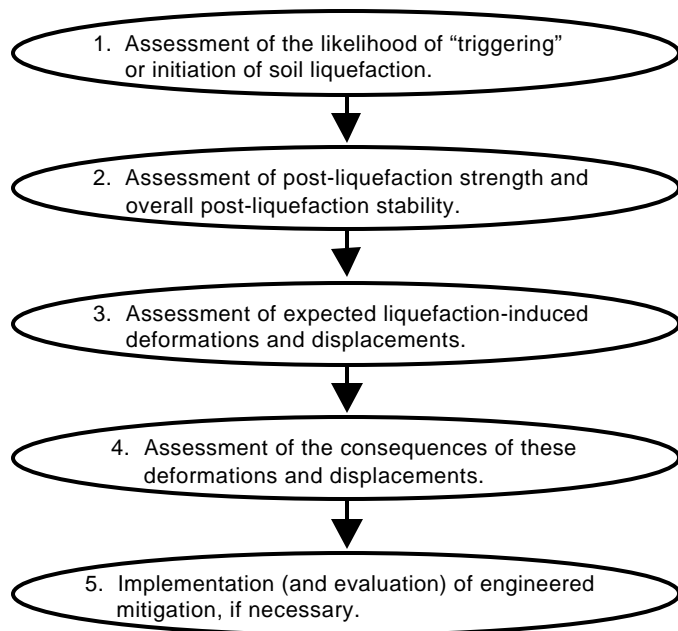


**Fig. 1: Key Elements of Soil Liquefaction Engineering**

evaluation of post-liquefaction strengths and stability over the past fifteen years. If post-liquefaction stability is found wanting, then deformation/displacement potential is large, and engineered remediation is typically warranted.

If post-liquefaction overall stability is not unacceptable, then attention is next directed towards (3) assessment of anticipated deformations and displacements. This is a very "soft" area of practice, and much remains to be done here with regard to development and calibration/verification of engineering tools and methods. Similarly, there are few engineering tools and guidelines regarding (4) the effects of liquefaction-induced deformations and displacements on the performance of structures and other engineered facilities, and criteria for "acceptable" performance are not well established.

Finally, in cases in which the engineer(s) conclude that satisfactory performance cannot be counted on, (5) engineered mitigation of liquefaction risk is generally warranted. This, too, is a rapidly evolving area, and one rife with potential controversy. Ongoing evolution of new methods for mitigation of liquefaction hazard provides an ever increasing suite of engineering options, but the efficacy and reliability of some of these remain contentious, and accurate and reliable engineering analysis of the improved performance provided by many of these mitigation techniques continues to be difficult.

It is not possible, within the confines of this paper, to fully address all of these issues (a textbook would be required!) Instead, a number of important recent and ongoing advances will be highlighted, and resultant issues and areas of controversy, as well as areas in urgent need of further advances either in practice or understanding, will be noted.

## 2.0 ASSESSMENT OF SUSCEPTIBILITY

### 2.1 Liquefiable Soil Types:

The first step in engineering assessment of the potential for "triggering" or initiation of soil liquefaction is the determination of whether or not soils of "potentially liquefiable nature" are present at a site. This, in turn, raises the important question regarding which types of soils are potentially vulnerable to soil liquefaction.

It has long been recognized that relatively "clean" sandy soils, with few fines, are potentially vulnerable to seismically-induced liquefaction. There has, however, been significant controversy and confusion regarding the liquefaction potential of silty soils (and silty/clayey soils), and also of coarser, gravelly soils and rockfills.

Coarser, gravelly soils are the easier of the two to discuss, so we will begin there. The cyclic behavior of coarse, gravelly soils differs little from that of "sandy" soils, as Nature has little or no respect for the arbitrary criteria established by the standard #4 sieve. Coarse, gravelly soils are potentially vulnerable to cyclic pore pressure generation and liquefaction. There are now a number of well-documented field cases of liquefaction of coarse, gravelly soils (e.g.: Evans, 1987; Harder, 1988; Hynes, 1988; Andrus, 1994). These soils do, however, often differ in behavior from their finer, sandy brethren in two ways: (1) they can be much more pervious, and so can often rapidly dissipate cyclically generated pore pressures, and (2) due to the mass of their larger particles, the coarse gravelly soils are seldom deposited "gently" and so do not often occur in the very loose states more often encountered with finer sandy soils. Sandy soils can range from very loose to very dense, while the "very" loose state is relatively uncommon in gravelly deposits and coarser soils.

The apparent drainage advantages of coarse, gravelly soils can be defeated if their drainage potential is circumvented by either; (1) their being surrounded and encapsulated by finer, less pervious materials, (2) if drainage is internally impeded by the presence of finer soils in the void spaces between the coarser particles (it should be noted that the  $D_{10}$  particle size, not the mean or  $D_{50}$  size, most closely correlates with the permeability of a broadly graded soil mix), or (3) if the layer or stratum of coarse soil is of large dimension, so that the distance over which drainage must occur (rapidly) during an earthquake is large. In these cases, the coarse soils should be considered to be of potentially liquefiable type, and should be evaluated accordingly.

Questions regarding the potential liquefiability of finer, "cohesive" soils (especially "silts" and "silty clays") are increasingly common at meetings and professional short courses and seminars. There is considerable new field data regarding this issue from recent major earthquakes, and this is an area in which major changes in both understanding and practice are occurring.

1. Percent Finer than 0.005mm  $\leq 15\%$
2. Liquid Limit (LL)  $\leq 35\%$
3. Water Content (W)  $\geq 0.9 \times LL$

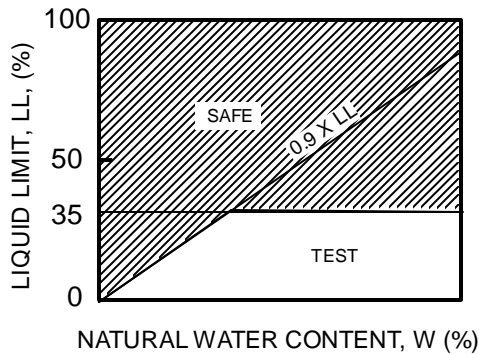


**Fig. 2: Modified Chinese Criteria (After Wang (1979) and Seed and Idriss (1982))**

Figure 2 illustrates the “Modified Chinese Criteria” (Wang (1979), and Seed and Idriss (1982)), which represent the criteria most widely used for defining potentially liquefiable soils over the past two decades. According to these criteria, fine (cohesive) soils that plot above the A-line are considered to be of potentially liquefiable type and character if: (1) there are less than 15% “clay” fines (based on the Chinese definition of “clay” sizes as less than 0.005 mm), (2) there is a Liquid Limit of  $LL \leq 35\%$ , and (3) there is a current in-situ water content greater than or equal to 90% of the Liquid Limit.

Andrews and Martin (2000) re-evaluated the liquefaction field case histories from the database of Wang (1979), as well as a number of subsequent earthquakes, and have transposed the “Modified Chinese Criteria” to U.S. conventions (with clay sizes defined as those less than about 0.002 mm). Their findings are largely summarized in Figure 3. Andrews and Martin recommended: (1) that soils with less than about 10% clay fines ( $< 0.002$  mm), and a Liquid Limit (LL) in the minus #40 sieve fraction of less than 32%, be considered potentially liquefiable, (2) that soils with more than about 10% clay fines and  $LL \geq 32\%$  are unlikely to be susceptible to classic cyclically-induced liquefaction, and (3) that soils intermediate between these criteria should be sampled and tested to assess whether or not they are potentially liquefiable.

Over the period from 1994 to 1999, a group of approximately two dozen leading experts worked to achieve consensus regarding a number of issues involved in the assessment of liquefaction potential. This group, referred to hereafter as the NCEER Working Group, have published many of their consensus findings (or at least near-consensus findings) in the NSF-sponsored workshop summary paper (NCEER, 1997), and the summary article in the ASCE Journal of Geotechnical and Geoenvironmental Engineering (Youd et al., 2001). The NCEER Working Group addressed this issue, and it was

agreed that there was a need to reexamine the “Modified Chinese Criteria” for defining the types of fine “cohesive” soils potentially vulnerable to liquefaction, but no improved consensus position could be reached at that time, and more study was warranted.

Two major earthquakes in 1999 then dramatically altered the picture. Widespread soil liquefaction occurred throughout much of the city of Adapazari in the 1999 Kocaeli (Turkey) Earthquake, and widespread liquefaction-induced damages also occurred in the cities of Wu Feng, Yuan Lin and Nantou in the 1999 Chi-Chi (Taiwan) Earthquake. In all four of these cities, significant liquefaction-type damages (including settlements and/or partial or complete bearing failures of shallow-founded structures) occurred at sites where the soils responsible appear to be more “cohesive” than would be expected based on the Modified Chinese Criteria.

There is significant ongoing research with regard to the field performance of increasingly cohesive soils in Adapazari; work is in progress both at U.C. Berkeley (Sancio, 2003) and at the Middle East Technical University in Ankara (Cetin, 2003), and more detailed publications can be anticipated in the very near future as these efforts are completed. Similarly, studies are also in progress by a number of research teams (including Stewart, et al., 2003) regarding performance of increasingly cohesive soils in Wu Feng, Yuan Lin and Nantou during the Chi-Chi Earthquake.

In the “new” field performance cases in these four cities, it is often difficult to reliably discern whether or not soils with cohesive fines “liquefied”. Soils with large fines contents do not generally exude excess pore pressures rapidly, and so are less prone to produce surface boil ejecta than are “cleaner” cohesionless soils.

As a result, soils with significant (and plastic) fines have been sampled and then subjected to cyclic testing in the laboratory by a number of researchers. This laboratory testing, much like

	Liquid Limit <sup>1</sup> < 32	Liquid Limit $\geq 32$
Clay Content <sup>2</sup> < 10%	Susceptible	Further Studies Required <i>(Considering plastic non-clay sized grains – such as Mica)</i>
Clay Content <sup>2</sup> $\geq 10\%$	Further Studies Required <i>(Considering non-plastic clay sized grains – such as mine and quarry tailings)</i>	Not Susceptible

Notes:

1. Liquid limit determined by Casagrande-type percussion apparatus.
2. Clay defined as grains finer than 0.002 mm.

**Fig. 3: Liquefaction Susceptibility of Silty and Clayey Sands (after Andrews and Martin, 2000)**

the observed field performance, suggests that: (1) soils of higher plasticity may be susceptible to significant cyclic pore pressure increase and consequent loss of strength than is suggested by the Modified Chinese Criteria, and (2) the transition in behavior to soils of even higher plasticity, which do not appear to be prone to similarly severe cyclic pore pressure generation and strength loss, is gradual (rather than abrupt).

Some of the confusion here is related to the definition of liquefaction. In this paper, the term “classic” cyclic liquefaction will refer to significant loss of strength and stiffness due to cyclic pore pressure generation, in contrast to “sensitivity” or loss of strength due to monotonic shearing and/or remolding as a result of larger, monotonic (uni-directional) shear displacements. By making these distinctions, we are able to separately discuss “classic” cyclically-induced liquefaction and the closely-related (but different) phenomenon of strain-softening or sensitivity.

Sandy soils, and silty soils of very low plasticity, tend to experience “triggering” of cyclically induced soil liquefaction at relatively low shear strains (typically on the order of 3% to 6%), and the loss of strength can be severe. Soils of higher plasticity, on the other hand, may also exhibit loss of strength and stiffness, accompanied by increased pore pressures, but the pore pressure ratios achieved may be somewhat lower than those associated with more “classically” liquefiable soils, and the loss of strength and stiffness becomes pronounced at somewhat larger shear strains. In other words, there is a transition in behaviors; as soils’ behaviors become controlled by fines of increasing plasticity their cyclic behavior becomes more “ductile”, and the boundary between soils which are potentially susceptible to “classic” cyclic liquefaction and

those that are not is not a sharp transition.

It is recommended herein that the Modified Chinese Criteria be relegated to history, and that we move forward to broader consideration of potentially liquefiable soil types. One element of the Modified Chinese Criteria has been clearly shown to be flawed, and that is the “percent clay fines” rule (e.g.: Bray et al. 2001; Sancio et al.; 2002, 2003). Percent clay fines is less important than the overall contribution of the fines to plasticity, and there are numerous cases of liquefaction of soils with more than 10 or 15% clay-sized fines. The other elements of the Modified Chinese Criteria (Liquid Limit, and water content as a fraction of the liquid limit) both appear better directed, but warrant some revision as well.

Post-earthquake reconnaissance efforts (e.g. Bray and Stewart, 2000) and follow-on studies (e.g. Sancio et al., 2002), clearly found ample evidence of liquefaction and ground softening at sites where critical soil layers contained more than 15% particles finer than 5 mm. As suggested in Bray et al. (2001), Sancio et al. (2002), and Sancio et al. (2003), the percent “clay-size” criterion of the Chinese criteria and Andrews and Martin (2000) criteria is misleading, because it is not the percent of “clay-size” particles that is important. Rather, it is the percent of clay minerals present in the soil and their activity that are important. Fine quartz particles may be smaller than either 2 or 5 mm, but if largely nonplastic, these soils respond as a cohesionless material in terms of liquefaction under cyclic loading. Accordingly, use of the percent “clay size” criterion as is commonly done in current engineering practice (e.g.: “Guidelines for Analyzing and Mitigating Liquefaction Hazards in California”; edited by Martin and Lew, 1999), can be unconservative, because soils that are susceptible to liquefaction can be incorrectly classified as non-liquefiable.

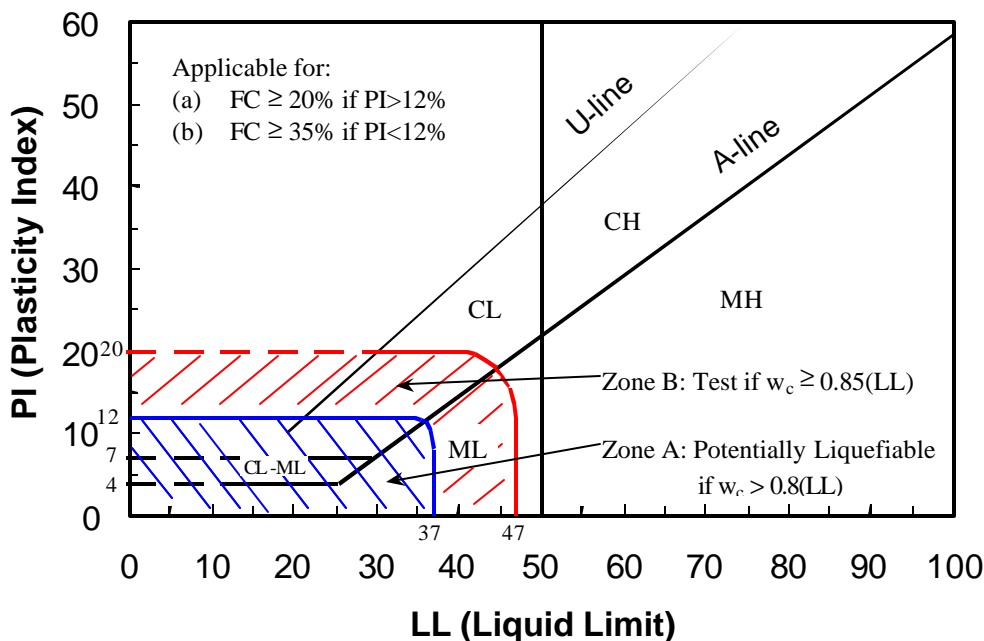


Fig 4: Recommendations Regarding Assessment of “Liquefiable” Soil Types

Figure 4 represents interim recommendations regarding “liquefiability” of soils with significant fines contents. This may evolve further, based on work in progress, but is a good summary of what we know to date. For soils with sufficient fines content that the fines separate the coarser particles and control overall behavior: (1) Soils within Zone A are considered potentially susceptible to “classic” cyclically induced liquefaction, (2) Soils within Zone B may be liquefiable, and (3) Soils in Zone C (not within Zones A or B) are not generally susceptible to “classic” cyclic liquefaction, but should be checked for potential sensitivity (loss of strength with remolding or monotonic accumulation of shear deformation).

Both experimental research and review of liquefaction field case histories show that for soils with sufficient “fines” (particles finer than 0.074 mm, or passing a #200 sieve) to separate the coarser (larger than 0.074 mm) particles, the characteristics of the fines control the potential for cyclically-induced liquefaction. This separation of the coarser particles typically occurs as the fines content exceeds about 15% to 35%, with the precise fines content required being dependent principally on the overall soil gradation and the character of the fines. Well-graded soils have lesser void ratios than uniformly-graded or gap-graded soils, and so require lesser fines contents to fill the remaining available void space and thus separate (or “float”) the coarser particles in a matrix of the fines. Similarly, clay fines carry higher void ratios than silty particles and so are more rapidly effective at over-filling the void space available between the coarser (larger than 0.074mm) particles; a lesser weight (or percentage) of clay fines is required than would be required if the fines were lower plasticity silty particles.

In soils wherein the fines content is sufficient as to separate the coarser particles and control behavior, cyclically-induced soil liquefaction appears to occur primarily in soils where these fines are either non-plastic or are low plasticity silts and/or silty clays ( $PI \leq 12\%$ , and  $LL \leq 37\%$ ), and with high water content relative to their Liquid Limit ( $w_c > 0.85 \cdot LL$ ). In fact, low plasticity or non-plastic silts and silty sands can be among the most dangerous of liquefiable soils, as they not only can cyclically liquefy; they also “hold their water” well and dissipate excess pore pressures slowly due to their low permeabilities.

Soils with sufficient fines that the fines control their behavior, and falling within Zone A in Figure 4, are considered potentially susceptible to “classic” cyclically-induced soil liquefaction. Soils within Zone B fall into a transition range; they may in some cases be susceptible to liquefaction (especially if their in situ water content is greater than about 85% of their Liquid Limit), but tend to be more ductile and may not “liquefy” in the classic sense of losing a large fraction of their strength and stiffness at relatively low cyclic shear strains. These soils are also, in many cases, not well suited to evaluation based on conventional in-situ “penetration-based” liquefaction hazard assessment methods. These types of soils usually are amenable to reasonably “undisturbed” (e.g.: thin-walled, or better) sampling, however, and so can be tested in the laboratory. It should be remembered to check for “sensitivity” of these cohesive soils as well as for potential cyclic liquefiability. Soils in Zone C are generally not susceptible to “classic” cyclically-induced soil liquefaction, but they may be “sensitive” and vulnerable to strength loss with remoulding or large shear displacements.

This is a step forward, as it extends the previous “Modified Chinese” criteria to encompass important new field performance data (and corollary laboratory test data) from recent earthquakes. It should also be noted that there is a common lapse in engineering practice inasmuch as engineers often tend to become distracted by the presence of potentially

“classically” liquefiable soils, and then often neglect cohesive soils (clays and plastic silts) that are highly “sensitive” and vulnerable to major loss of strength if sheared or remolded. These types of “sensitive” soils (which can exist in Zones B and C) often co-exist in close proximity with potentially liquefiable soils, and can be similarly dangerous in their own right.

Appropriate sampling and testing protocols for soils of Zone B are not yet well established, and further research is needed here. Issues of sample disturbance, and sample densification during reconsolidation, and the potential applicability of “SHANSEP-like” laboratory reconsolidation approaches to offset these potential problems, are not yet well studied. Accordingly, sampling and testing of these types of soils may produce important qualitative data regarding likely soil performance, but it is difficult to rigorously quantitatively assess the levels of seismic loading necessary to “trigger” liquefaction in these soil types at present. It should also be noted that soils of Zone B may sometimes exhibit relatively innocuous behavior under cyclic loading in the absence of “static” driving shear stresses, but may exhibit much more significant softening and pore pressure increase if cyclically loaded while also subjected to significant “static” driving shear stresses. Accordingly, it appears that cyclic testing of these types of soils with non-zero static driving shear stresses ( $\dot{\sigma} > 0$ ) is advisable if this is potentially applicable to field conditions.

The criteria of this section do not fully cover all types of liquefiable soils. As an example, a well-studied clayey sand (SC) at a site in the southeastern U.S. has been clearly shown to be potentially susceptible to cyclic liquefaction, despite a clay content on the order of 15 %, and a Plasticity Index of up to 30% (Riemer et al., 1993). This is a highly unusual material, however, as it is an ancient sand that has weathered in place, with the clay largely coating the exterior surfaces of the individual weathered grains, and the overall soil is unusually “loose”. Exceptions must be anticipated, and judgement will continue to be necessary in evaluating whether or not specific soils are potentially liquefiable.

Finally, two additional conditions necessary for potential liquefiability are: (1) saturation (or at least near-saturation), and (2) “rapid” (largely “undrained”) loading. It should be remembered that phreatic conditions are variable both with seasonal fluctuations and irrigation, and that the rapid cyclic loading induced by seismic excitation represents an ideal loading type for initiation of soil liquefaction.

### 3.0 ASSESSMENT OF TRIGGERING POTENTIAL

Quantitative assessment of the likelihood of “triggering” or initiation of liquefaction is the necessary first step for most projects involving potential seismically-induced liquefaction. There are two general types of approaches available for this: (1) use of laboratory testing of “undisturbed” samples, and (2) use of empirical relationships based on correlation of observed field behavior with various in-situ “index” tests.

The use of laboratory testing is complicated by difficulties associated with sample disturbance during both sampling and reconsolidation. It is also difficult and expensive to perform high-quality cyclic simple shear testing, and cyclic triaxial testing poorly represents the loading conditions of principal interest for most seismic problems. Both sets of problems can be ameliorated, to some extent, by use of appropriate “frozen” sampling techniques, and subsequent testing in a high quality cyclic simple shear or torsional shear apparatus. The difficulty and cost of these delicate techniques, however, places their use beyond the budget and scope of most engineering studies. In addition, frozen sampling can be infeasible in soils with significant fines content, as the low permeability of these can lead to ice expansion completely disturbing the soils rather than preventing disturbance.

Accordingly, the use of in-situ “index” testing is the dominant approach in common engineering practice. As summarized in the recent state-of-the-art paper (Youd et al.; 1997, 2001), four in-situ test methods have now reached a level of sufficient maturity as to represent viable tools for this purpose, and these are (1) the Standard Penetration Test (SPT), (2) the cone penetration test (CPT), (3) measurement of in-situ shear wave

velocity ( $V_s$ ), and (4) the Becker penetration test (BPT). The oldest, and still the most widely used of these, is the SPT, and this will be the focus of the next section of this paper.

### 3.1 SPT-Based Triggering Assessment:

#### 3.1.1 Existing SPT-Based Correlations

The use of the SPT as a tool for evaluation of liquefaction potential first began to evolve in the wake of a pair of devastating earthquakes that occurred in 1964; the 1964 Great Alaskan Earthquake ( $M = 8+$ ) and the 1964 Niigata Earthquake ( $M \approx 7.5$ ), both of which produced significant liquefaction-related damage (e.g.: Kishida, 1966; Koizumi, 1966; Ohsaki, 1966; Seed and Idriss, 1971). Numerous additional researchers have made subsequent progress, and these types of SPT-based methods continue to evolve today.

As discussed by the NCEER Working Group (NCEER, 1997; Youd et al., 2001), one of the most widely accepted and widely used SPT-based correlations is the “deterministic” relationship proposed by Seed, et al. (1984, 1985). Figure 5 shows this relationship, with minor modification at low CSR (as recommended by the NCEER Working Group; NCEER, 1997). This familiar relationship is based on comparison between SPT  $N$ -values, corrected for both effective overburden stress and energy, equipment and procedural factors affecting SPT testing (to  $N_{1,60}$ -values) vs. intensity of cyclic loading, expressed as magnitude-weighted equivalent uniform cyclic stress ratio ( $CSR_{eq}$ ). The relationship between corrected  $N_{1,60}$ -values and the intensity of cyclic loading required to trigger liquefaction is also a function of fines content in this relationship, as shown in Figure 5.

Although widely used in practice, this relationship is dated, and does not make use of an increasing body of field case history data from seismic events that have occurred since 1984. It is particularly lacking in data from cases wherein peak ground shaking levels were high ( $CSR > 0.25$ ), an increasingly common design range in regions of high seismicity. This correlation also has no formal probabilistic basis, and so provides no insight regarding either uncertainty or probability of liquefaction.

Efforts at development of similar, but formally probabilistically-based, correlations have been published by a number of researchers, including Liao et al. (1988, 1998), and more recently Youd and Noble (1997), and Toprak et al. (1999). Figures 6(a) through (c) show these relationships, expressed as contours of probability of triggering of liquefaction, with the deterministic relationship of Seed et al. from Figure 5 superimposed (dashed lines) for reference. In each of the figures on this page, contours of probability of triggering or initiation of liquefaction for  $R_L = 5, 20, 50, 80$  and 95% are shown.

The probabilistic relationship proposed by Liao et al. employs a larger number of case history data points than were used by Seed et al. (1984), but this larger number of data points is the

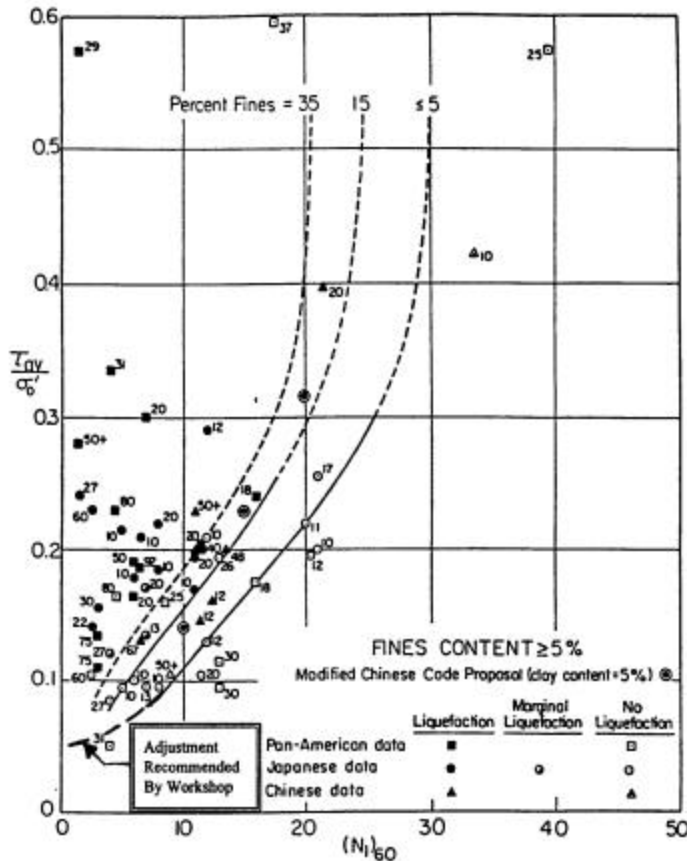


**Fig. 5: Correlation Between Equivalent Uniform Cyclic Stress Ratio and SPT  $N_{1,60}$ -Value for Events of Magnitude  $M_w$  7.5 for Varying Fines Contents, With Adjustments at Low Cyclic Stress Ratio as Recommended by NCEER Working Group (Modified from Seed, et al., 1984)**

result of less severe screening of points for data quality, and so includes a number of low quality data. This relationship was developed using the maximum likelihood estimation method for probabilistic regression (binary regression of logistic models). The way the likelihood function was formulated did not permit separate treatment of aleatory and epistemic sources of uncertainty, and so overstates the overall variance or uncertainty of the proposed correlation. This can lead to over-conservatism at low levels of probability of liquefaction. An additional shortcoming was that Liao et al. sought, but failed to find, a significant impact of fines content on the regressed relationship between SPT penetration resistance and liquefaction resistance, and so developed reliable curves (Figure 6(a)) only for sandy soils with less than 12% fines.

The relationship proposed by Youd and Noble employs a number of field case history data points from earthquakes which have occurred since the earlier relationships were developed, and excludes the most questionable of the data used by Liao et al. The basic methodology employed, maximum likelihood estimation, is the same, however, and as a result this correlation continues to overstate the overall uncertainty. The effects of fines content were judgmentally prescribed, a priori, in these relationships, and so were not developed as part of the regression. This correlation is applicable to soils of variable fines contents, and so can be employed for both sandy and silty soils. As shown in Figure 6(b), however, uncertainty (or variance) is high.

The relationship proposed by Toprak et al. also employs an enlarged and updated field case history database, and deletes the most questionable of the data used by Liao et al. As with the studies of Youd et al., the basic regression tool was binary regression, and the resulting overall uncertainty is again very large. Similarly, fines corrections and magnitude-correlated duration weighting factors were prescribed a priori, rather than being regressed from the field case history data, further decreasing model “fit” (and increasing variance and uncertainty).

Overall, the four prior relationships presented in Figures 5 and 6(a) through (c) are all excellent efforts, and are among the best of their types. It is proposed that more can now be achieved, however, using more powerful and flexible probabilistic tools, and taking fullest possible advantage of the currently available field case histories and current knowledge affecting the processing and interpretation of these.

### 3.1.2 Proposed New SPT-Based Correlations:

This section presents new correlations for assessment of the likelihood of initiation (or “triggering”) of soil liquefaction (Cetin, et al.; 2000, 2003). These new correlations eliminate several sources of bias intrinsic to previous, similar correlations, and provide greatly reduced overall uncertainty and variance. Figure 6(d) shows the new correlation, with contours of probability of liquefaction again plotted for  $P_L = 5, 20, 50, 80$  and 95%, and plotted to the same scale as the earlier

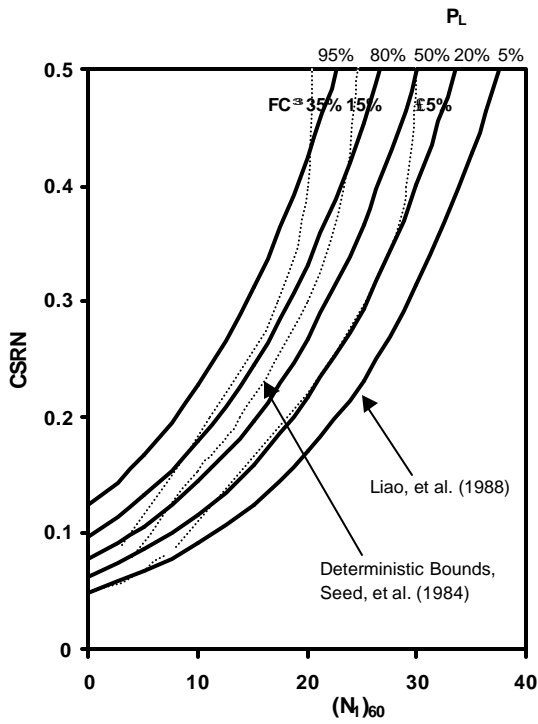
correlations. As shown in this figure, the new correlation provides greatly reduced overall uncertainty. Indeed, the uncertainty is now sufficiently reduced that the principal uncertainty now resides where it belongs; in the engineer’s ability to assess suitable CSR and representative  $N_{1,60}$  values for design cases.

Key elements in the development of this new correlation were: (1) accumulation of a significantly expanded database of field performance case histories, (2) use of improved knowledge and understanding of factors affecting interpretation of SPT data, (3) incorporation of improved understanding of factors affecting site-specific ground motions (including directivity effects, site-specific response, etc.), (4) use of improved methods for assessment of in-situ cyclic shear stress ratio (CSR), (5) screening of field data case histories on a quality/uncertainty basis, and (6) use of higher-order probabilistic tools (Bayesian Updating). These Bayesian methods (a) allowed for simultaneous use of more descriptive variables than most prior studies, and (b) allowed for appropriate treatment of various contributing sources of aleatory and epistemic uncertainty. The resulting relationships not only provide greatly reduced uncertainty, they also help to resolve a number of corollary issues that have long been difficult and controversial, including: (1) magnitude-correlated duration weighting factors, (2) adjustments for fines content, and (3) corrections for effective overburden stress.

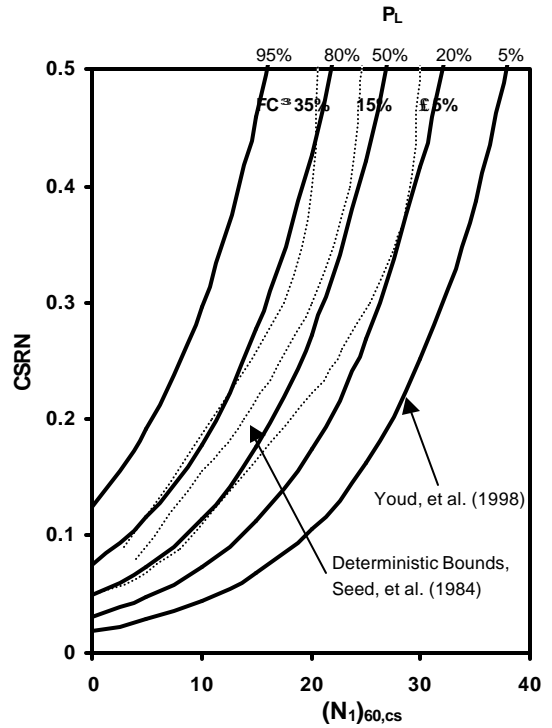
As a starting point, all of the field case histories employed in the correlations shown in Figures 5 and 6(a) through (c) were obtained and studied. Additional cases were also obtained, including several proprietary data sets. Eventually, approximately 450 liquefaction (and “non-liquefaction”) field case histories were evaluated in detail. A formal rating system was established for rating these case histories on the basis of data quality and uncertainty, and standards were established for inclusion of field cases in the final data set used to establish the new correlations. In the end, 203 of the field case histories were judged to meet these new and higher standards, and were employed in the final development of the proposed new correlations.

A significant improvement over previous efforts was the improved evaluation of peak horizontal ground acceleration at each earthquake field case history site. Specific details are provided by Cetin et al. (2001, 2003). Significant improvements here were principally due to improved understanding and treatment of issues such as (a) directivity effects, (b) effects of site conditions on response, (c) improved attenuation relationships, and (d) availability of strong motion records from recent (and well-instrumented) major earthquakes. In these studies, peak horizontal ground acceleration ( $a_{max}$ ) was taken as the geometric mean of two recorded orthogonal horizontal components. Whenever possible, attenuation relationships were calibrated on an earthquake-specific basis, based on local strong ground motion records, significantly reducing uncertainties. For all cases wherein sufficiently detailed data and suitable nearby recorded ground motions were available, site-specific site response analyses were

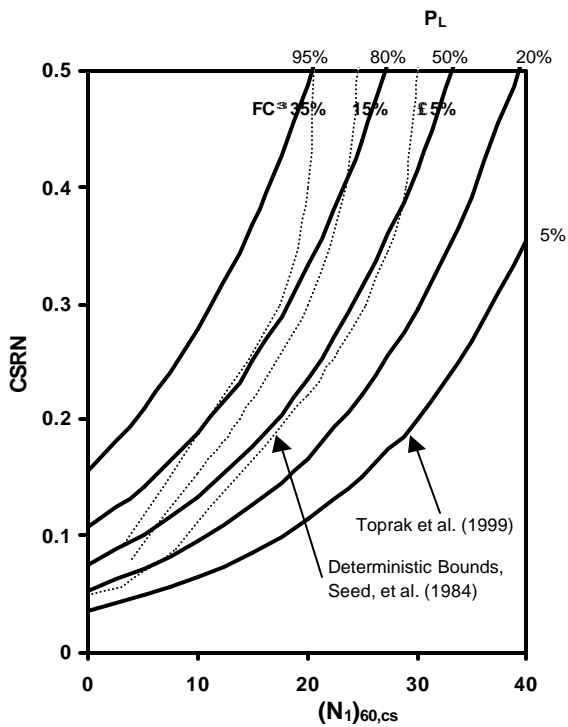
(a) Liao et al., 1988



(b) Youd et al., 1998



(c) Toprak et al., 1999



(d) This Study ( $s\zeta=1300$  psf.)

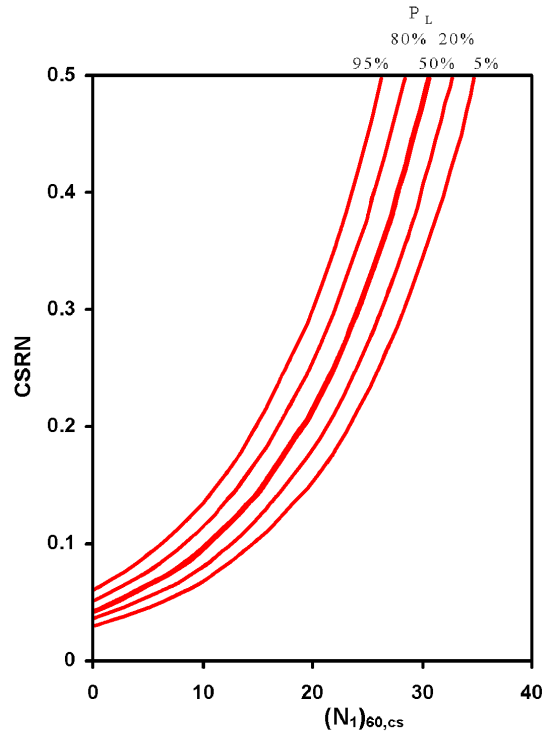


Fig. 6: Comparison of Best Available Probabilistic Correlations for Evaluation of Liquefaction Potential (All Plotted for  $M_W=7.5$ ,  $s_v'=0.65$  atm, and Fines Content  $\leq 5\%$ )

performed. In all cases, both local site effects and rupture-mechanism-dependent potential directivity effects were also considered.

A second major improvement was better estimation of in-situ CSR within the critical stratum for each of the field case histories. All of the previous studies described so far used the “simplified” method of Seed and Idriss (1971) to estimate CSR at depth (within the critical soil stratum) as

$$CSR_{peak} = \left( \frac{a_{max}}{g} \right) \cdot \left( \frac{\sigma_v}{\sigma'_v} \right) \cdot (r_d) \quad (\text{Eq. 1})$$

where

- $a_{max}$  = the peak horizontal ground surface acceleration,
- $g$  = the acceleration of gravity,
- $\sigma_v$  = total vertical stress,
- $\sigma'_v$  = effective vertical stress, and
- $r_d$  = the nonlinear shear mass participation factor.

The original  $r_d$  values proposed by Seed and Idriss (1971) are shown by the heavy lines in Figure 6(a). These are the values used in the previous studies by Seed et al. (1984), Liao et al. (1988, 1998), Youd et al. (1997), and Toprak et al. (1999).

Recognition that  $r_d$  is nonlinearly dependent upon a suite of factors led to studies by Cetin and Seed (2000) to develop improved correlations for estimation of  $r_d$ . The numerous light gray lines in Figures 7(a) and (b) show the results of 2,153 seismic site response analyses performed to assess the variation of  $r_d$  over ranges of (1) site conditions, and (2) ground motion excitation characteristics. The mean and  $\pm 1$  standard deviation values for these 2,153 analyses are shown by the heavy lines in Figure 7(b). As shown in Figures 7(a) and (b), the earlier  $r_d$  proposal of Seed and Idriss (1971) understates the variance, and provides biased (generally high) estimates of  $r_d$  at depths of between 10 and 50 feet (3 to 15 m.) Unfortunately, it is in this depth range that the critical soil strata for most of the important liquefaction (and non-liquefaction) earthquake field case histories occur. This, in turn, creates some degree of corresponding bias in relationships developed on this basis.

Cetin and Seed (2000, 2003) propose a new, empirical basis for estimation of  $r_d$  as a function of; (1) depth, (2) earthquake magnitude, (3) intensity of shaking, and (4) site stiffness (as expressed in Equation 2).

Figure 8 shows the values of  $r_d$  from the 2,153 site response analyses performed as part of these studies sub-divided into 12 “bins” as a function of peak ground surface acceleration ( $a_{max}$ ),

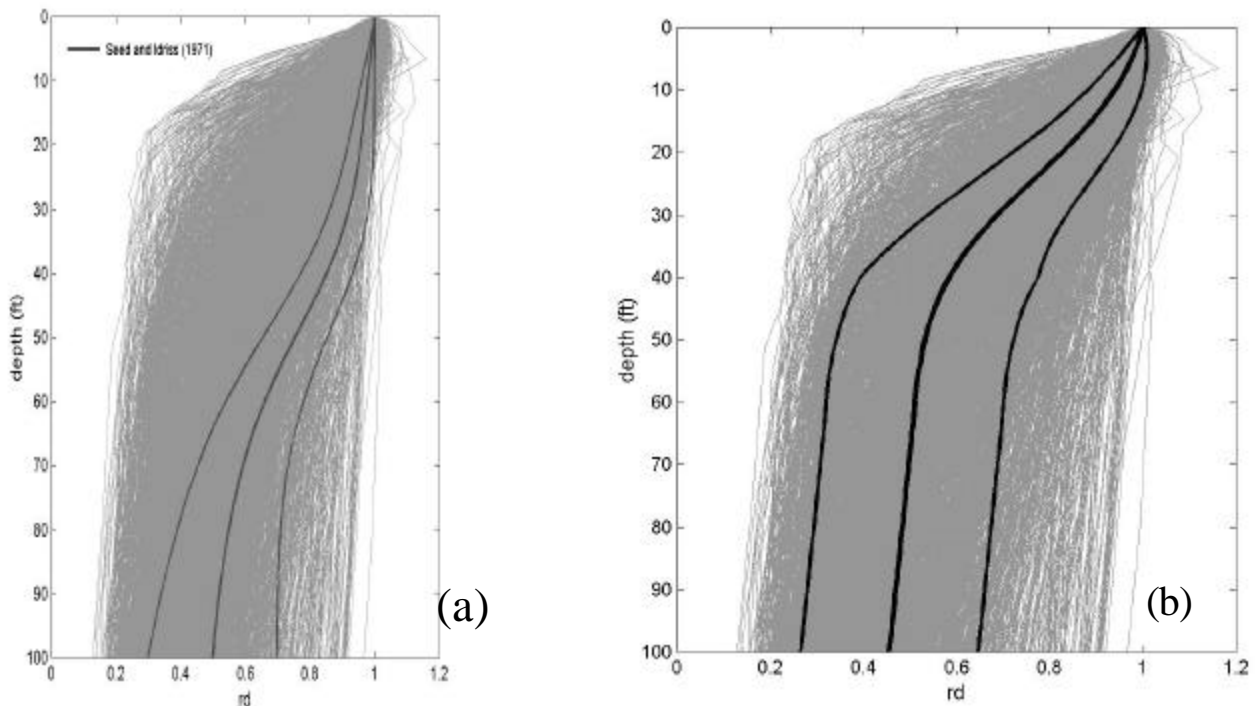


**Fig. 7:  $r_d$  Results from Response Analyses for 2,153 Combinations of Site Conditions and Ground Motions, Superimposed with Heavier Lines Showing (a) the Earlier Recommendations of Seed and Idriss (1971), and (b) the Mean and  $\pm 1$  Standard Deviation Values for the 2,153 Cases Analyzed (After Cetin and Seed, 2000).**

site stiffness ( $V_{s,40ft}$ ), earthquake magnitude ( $M_w$ ), and depth ( $d$ ). [ $V_{s,40ft}$  is the “average” shear wave velocity over the top 40 feet of a site (in units of ft./sec.), taken as 40 feet divided by the shear wave travel time in traversing this 40 feet.] Superimposed on each figure are the mean and  $\pm 1$  standard deviation values central to each “bin” from Equation 2. Either Equation 2, or Figure 8, can be used to derive improved (and statistically unbiased) estimates of  $r_d$ .

It is noted, however, that in-situ CSR (and  $r_d$ ) can “jump” or transition irregularly within a specific soil profile, especially near sharp transitions between “soft” and “stiff” strata, and that CSR (and  $r_d$ ) are also a function of the interaction between a site and each specific excitation motion. Accordingly, the best means of estimation of in-situ CSR within any given stratum is to directly calculate CSR by means of appropriate site-specific, and event-specific, seismic site response analyses, when this is feasible. As the new correlations were developed using both directly-calculated  $r_d$  values (from site response analyses) as well as  $r_d$  values from the statistically unbiased correlation of Equation 2, there is no intrinsic a priori bias associated with either approach.

This represents an important improvement over all previous SPT-based “triggering” correlations. All prior correlations had been based on use of the “simplified”  $r_d$  of Seed and Idriss (1971) for back-analysis of field performance case histories, and were as a result unconservatively biased relative to actual case-specific seismic response analysis. These previous methods could be used in forward engineering so long as the “simplified”  $r_d$  was used to assess CSR, but could be unconservative if used in conjunction with (1-D or 2-D or 3-D) seismic response analyses (as they often are for “important” projects such as dams and other critical facilities.) The new correlations, on the other hand, can be safely used in

conjunction with project-specific dynamic response analyses without introducing bias.

In the new correlations proposed herein, in-situ cyclic stress ratio (CSR) is taken as the “equivalent uniform CSR” equal to 65% of the single (one-time) peak CSR (from Equation 1) as

$$CSR_{eq} = (0.65) \cdot CSR_{peak} \quad (\text{Eq. 3})$$

In-situ  $CSR_{eq}$  was evaluated directly, based on performance of full seismic site response analyses (using SHAKE 90; Idriss and Sun, 1992), for cases where (a) sufficient sub-surface data was available, and (b) where suitable “input” motions could be developed from nearby strong ground motion records. For cases wherein full seismic site response analyses were not performed,  $CSR_{eq}$  was evaluated using the estimated  $a_{max}$  and Equations 1 and 2. In addition to the best estimates of  $CSR_{eq}$ , the variance or uncertainty of these estimates (due to all contributing sources of uncertainty) was also assessed (Cetin et al., 2001).

At each case history site, the critical stratum was identified as the stratum most susceptible to triggering of liquefaction. Only one critical stratum was analyzed at any one site, and in many cases two or more SPT borings were combined jointly to characterize a single critical stratum. When possible, collected surface boil materials were also considered, but problems associated with mixing and segregation during transport, and recognition that liquefaction of underlying strata can result in transport of overlying soils to the surface through boils, limited the usefulness of some of this data.

The  $N_{1,60}$ -values employed were “truncated mean values” within the critical stratum. Measured  $N$ -values (from one or more points) within a critical stratum were corrected for

**$d < 65$  ft:**

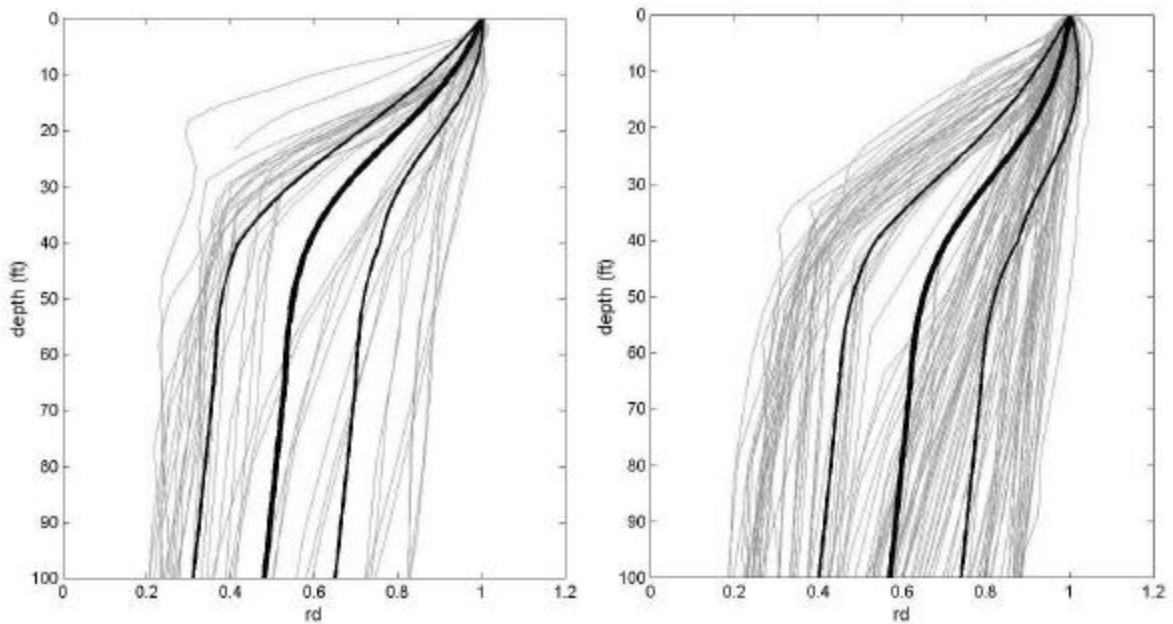
$$r_d(d, M_w, a_{max}, V_{s,40'}^*) = \frac{1 + \frac{-23.013 - 2.949 \cdot a_{max} + 0.999 \cdot M_w + 0.016 \cdot V_{s,40'}^*}{16.258 + 0.201 \cdot e^{0.104 \cdot (-d + 0.0785 \cdot V_{s,40'}^* + 24.888)}}}{1 + \frac{-23.013 - 2.949 \cdot a_{max} + 0.999 \cdot M_w + 0.016 \cdot V_{s,40'}^*}{16.258 + 0.201 \cdot e^{0.104 \cdot (0.0785 \cdot V_{s,40'}^* + 24.888)}}} \pm \sigma_{\varepsilon_{r_d}} \quad (\text{Eq 2})$$

**$d \geq 65$  ft:**

$$r_d(d, M_w, a_{max}, V_{s,40'}^*) = \frac{1 + \frac{-23.013 - 2.949 \cdot a_{max} + 0.999 \cdot M_w + 0.016 \cdot V_{s,40'}^*}{16.258 + 0.201 \cdot e^{0.104 \cdot (-65 + 0.0785 \cdot V_{s,40'}^* + 24.888)}}}{1 + \frac{-23.013 - 2.949 \cdot a_{max} + 0.999 \cdot M_w + 0.016 \cdot V_{s,40'}^*}{16.258 + 0.201 \cdot e^{0.104 \cdot (0.0785 \cdot V_{s,40'}^* + 24.888)}}} - 0.0014 \cdot (d - 65) \pm \sigma_{\varepsilon_{r_d}}$$

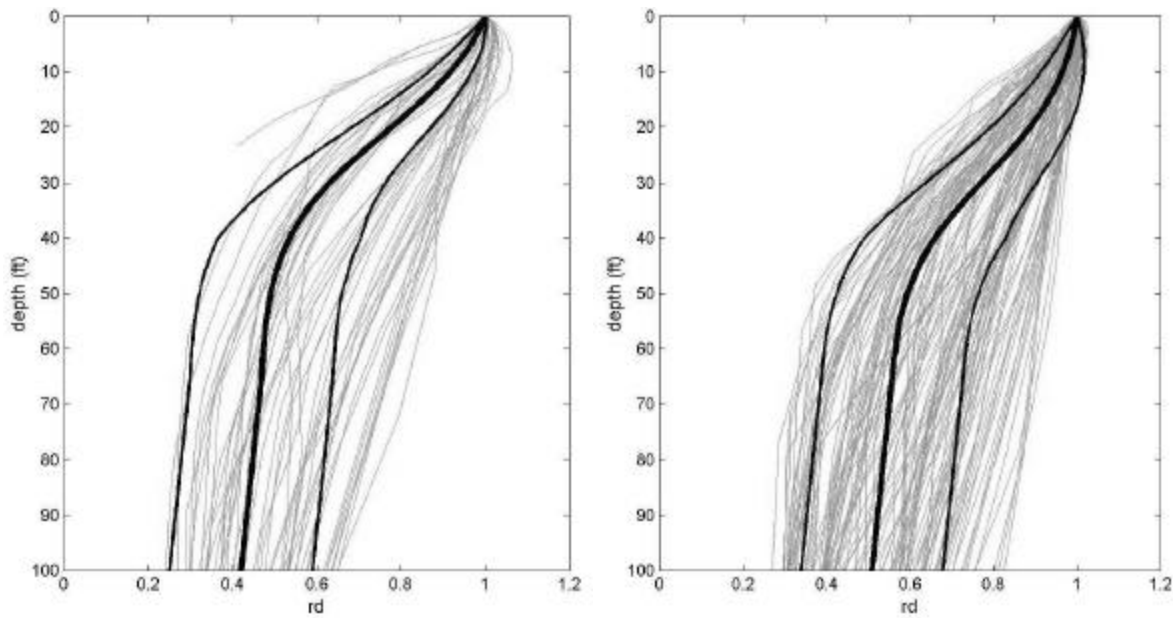
**where**

$$\sigma_{\varepsilon_{r_d}}(d) = d^{0.850} \cdot 0.0072 \quad [\text{for } d < 40 \text{ ft}], \text{ and} \quad \sigma_{\varepsilon_{r_d}}(d) = 40^{0.850} \cdot 0.0072 \quad [\text{for } d \geq 40 \text{ ft}]$$



(a)  $M_w \geq 6.8$ ,  $a_{max} \leq 0.12g$ ,  $V_{s,40 ft.} \leq 525$  fps

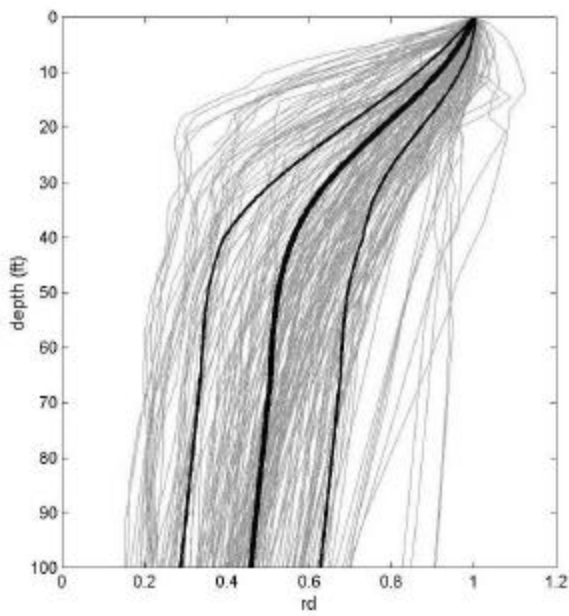
(b)  $M_w \geq 6.8$ ,  $a_{max} \leq 0.12g$ ,  $V_{s,40 ft.} > 525$  fps



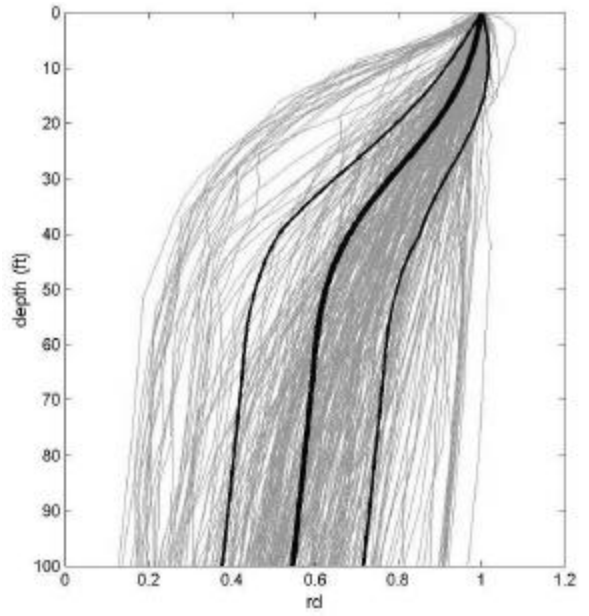
(c)  $M_w < 6.8$ ,  $a_{max} \leq 0.12g$ ,  $V_{s,40 ft.} \leq 525$  fps

(d)  $M_w < 6.8$ ,  $a_{max} \leq 0.12g$ ,  $V_{s,40 ft.} > 525$  fps

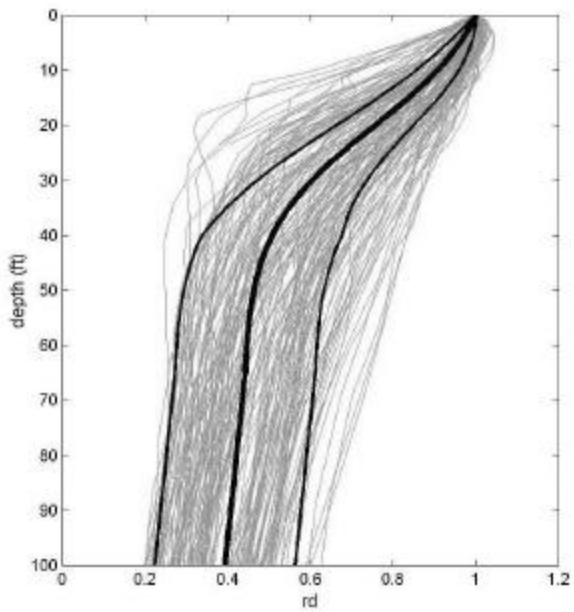
**Fig. 8:  $R_d$  Results for Various “Bins” Superimposed with the Predictions (Mean and Mean  $\pm 1s$ ) Based on Bin Mean Values of  $V_{s,40 ft.}$ ,  $M_w$ , and  $a_{max}$  (continued...)**



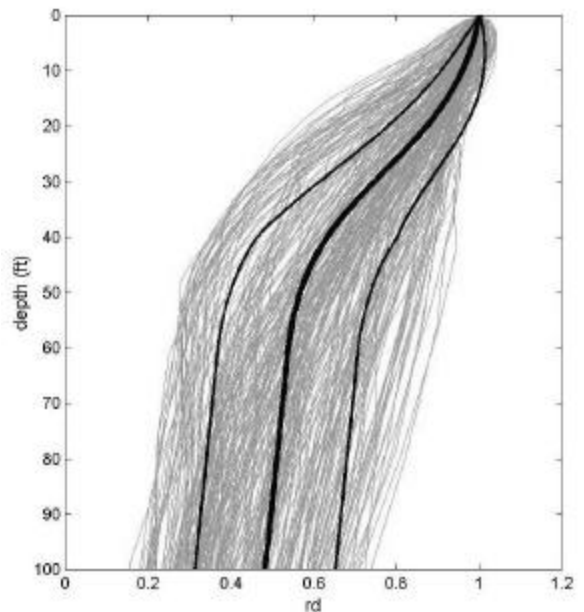
(e)  $M_w \geq 6.8, 0.12 < a_{\max} \leq 0.23g, V_{s,40 \text{ ft.}} \leq 525 \text{ fps}$



(f)  $M_w \geq 6.8, 0.12 < a_{\max} \leq 0.23g, V_{s,40 \text{ ft.}} > 525 \text{ fps}$

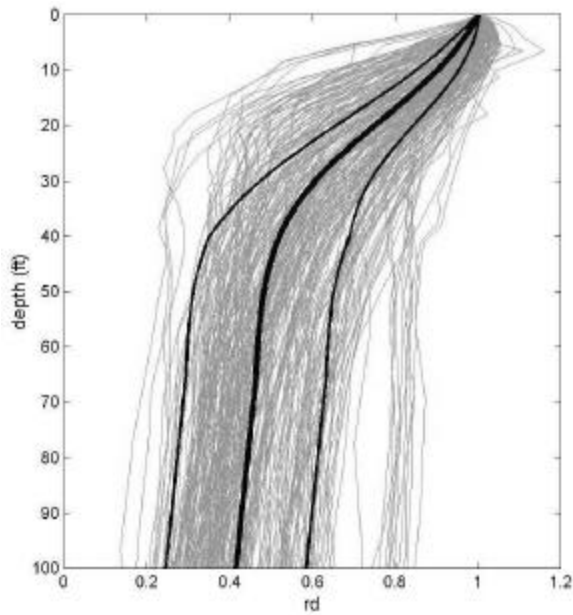


(g)  $M_w < 6.8, 0.12 < a_{\max} \leq 0.23g, V_{s,40 \text{ ft.}} \leq 525 \text{ fps}$

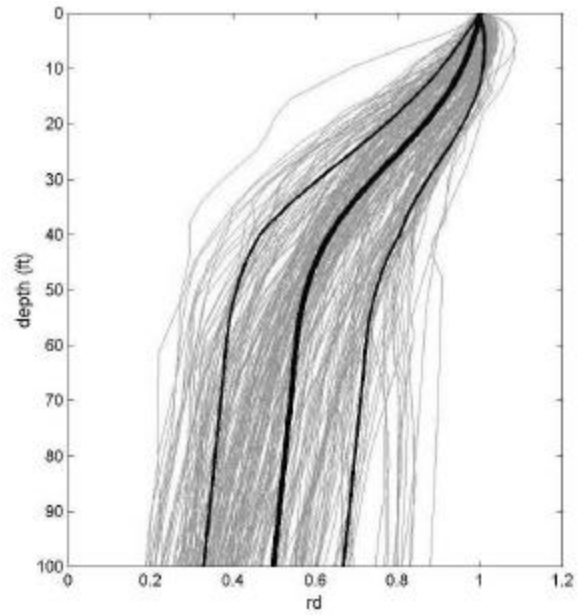


(h)  $M_w < 6.8, 0.12 < a_{\max} \leq 0.23g, V_{s,40 \text{ ft.}} > 525 \text{ fps}$

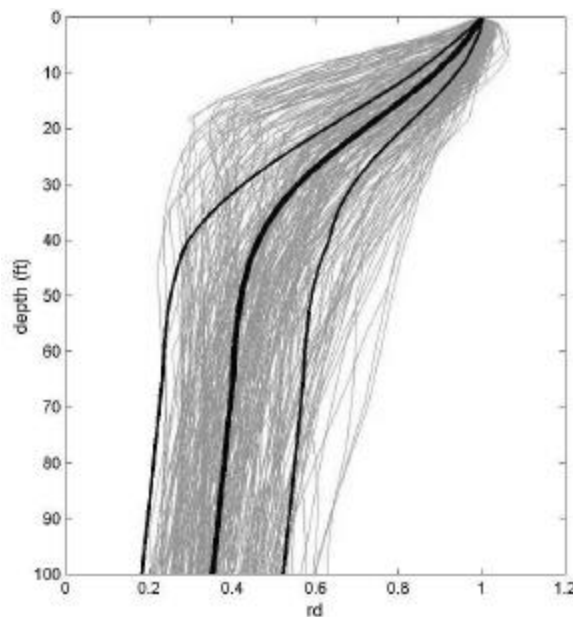
**Fig. 8:  $R_d$  Results for Various “Bins” Superimposed with the Predictions (Mean and Mean  $\pm 1s$ ) Based on Bin Mean Values of  $V_{s,40 \text{ ft.}}$ ,  $M_w$ , and  $a_{\max}$  (continued...)**



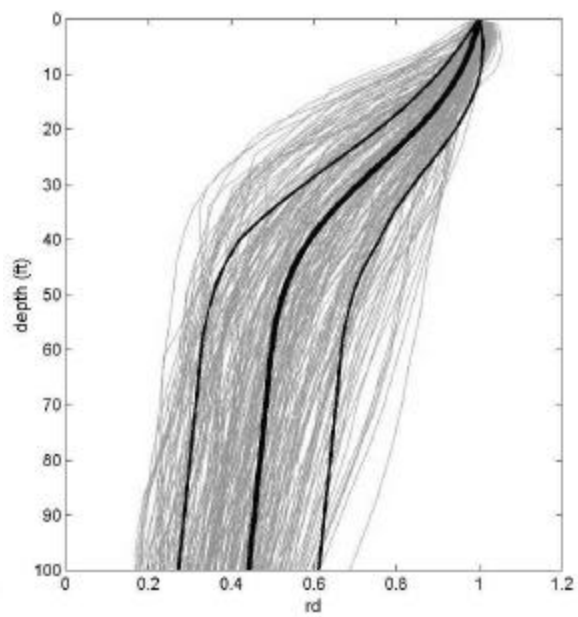
(i)  $M_w \geq 6.8, 0.23 < a_{max}, V_{s,40 ft.} \leq 525$  fps



(j)  $M_w \geq 6.8, 0.23 < a_{max}, V_{s,40 ft.} > 525$  fps



(k)  $M_w < 6.8, 0.23 < a_{max}, V_{s,40 ft.} \leq 525$  fps



(l)  $M_w < 6.8, 0.23 < a_{max}, V_{s,40 ft.} > 525$  fps

**Fig. 8:  $R_d$  Results for Various “Bins” Superimposed with the Predictions (Mean and Mean  $\pm 1s$ ) Based on Bin Mean Values of  $V_{s,40 ft.}$ ,  $M_w$ , and  $a_{max}$**

overburden, energy, equipment, and procedural effects to  $N_{1,60}$  values, and were then plotted vs. elevation. In many cases, a given soil stratum would be found to contain an identifiable sub-stratum (based on a group of localized low  $N_{1,60}$ -values) that was significantly more critical than the rest of the stratum. In such cases, the sub-stratum was taken as the “critical stratum”. Occasional high values, not apparently representative of the general characteristics of the critical stratum, were considered “non-representative” and were deleted in a number of the cases. Similarly, though less often, very low  $N_{1,60}$  values (very much lower than the apparent main body of the stratum, and often associated with locally high fines content) were similarly deleted. The remaining, corrected  $N_{1,60}$  values were then used to evaluate both the mean of  $N_{1,60}$  within the critical stratum, and the variance in  $N_{1,60}$ .

For those cases wherein the critical stratum had only one single useful  $N_{1,60}$ -value, the coefficient of variation was taken as 20%; a value typical of the larger variances among the cases with multiple  $N_{1,60}$  values within the critical stratum (reflecting the increased uncertainty due to lack of data when only a single value was available).

All  $N$ -values were corrected for overburden effects (to the hypothetical value,  $N_1$ , that “would” have been measured if the effective overburden stress at the depth of the SPT had been 1 atmosphere) [1 atm.  $\approx$  2,000 lb/ft<sup>2</sup>  $\approx$  1 kg/cm<sup>2</sup>  $\approx$  14.7 lb/in<sup>2</sup>  $\approx$  101 kPa] as

$$N_1 = N \cdot C_N \quad (\text{Eq. 4(a)})$$

where  $C_N$  is taken (after Liao and Whitman, 1986) as

$$C_N = \left( \frac{1}{\sigma'_v} \right)^{0.5} \quad (\text{Eq. 4(b)})$$

where  $\sigma'_v$  is the actual effective overburden stress at the depth of the SPT in atmospheres.

The resulting  $N_1$  values were then further corrected for energy, equipment, and procedural effects to fully standardized  $N_{1,60}$  values as

$$N_{1,60} = N_1 \cdot C_R \cdot C_S \cdot C_B \cdot C_E \quad (\text{Eq. 5})$$

where  $C_R$  = correction for “short” rod length,  
 $C_S$  = correction for non-standardized sampler configuration,  
 $C_B$  = correction for borehole diameter, and  
 $C_E$  = correction for hammer energy efficiency.

The corrections for  $C_R$ ,  $C_S$ ,  $C_B$  and  $C_E$  employed correspond largely to those recommended by the NCEER Working Group (NCEER, 1997; Youd et al., 2001).

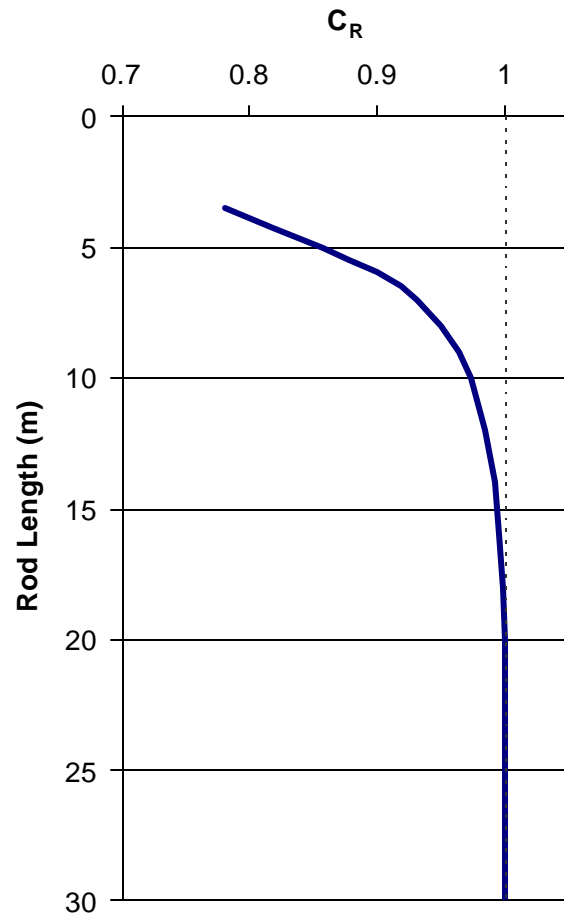


**Fig. 9: Recommended  $C_R$  Values (rod length from point of hammer impact to tip of sampler).**

Table 1 summarizes the correction factors used in these studies. The correction for “short” rod length between the driving hammer and the penetrating sampler was taken as a nonlinear “curve” (Figure 9), rather than the incremental values of the NCEER Workshop recommendations, but the two agree reasonably well at all NCEER mid-increments of length.

$C_S$  was applied in cases wherein a “nonstandard” (though very common) SPT sampler was used in which the sampler had an internal space for sample liner rings, but the rings were not used. This results in an “indented” interior liner annulus of enlarged diameter, and reduces friction between the sample and the interior of the sampler, resulting in reduced overall penetration resistance (Seed et al., 1984 and 1985). The reduction in penetration resistance is on the order of ~10 % in loose soils ( $N_1 < 10$  blows/ft), and ~30 % in very dense soils ( $N_1 > 30$  blows/ft), so  $C_S$  varied from 1.1 to 1.3 over this range.

Borehole diameter corrections ( $C_B$ ) were as recommended in the NCEER Workshop Proceedings (NCEER, 1997; Youd et al., 2001).

**Table 1: Recommended Corrections for SPT Equipment Energy and Procedures**

$C_R$	(See Fig. 9 for Rod Length Correction Factors)	
$C_S$	For samplers with an indented space for interior liners, but with liners omitted during sampling,	
	$C_s = 1 + \frac{N_{1,60}}{100} \quad (\text{Eq. T-1})$	
	With limits as $1.10 \leq C_S \leq 1.30$	
$C_B$	<u>Borehole diameter</u>	<u>Correction (<math>C_B</math>)</u>
	65 to 115 mm	1.00
	150 mm	1.05
	200 mm	1.15
$C_E$	$C_E = \frac{ER}{60\%} \quad (\text{Eq. T-2})$	
	where ER (efficiency ratio) is the fraction or percentage of the theoretical SPT impact hammer energy actually transmitted to the sampler, expressed as %	
	<ul style="list-style-type: none"> <li>• The best approach is to directly measure the impact energy transmitted with each blow. When available, direct energy measurements were employed.</li> <li>• The next best approach is to use a hammer and mechanical hammer release system that has been previously calibrated based on direct energy measurements.</li> <li>• Otherwise, ER must be estimated. For good field procedures, equipment and monitoring, the following guidelines are suggested:</li> </ul>	
	<u>Equipment</u>	<u>Approximate ER (see Note 3)</u> <u><math>C_E</math> (see Note 3)</u>
	-Safety Hammer <sup>1</sup>	0.4 to 0.75      0.7 to 1.2
	-Donut Hammer <sup>1</sup>	0.3 to 0.6      0.5 to 1.0
	-Donut Hammer <sup>2</sup>	0.7 to 0.85      1.1 to 1.4
	-Automatic -Trip Hammer (Donut or Safety Type)	0.5 to 0.8      0.8 to 1.4
	<ul style="list-style-type: none"> <li>• For lesser quality fieldwork (e.g.: irregular hammer drop distance, excessive sliding friction of hammer on rods, wet or worn rope on cathead, etc.) further judgmental adjustments are needed.</li> </ul>	

- Notes: (1) Based on rope and cathead system, two turns of rope around cathead, “normal” release (not the Japanese “throw”), and rope not wet or excessively worn.  
(2) Rope and cathead with special Japanese “throw” release. (See also Note 4.)  
(3) For the ranges shown, values roughly central to the mid-third of the range are more common than outlying values, but ER and  $C_E$  can be even more highly variable than the ranges shown if equipment and/or monitoring and procedures are not good.  
(4) Common Japanese SPT practice requires additional corrections for borehole diameter and for frequency of SPT hammer blows. For “typical” Japanese practice with rope and cathead, donut hammer, and the Japanese “throw” release, the overall product of  $C_B \times C_E$  is typically in the range of 1.0 to 1.3.

Corrections for hammer energy ( $C_E$ ), which were often significant, were largely as recommended by the NCEER Working Group, except in those cases where better hammer/system-specific information was available. Cases where better information was available included cases where either direct energy measurements were made during driving of the SPT sampler, or where the hammer and the raising/dropping system (and the operator, when appropriate) had been reliably calibrated by means of direct driving energy measurements.

Within the Bayesian updating analyses, which were performed using a modified version of the program BUMP (Geyskens et al., 1993), all field case history data were modeled not as “points”, but rather as distributions, with variances in both CSR and  $N_{1,60}$ . These regression-type analyses were simultaneously applied to a number of contributing variables, and the resulting proposed correlations are illustrated in Figures 6(d) and 10 through 12, and are expressed in Equations 6 through 12.

Figure 10 shows the proposed probabilistic relationship between duration-corrected equivalent uniform cyclic stress ratio ( $CSR_{eq}$ ), and fines-corrected penetration resistances ( $N_{1,60,cs}$ ), with the correlations as well as all field data shown normalized to an effective overburden stress of  $\sigma'_v = 0.65$  atm. (1,300 lb/ft<sup>2</sup>). The contours shown (solid lines) are for probabilities of liquefaction of  $P_L=5\%$ , 20%, 50%, 80%, and 95%. All “data points” shown represent median values, also corrected for duration and fines. These are superposed (dashed lines) with the relationship proposed by Seed et al. (1984) for reference.

As shown in this figure, the “clean sand” (Fines Content 5%) line of Seed et al. (1984) appears to corresponds roughly to  $P_L=50\%$ . This is not the case, however, as the Seed et al. (1984) line was based on biased values of CSR (as a result of biased  $r_d$  at shallow depths, as discussed earlier). The new correlation uses actual event-specific seismic site response analyses for evaluation of in-situ CSR in 53 of the back-analyzed case histories, and the new (and statistically unbiased) empirical estimation of  $r_d$  (as a function of level of shaking, site stiffness, and earthquake magnitude) as presented in Equation 2 and Figure 8 (Cetin and Seed, 2000) for the remaining 148 case histories. The new (improved) estimates of in-situ CSR tend to be slightly lower, typically on the order of ~ 5 to 15% lower, at the shallow depths that are critical in most of the field case histories. Accordingly, the CSR’s of the new correlation are also, correspondingly, lower by about 5 to 15%, and a fully direct comparison between the new correlation and the earlier recommendations of Seed et al. (1984) cannot be made.

It should be noted that the use of slightly biased (high) values of  $r_d$  was not problematic in the earlier correlation of Seed et al. (1984), so long as the same biased ( $r_d$ ) basis was employed in forward application of this correlation to field engineering works. It was a slight problem, however, when forward applications involved direct, response-based calculation of in-

situ CSR, as often occurs on analyses of major dams, etc.

It was Seed’s intent that the recommended (1984) boundary should represent approximately a 10 to 15% probability of liquefaction, and with allowance for the “shift” in (improved) evaluation of CSR, the 1984 deterministic relationship for clean sands (<5% fines) does correspond to approximately  $P_L \approx 10$  to 30%, except at very high CSR ( $CSR > 0.3$ ), a range in which data were previously scarce.

Also shown in Figure 10 is the boundary curve proposed by Yoshimi et al. (1994), based on high quality cyclic testing of frozen samples of alluvial sandy soils. The line of Yoshimi et al. is arguably unconservatively biased at very low densities (low N-values) as these loose samples densified during laboratory thawing and reconsolidation. Their testing provides potentially valuable insight, however, at high N-values where reconsolidation densification was not significant. In this range, the new proposed correlation provides slightly better agreement with the test data than does the earlier relationship proposed by Seed et al. (1984). Improvement of the new correlation at high CSR values is due, in large part, to the availability of significant new data (at high CSR) from recent earthquakes that had not been available in 1984.

The new correlation is also presented in Figure 6(d), where it can be compared directly with the earlier probabilistic relationships of Figures 6(a) through (c). Here, again, the new correlation is normalized to  $\sigma'_v = 0.65$  atm. in order to be fully compatible with the basis of the other relationships shown. As shown in this figure, the new correlation provides a tremendous reduction in overall uncertainty (or variance).

### 3.1.3 Adjustments for Fines Content:

The new (probabilistic) boundary curve for  $P_L = 15\%$  (again normalized to an effective overburden stress of  $\sigma'_v = 0.65$  atm.) represents a suitable basis for illustration of the new correlation’s regressed correction for the effects of fines content, as shown in Figure 11. In this figure, both the correlation as well as the mean values (CSR and  $N_{1,60}$ ) of the field case history data are shown not corrected for fines (this time the N-value axis is not corrected for fines content effects, so that the ( $P_L=20\%$ ) boundary curves are, instead, offset to account for varying fines content.) In this figure, the earlier correlation proposed by Seed et al. (1984) is also shown (with dashed lines) for approximate comparison.

In these current studies, based on the overall (regressed) correlation, the energy- and procedure- and overburden-corrected N-values ( $N_{1,60}$ ) are further corrected for fines content as

$$N_{1,60,CS} = N_{1,60} * C_{FINES} \quad (\text{Eq. 6})$$

where the fines correction was “regressed” as a part of the Bayesian updating analyses. The fines correction is equal to 1.0 for fines contents of  $FC \leq 5\%$ , and reaches a maximum (limiting) value for  $FC \geq 35\%$ . As illustrated in Figure 11,

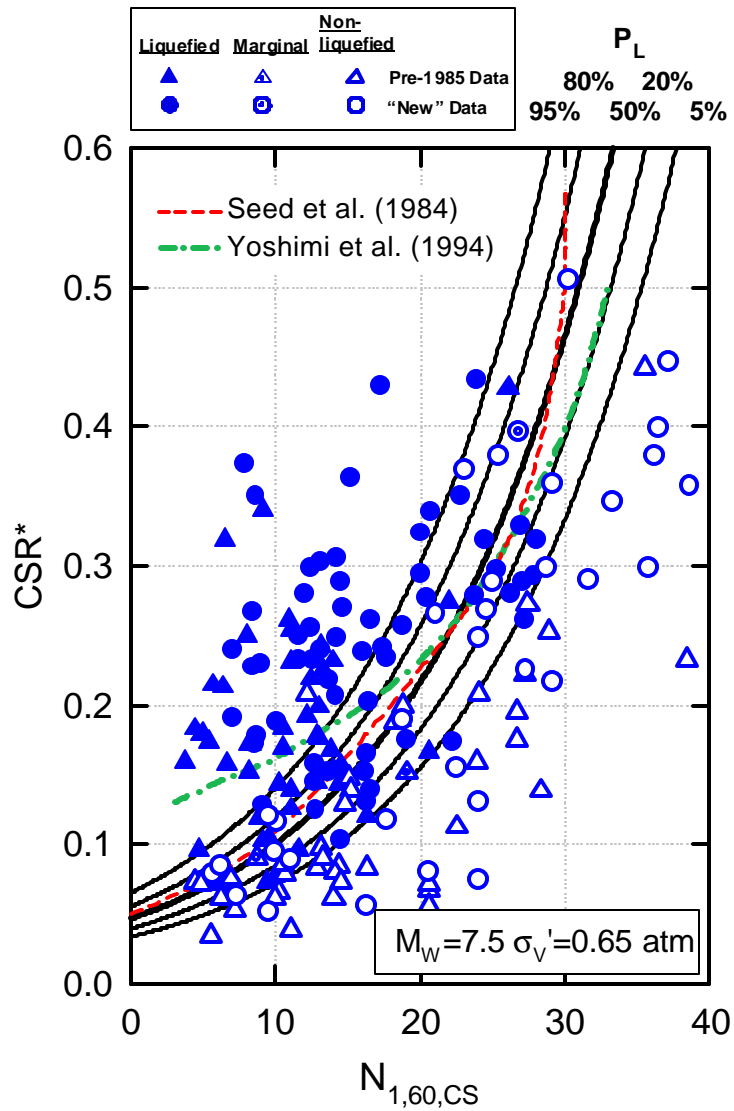


Fig. 10: Recommended Probabilistic SPT-Based Liquefaction Triggering Correlation (for  $M_w=7.5$  and  $\sigma'_v=0.65$  atm), and the Relationship for “Clean Sands” Proposed by Seed et al. (1984)

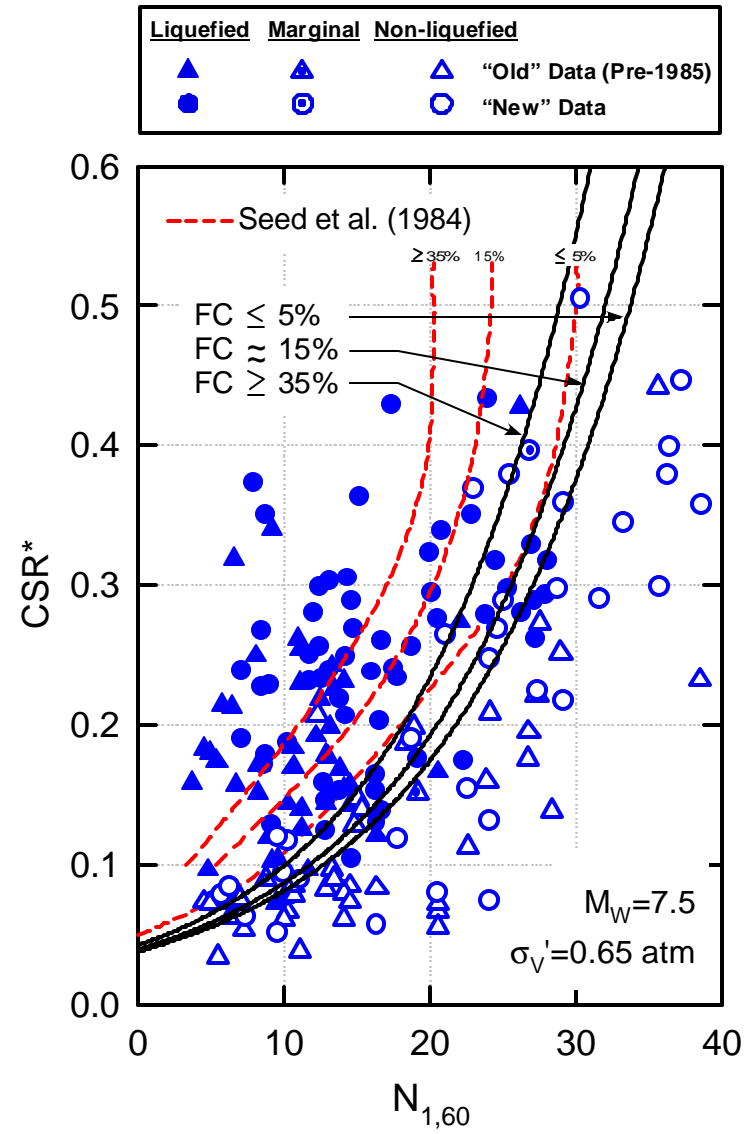


Fig. 11: Recommended “Deterministic” SPT-Based Liquefaction Triggering Correlation (for  $M_w=7.5$  and  $\sigma'_v=0.65$  atm), with Adjustments for Fines Content Shown

the maximum fines correction results in an increase of  $N$  values of about +6 blows/ft. (at  $FC \geq 35\%$ , and high CSR). As illustrated in this figure, this maximum fines correction is somewhat smaller than the earlier maximum correction of +9.5 blows/ft proposed by Seed et al. (1984).

The regressed relationship for  $C_{FINES}$  is

$$C_{FINES} = (1 + 0.004 \cdot FC) + 0.05 \cdot \left( \frac{FC}{N_{1,60}} \right) \quad (\text{Eq. 7})$$

lim:  $FC \geq 5\%$  and  $FC < 35\%$

where  $FC$  = percent fines content (percent by dry weight finer than 0.074mm), expressed as an integer (e.g. 15% fines is expressed as 15), and  $N_{1,60}$  is in units of blows/ft.

*Magnitude-Correlated Duration Weighting:*

Both the probabilistic and “deterministic” (based on  $P_L=20\%$ ) new correlations presented in Figures 10 and 11 are based on the correction of “equivalent uniform cyclic stress ratio” ( $CSR_{eq}$ ) for duration (or number of equivalent cycles) to  $CSR_N$ , representing the equivalent CSR for a duration typical of an “average” event of  $M_W = 7.5$ . This was done by means of a magnitude-correlated duration weighting factor ( $DWF_M$ ) as

$$CSR_N = CSR_{eq,M=7.5} = CSR_{eq,M=M} / DWF_M \quad (\text{Eq. 8})$$

This duration weighting factor has been somewhat controversial, and has been developed by a variety of different approaches (using cyclic laboratory testing and/or field case history data) by a number of investigators. Figure 12 summarizes a number of recommendations, and shows (shaded zone) the recommendations of the NCEER Working Group (NCEER, 1997). In these current studies, this important and controversial factor could be regressed as a part of the Bayesian Updating analyses. Moreover, the factor ( $DWF_M$ ) could also be investigated for possible dependence on density (correlation with  $N_{1,60}$ ). Figures 13 shows the resulting values of  $DWF_M$ , as a function of varying corrected  $N_{1,60}$ -values. As shown in Figure 13, the dependence on density, or  $N_{1,60}$ -values, was found to be relatively minor.

The duration weighting factors shown in Figures 12 and 13 fall slightly below those recommended by the NCEER Working group, and very close to recent recommendations of Idriss (2000). Idriss’ recommendations are based on a judgmental combination of interpretation of high-quality cyclic simple shear laboratory test data and empirical assessment of “equivalent” numbers of cycles from recorded strong motion time histories, and are the only other values shown that account for the cross-correlation of  $r_d$  with magnitude. The close agreement of this very different (and principally laboratory data based) approach, and the careful (field data based) probabilistic assessments of these current studies, are strongly mutually supportive.

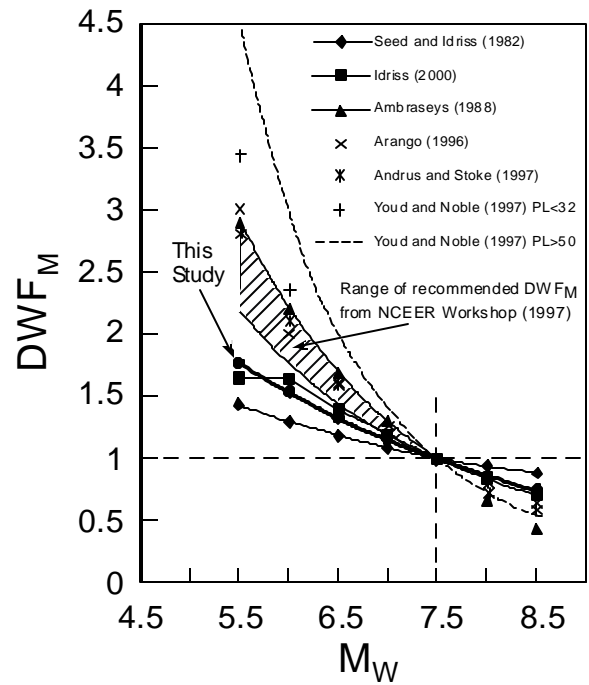


**Fig. 12: Previous Recommendations for Magnitude-Correlated Duration Weighting Factor, with Recommendations from Current Studies**

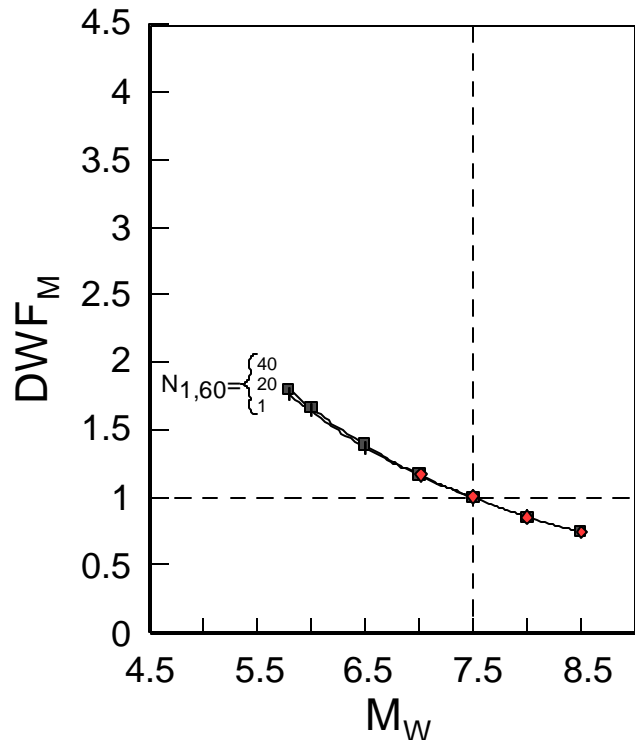


**Fig. 13: Recommended Magnitude-Correlated Duration Weighting Factor as a Function of  $N_{1,60}$**

### 3.1.5 Adjustments for Effective Overburden Stress:

An additional factor not directly resolved in prior studies based on field case histories is the increased susceptibility of soils to cyclic liquefaction, at the same CSR, with increases in effective overburden stress. This is in addition to the normalization of N-values for overburden effects as per Equation 4.

The additional effects of reduction of normalized liquefaction resistance with increased effective initial overburden stress ( $\sigma'_v$ ) has been demonstrated by means of laboratory testing, and this is a manifestation of “critical state” type of behavior (soils become less dilatant at increased effective stress). Figure 14 shows the recommendations of the NCEER Working Group (Youd et al., 2001) regarding the correction factor  $K_\sigma$  to be used to correct to the normalized resistance to liquefaction at an initial effective overburden stress of 1 atm. ( $CSR_{liq,1atm}$ ) as

$$CSR_{liq} = CSR_{liq,1atm} \cdot K_\sigma \quad (\text{Eq. 9})$$

These current studies were not very sensitive to  $K_\sigma$ , as the range of  $\sigma'_v$  in the case history data base was largely between  $\sigma'_v = 600$  to  $2,600$  lb/ft<sup>2</sup>, but it was possible to “regress”  $K_\sigma$  as part of the Bayesian updating. The results are shown in Figure 15, over the range of  $\sigma'_v = 600$  to  $3,600$  lb/ft<sup>2</sup> for which they

are considered valid. These are in good agreement with the earlier recommendations of Figure 14, and it is recommended that  $K_\sigma$  can be estimated as

$$K_\sigma = (\sigma'_v)^{f-1} \quad (\text{Eq. 10})$$

where  $f \approx 0.6$  to  $0.8$  (as  $N_{1,60,cs}$  varies from 1 to 40 blows/ft.) The field case history data of these current studies are not a sufficient basis for extrapolation of  $K_\sigma$  to much higher values of  $\sigma'_v$ , and the authors recommend use of Figure 14 for  $\sigma'_v > 2$  atm.

The earlier relationships proposed by Seed et al. (1984), Liao et al. (1988, 1998), Youd and Noble (1997), and Toprak et al. (1999) were all stated to be normalized to an effective overburden stress of approximately  $\sigma'_v = 1$  atm (2,000 lb/ft<sup>2</sup>). The correlation of Seed et al. (1984) was never formally corrected to  $\sigma'_v = 1$  atm., however, as it was noted that the field case histories of the database were “shallow”, and approximately in this range. The database was, however, not centered at  $\sigma'_v = 1$  atm., but rather at lesser overburden (Mean  $\sigma'_v = 1,300$  lb/ft<sup>2</sup> or 0.65 atm), and this proves to render this earlier relationship slightly unconservative if taken as normalized to  $\sigma'_v = 1$  atm. (The same is true of all of the previous relationships discussed.) It should be noted, however, that this unconservatism is minimized if the correlations are applied at shallow depths.

$$P_L(N_{1,60}, CSR, M_w, s'_v, FC) = \Phi \left[ \frac{\left( N_{1,60} \cdot (1 + 0.004 \cdot FC) - 13.32 \cdot \ln(CSR) - 29.53 \cdot \ln(M_w) - 3.70 \cdot \ln(s'_v) + 0.05 \cdot FC + 44.97 \right)}{2.70} \right] \quad (\text{Eq. 11})$$

where

$P_L$  = the probability of liquefaction in decimals (i.e. 0.3, 0.4, etc.), and

$\Phi$  = the standard cumulative normal distribution.

Also the cyclic resistance ratio, CRR, for a given probability of liquefaction can be expressed as:

$$CRR(N_{1,60}, CSR, M_w, s'_v, FC, P_L) = \exp \left[ \frac{\left( N_{1,60} \cdot (1 + 0.004 \cdot FC) - 29.53 \cdot \ln(M_w) - 3.70 \cdot \ln(s'_v) + 0.05 \cdot FC + 44.97 + 2.70 \cdot \Phi^{-1}(P_L) \right)}{13.32} \right] \quad (\text{Eq. 12})$$

where

$\Phi^{-1}(P_L)$  = the inverse of the standard cumulative normal distribution (i.e. mean=0, and standard deviation=1)

note: for spreadsheet purposes, the command in Microsoft Excel for this specific function is “NORMINV( $P_L, 0, 1$ )”

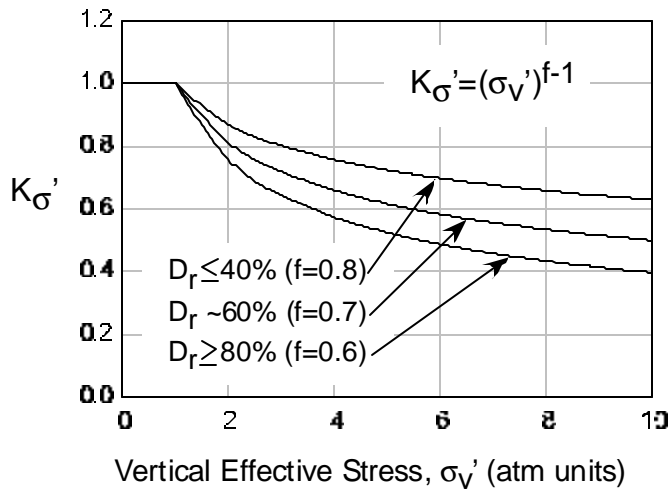


Fig. 14: Recommended  $K_s$  Values for  $s'_v > 2$  atm.

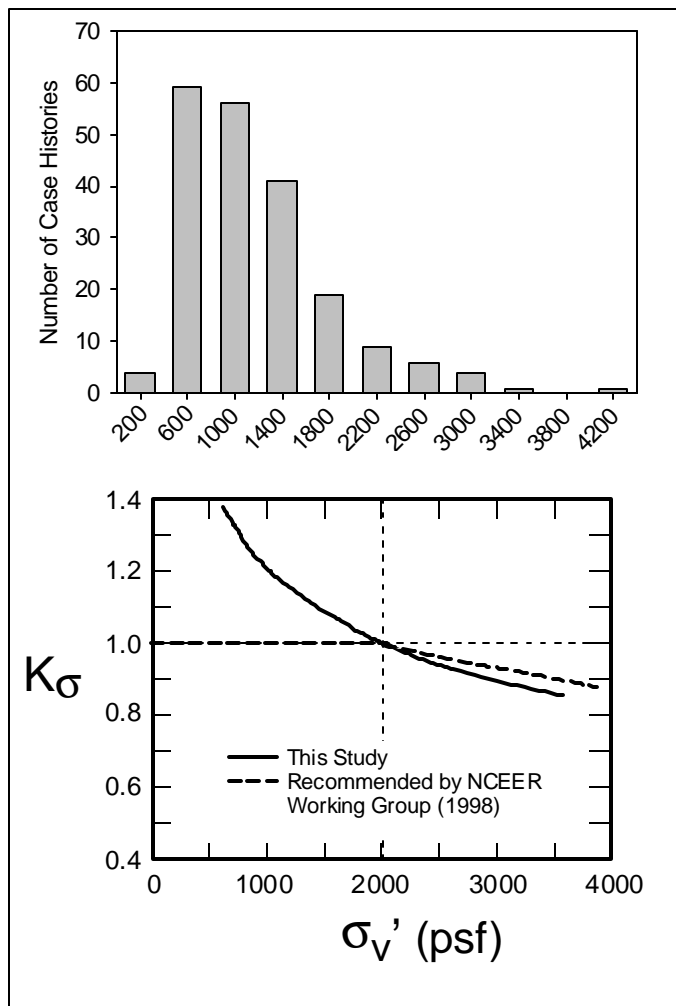


Fig. 15: Values of  $K_s$  Developed and Used in These Studies, NCEER Working Group Recommendations (for  $n=0.7$ ,  $D_R \geq 60\%$ ) for Comparison

For correctness, and to avoid ambiguity, both the earlier relationship of Seed et al. (1984), and the correlations developed in these current studies, need to be formally normalized to  $\sigma'_v = 1$  atm. Accordingly, in these present studies, all data are corrected for  $K_\sigma$ -effects (by Equations 9 and 10); not just those data for which  $\sigma'_v$  was greater than 1 atm. A recommended limit is  $K_\sigma \leq 1.5$  (at very shallow depths.) Figures 16 and 17 show the proposed new correlations, this time for  $\sigma'_v = 1$  atm, and these figures represent the final, fully normalized recommended correlations.

The overall correlation can be expressed in parts, as in the previous sections (and Equations 6 - 12, and Figures 7 - 17). It can also be expressed concisely as a single, composite relationship as shown in Equation 11.

*Recommended Use of the New SPT-Based Correlations:*

The proposed new probabilistic correlations can be used in either of two ways. They can be used directly, all at once, as summarized in Equations 11 and 12. Alternatively, they can be used “in parts” as has been conventional for most previous, similar methods. To do this, measured  $N$  values must be corrected to  $N_{1,60}$ -values, using Equations 3, 4 and 5. The resulting  $N_{1,60}$ -values must then be further corrected for fines content to  $N_{1,60,cs}$ -values, using Equations 6 and 7 (or Figure 17). Similarly, in-situ equivalent uniform cyclic stress ratio ( $CSR_{eq}$ ) must be evaluated, and this must then be adjusted by the magnitude-correlated Duration Weighting Factor ( $DWF_M$ ) using Equation 8 (and Figure 13) as

$$CSR_N = CSR_{eq,M=7.5} = CSR_{eq} / DWF_M \quad (\text{Eq. 13})$$

The new  $CSR_{eq,M=7.5}$  must then be further adjusted for effective overburden stress by the inverse of Equation 9, as

$$CSR^* = CSR_{eq,M=7.5,1atm} = CSR_{eq,M=7.5} / K_\sigma \quad (\text{Eq. 14})$$

The resulting, fully adjusted and normalized values of  $N_{1,60,cs}$  and  $CSR_{eq,M=7.5,1atm}$  can then be used, with Figure 16, to assess probability of initiation of liquefaction.

For “deterministic” evaluation of liquefaction resistance, largely compatible with the intent of the earlier relationship proposed by Seed et al. (1984), the same steps can be undertaken (except for the fines adjustment) to assess the fully adjusted and normalized  $CSR_{eq,M=7.5,1atm}$  values, and normalized  $N_{1,60}$  values, and these can then be used in conjunction with the recommended “deterministic” relationship presented in Figure 17. The recommendations of Figure 17 correspond to the new probabilistic relationships (for  $R_L = 15\%$ , except at very high  $CSR$  ( $CSR > 0.4$ )). At these very high  $CSR$ ; (a) there is virtually no conclusive field data, and (b) the very dense soils ( $N_{1,60} \geq 30$  blows/ft) of the boundary region are strongly dilatant and have only very limited post-liquefaction strain potential. Behavior in this region is thus not conducive to large liquefaction-related

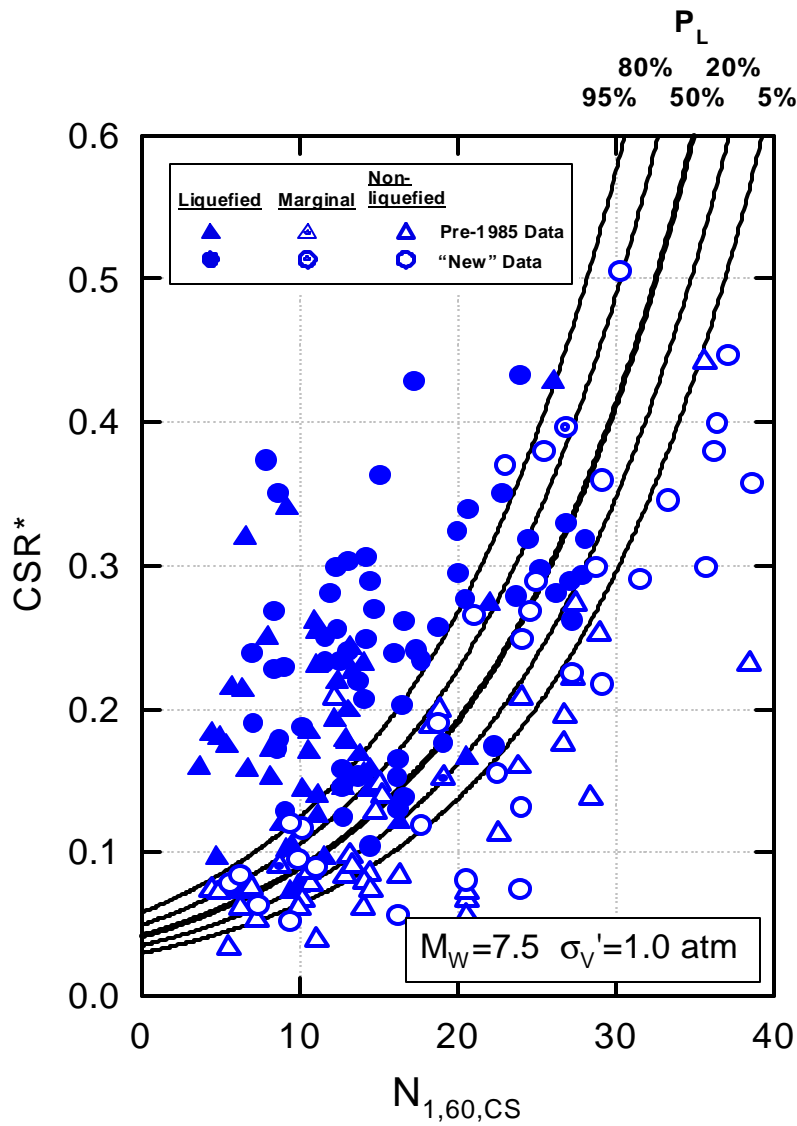


Fig. 16: Recommended “Probabilistic” SPT-Based Liquefaction Triggering Correlation (For  $M_W=7.5$  and  $\sigma_v'=1.0$  atm)

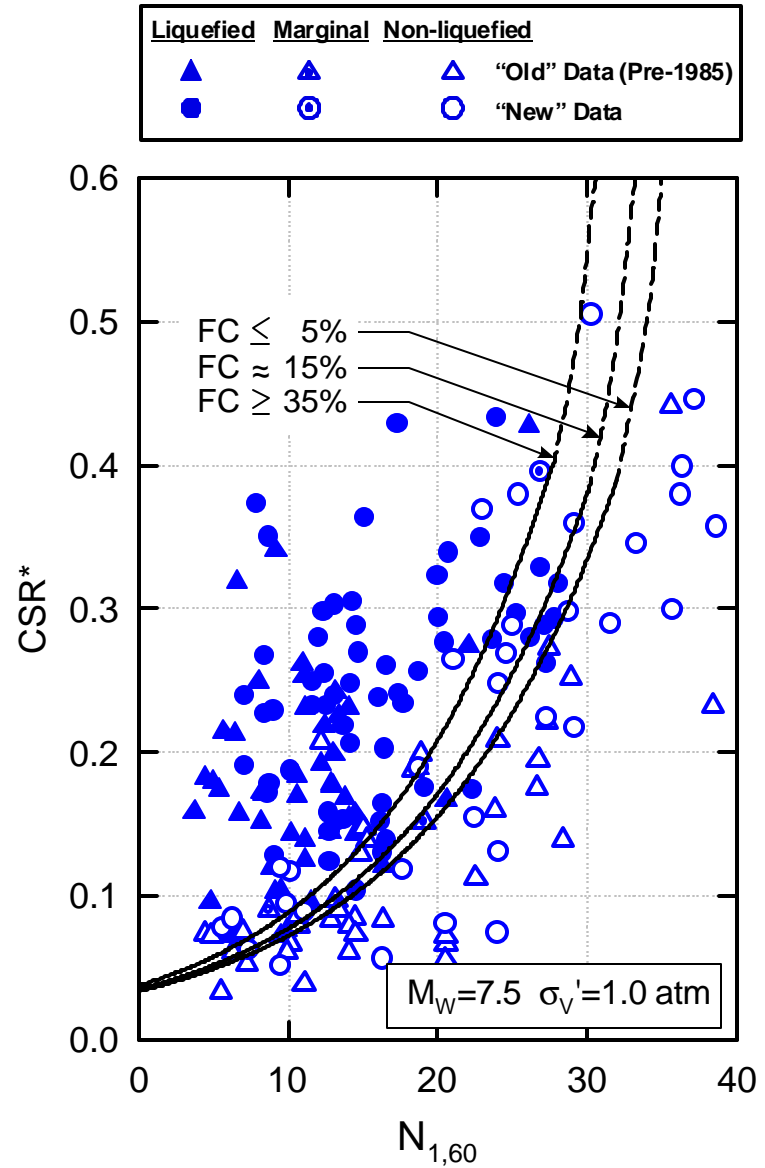


Fig. 17: Recommended “Deterministic” SPT-Based Liquefaction Triggering Correlation (For  $M_W=7.5$  and  $\sigma_v'=1.0$  atm) with Adjustments for Fines Content Shown

displacements, and the heavy dashed lines shown in the upper portion of Figure 17 represent the authors' recommendations in this region based on data available at this time.

### 3.1.7 Summary

This section of this paper has presented the development of recommended new probabilistic and "deterministic" relationships for assessment of likelihood of initiation of liquefaction. Stochastic models for assessment of seismic soil liquefaction initiation risk have been developed within a Bayesian framework. In the course of developing the proposed stochastic models, the relevant uncertainties including: (a) measurement/estimation errors, (b) model imperfection, (c) statistical uncertainty, and (d) those arising from inherent variability were addressed.

The resulting models provide a significantly improved basis for engineering assessment of the likelihood of liquefaction initiation, relative to previously available models, as shown in Figure 5(d). The new models presented and described in this paper deal explicitly with the issues of (1) fines content (FC), (2) magnitude-correlated duration weighting factors ( $DWF_M$ ), and (3) effective overburden stress ( $K_\sigma$  effects), and they provide both (1) an unbiased basis for evaluation of liquefaction initiation hazard, and (2) significantly reduced overall model uncertainty. Indeed, model uncertainty is now reduced sufficiently that overall uncertainty in application of these new correlations to field problems is now driven strongly by the difficulties/uncertainties associated with project-specific engineering assessment of the necessary "loading" and "resistance" variables, rather than uncertainty associated with the correlations themselves. This, in turn, allows/encourages the devotion of attention and resources to improved evaluation of these project-specific parameters. As illustrated in Figures 6(d), 16 and 17, this represents a significant overall improvement in our ability to accurately and reliably assess liquefaction hazard.

The new correlations also eliminate a bias intrinsic in all prior, similar relationships when using actual dynamic response analyses to directly calculate in-situ CSR, as all prior relationships were based on an unconservatively biased "simplified" ( $r_d$ -based) assessment of CSR. This was not a major problem when using these previous correlations in conjunction with the same  $r_d$  for "forward" engineering analyses, but it was a problem when using prior correlations in conjunction with direct calculation of in-situ CSR. The new correlations are unbiased in this regard, and can be used either in conjunction with "simplified" CSR assessments (based on the new  $r_d$  recommendations presented herein), or in conjunction with direct dynamic response analyses for calculation of in-situ CSR. The new correlations cannot, however, be used in conjunction with assessment of CSR based on the "old" (Seed and Idriss, 1971)  $r_d$  relationship.

## 3.2 CPT-Based Triggering Correlations:

### 3.2.1 Introduction

In addition to SPT, three other in-situ index tests are now sufficiently advanced as to represent suitable bases for correlation with soil liquefaction triggering potential, and these are (a) the cone penetration test (CPT), (b) in-situ shear wave velocity measurement ( $V_s$ ), and (c) the Becker Penetration Test (BPT).

Up to this point in time, the SPT-based correlations have been better defined, and have provided lesser levels of uncertainty, than these other three methods. CPT, however, is approaching near parity, and newly developed CPT-based correlations now represent nearly co-equal status with regard to accuracy and reliability relative to SPT-based correlations.

CPT-based correlations have, to date, been based on much less numerous and less well defined earthquake field case histories than SPT-based correlations. This is changing, however, as a number of research teams are working on development of improved CPT-based "triggering" correlations. This includes the authors of this paper, and the next sections will present a much-improved basis for CPT-based assessment of liquefaction initiation (or "triggering") potential.

It is important to develop high quality CPT-based correlations to complement and augment the new SPT-based correlations presented herein. The authors are often asked whether SPT or CPT is intrinsically a better test for liquefaction potential evaluation. The best answer is that both tests are far better when used together, as each offers significant advantages not available with the other.

SPT-based correlations are currently ahead of "existing" CPT-based correlations, due in large part to enhanced data bases and better data processing and correlation development. The new SPT-based correlations described in this paper are currently more accurate and reliable, and provide much lower levels of uncertainty or variance. An additional very significant advantage of SPT is that a sample is retrieved with each test, and so can be examined and evaluated to ascertain with certainty the character (gradation, fines content, PI, etc.) of the soils tested, as contrasted with CPT where soil character must be "inferred" based on cone tip and sleeve friction resistance data.

The CPT offers advantages with regard to cost and efficiency (as no borehole is required). A second advantage is consistency, as variability between equipment and operators is small (in contrast to SPT). The most important advantage of CPT, however, is continuity of data over depth. SPT can only be performed in 18-inch increments, and it is necessary to advance and clean out the borehole between tests. Accordingly, SPT can only be performed at vertical spacings of about 30 inches (75cm) or more. As a result, SPT can completely miss thin (but potentially important) liquefiable strata between test depths. Similarly, with a 12-inch test

height and allowance for effects of softer overlying and underlying strata, SPT can fail to suitably characterize strata less than about 3 to 4 feet in thickness.

CPT, in contrast, is fully continuous and so “misses” nothing. The need to penetrate about 4 to 5 diameters into a stratum to develop full tip resistance, to be at least 4 to 5 diameters from an underlying softer stratum, and the “drag length” of the following sleeve, cause the CPT test to poorly characterize strata of less than about 12 to 15 inches (30 to 40cm) in thickness, but this allows for good characterization of much thinner strata than SPT. Even for strata too thin to be adequately (quantifiably) characterized, the CPT at least provides some indications of potentially problematic materials if one examines the  $q_c$  and  $f_s$  traces carefully.

### 3.2.2 Existing CPT-Based Correlations

Owing to its attractive form and simplicity, as well as its endorsement by the NCEER Working Group, the CPT-based correlation of Robertson and Wride (1998) is increasingly used for liquefaction studies. This correlation is well described in the NCEER summary papers (NCEER, 1997; Youd, et al., 2001).

Robertson and Wride had access to a much smaller field case history database than is currently available, and so their correlation represents a valuable interim contribution as development of new correlations taking advantage of the wealth of new earthquake field case history data now available now proceeds.

Figure 18 shows the “baseline” triggering curve of Robertson and Wride for “clean” sandy soils. Adjustments for fines are based on combinations of sleeve friction ratios and tip resistances in such a manner that the “clean sand” boundary curve of Figure 18 is adjusted based on a composite parameter  $I_C$ .  $I_C$  is a measure of the distance (the radius) from a point above and to the left of the plot of normalized tip resistance ( $q_{c,1}$ ) and normalized Friction Ratio (F) as indicated in Figure 19. Tip resistance is corrected for increasing fines content and plasticity as

$$q_{c,1,mod} = q_{c,1} \cdot K_C \quad (\text{Eq. 15})$$

The recommended “fines” correction is a nonlinear function of  $I_C$ , and ranges from a multiplicative factor of  $K_C = 1.0$  at  $I_C = 1.64$ , to a maximum value of  $K_C = 3.5$  at  $I_C = 2.60$ . A further recommendation on the fines correction factor is that this factor be set at  $K_C = 1.0$  in the shaded zone within Area “A” of Figure 19 (within which  $1.64 < I_C < 2.36$ , and friction ratio  $F < 0.5$ ).

Based on cross-comparison with the new SPT-based correlation, it appears that the CPT-based correlation of Robertson and Wride is slightly unconservative for clean sands, especially at high CSR, and that it is very unconservative for soils of increasing fines content and

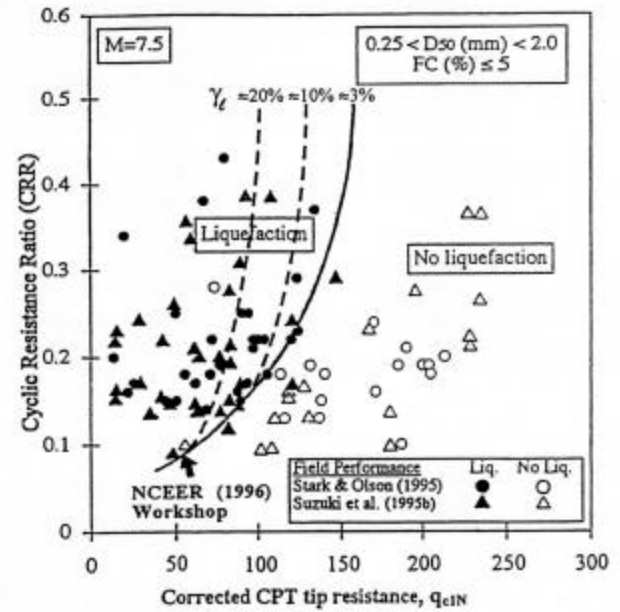
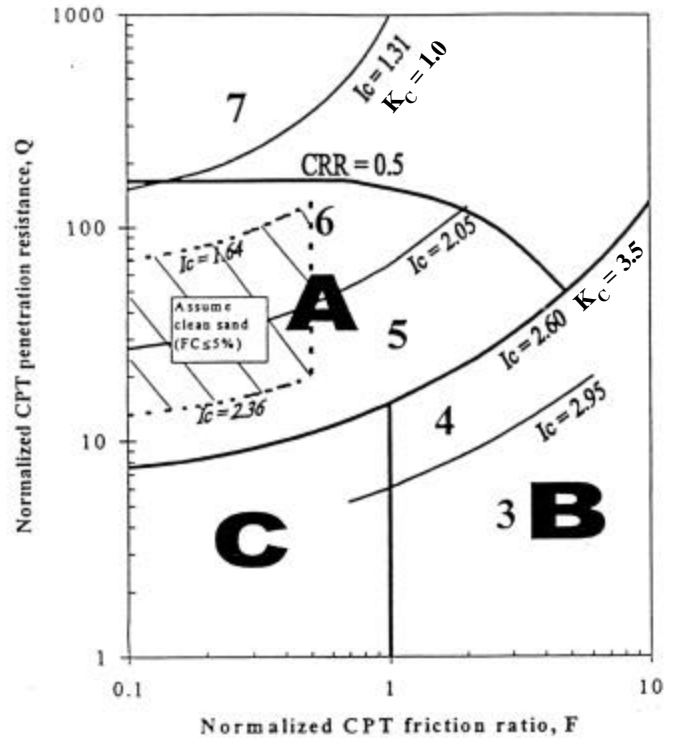


Fig. 18: CPT-Based Liquefaction Triggering Correlation for “Clean” Sands Proposed by Robertson and Wride (1998)



Zone A: Cyclic liquefaction possible – depends on size and duration of cyclic loading  
 Zone B: Liquefaction unlikely – check other criteria  
 Zone C: Flow/cyclic liquefaction possible – depends on soil plasticity and sensitivity as well as size and duration of cyclic loading.

Fig. 19: Fines Correction as Proposed by Robertson and Wride (1998)

plasticity. This, as it turns out, is verified by comparison with the new CPT-based correlations presented and described in the section that follows.

Additional researchers have been and are continuing to develop CPT-based correlations, but rather than discuss all of these we will, instead, present a recommended new CPT-based correlation with many of the attributes and strengths of the new SPT-based correlation presented previously.

### 3.3 Recommended New CPT-Based Triggering Correlation:

#### 3.3.1 Introduction

The approach followed in development of the new CPT-based correlation presented herein was similar in many ways to that followed in development of the SPT-based correlation presented previously. As a result, the new CPT-based relationship shares many of the same strengths.

Key elements in the development of this new correlation were: (1) accumulation of a significantly expanded database of field performance case histories, (2) use of improved knowledge and understanding of factors affecting interpretation of CPT data, (3) incorporation of improved understanding of factors affecting site-specific ground motions (including directivity effects, site-specific response, etc.), (4) use of improved methods for assessment of in-situ cyclic shear stress ratio (CSR), (5) screening of field data case histories on a quality/uncertainty basis, and (6) use of higher-order probabilistic tools (Bayesian Updating). Once again, detailed review of the processing and back-analyses of the field performance case histories by a group of leading experts, and establishment of consensus (or at least near-consensus) regarding all resulting critical parameters and variables, is a key feature of this effort.

These new correlations are not yet quite complete, as iterative review of some of the case history interpretations is still underway. The correlations are far enough along that they are nearly final, however, and as they already incorporate far more data (and of higher overall quality) than previous correlations, they represent a significant advance. The resulting relationships not only provide greatly reduced levels of uncertainty, they also help to resolve a number of corollary issues that have long been difficult and controversial, including: (1) adjustments for fines content, and (2) corrections for effective overburden stress.

#### 3.3.2 Improved Treatment of Normalization of CPT Tip and Sleeve Resistance for Effective Overburden Stress

In development of optimally improved CPT-based correlations, it was desirable to go after each of the issues that have historically contributed to the uncertainty (or variance) of previous correlations. One particularly significant issue was

the approach used to normalize CPT tip resistance ( $q_c$ ) and sleeve resistance ( $f_s$ ) for effective overburden stress effects.

Approaches have differed significantly here. Olsen and Mitchell (1995) presented the most comprehensive set of recommendations in this regard, and their recommendations (along with their recommended approximate soil classification scheme) are presented in Figure 20. This figure's axes (normalized CPT tip resistance  $q_{c,1}$  on the vertical axis, and sleeve friction ratio  $R_f$  on the horizontal axis) will provide a useful template for much of the rest of this section. [Friction Ratio is taken as  $R_f = f_s/q_c \cdot 100$ .]

In these current studies, a suite of four different cavity expansion models, each used for the soil type and density ( $D_R$ ) or overconsolidation ratio (OCR) range for which it is best suited, were used to study variation of CPT tip resistances with changes in effective overburden stress ( $\sigma'_v$ ). The model of Salgado & Randolph (2001) was used for dense (dilatant) cohesionless soils. The model of Boulanger (2003) was used for very high overburden stress conditions for the same dense (dilatant) cohesionless soils. The model of Yu (2000) with Ladanyi and Johnston (1974) was used for loose to medium dense cohesionless soils. The model of Cao et al. (2001) was used for overconsolidated cohesive (clayey) soils and the model of Yu (2000) was used for normally consolidated cohesive (clayey) soils. Each of these models was both constrained and calibrated using significant bodies of laboratory calibration chamber test data. The results of these laboratory and analytically based methods were then augmented using actual field data regarding variation of tip resistance vs. effective overburden stress. Details of all analyses, as well as field data summaries, will be presented in Moss (2003). The combined data was then judgmentally interpreted, and used to develop recommendations for normalization of CPT tip resistance to develop normalized  $q_{c,1}$  values as

$$q_{c,1} = C_q \cdot q_c \quad \text{where} \quad C_q = \left( \frac{P_a}{\mathbf{S}'_v} \right)^c \quad (\text{Eq. 16})$$

The normalization exponent (c) is a function of both normalized tip resistance and friction ratio ( $R_f$ ) as shown in Figure 21. Also shown, for purposes of comparison, are the earlier recommendations of Olsen and Mitchell (1995).

Cavity expansion models are not able to provide insight regarding similar normalization of sleeve friction ( $f_s$ ) for effective overburden stress effects, so a more approximate assessment was made, based largely on laboratory calibration chamber test data and field data, to develop similar corrections for sleeve resistance as,

$$f_{s,1} = C_f \cdot f_s \quad \text{where} \quad C_f = \left( \frac{P_a}{\mathbf{S}'_v} \right)^s \quad (\text{Eq. 17})$$

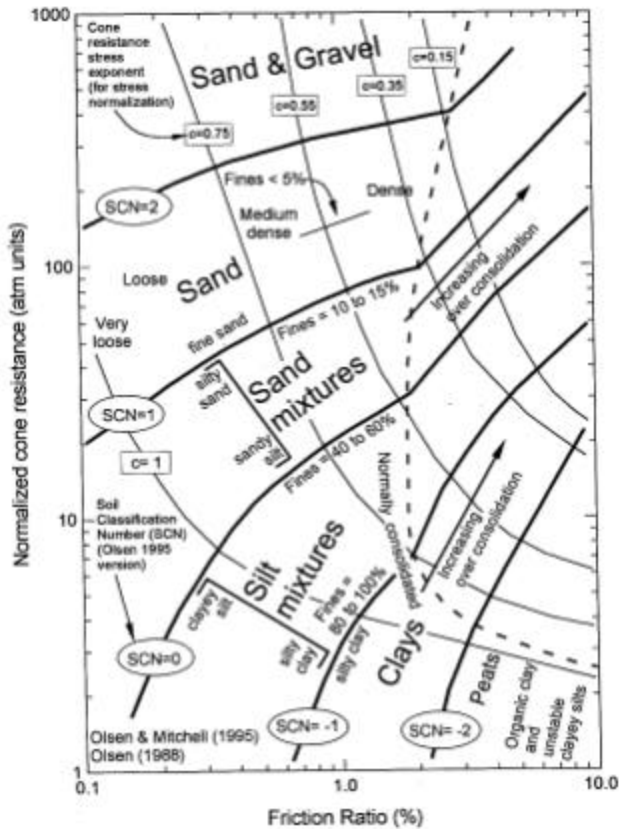


**Fig. 20: Recommended CPT Tip Normalization Exponents, and Approximate Soil Characterization Framework (After Olsen & Mitchell, 1995)**

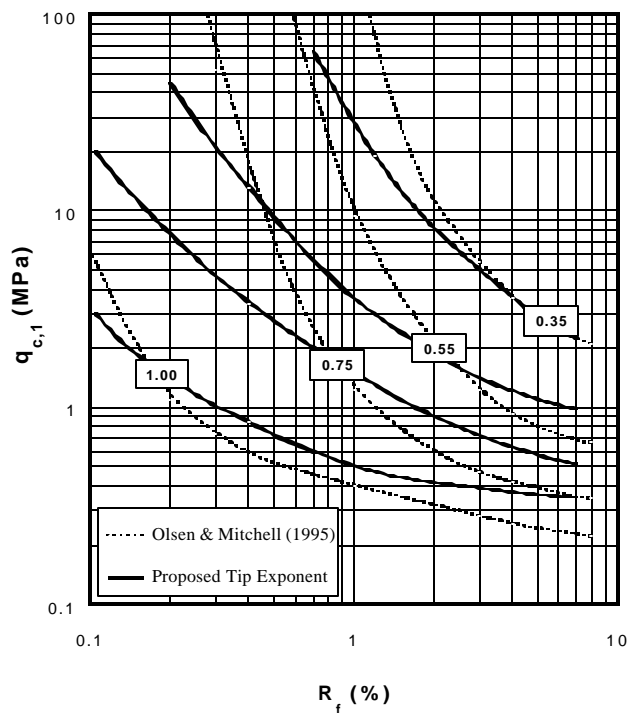


**Fig. 21: Recommended CPT Tip Normalization Exponents, and Previous Recommendations of Olsen & Mitchell (1995)**

The recommended normalization exponent (s) is shown, as a function of normalized tip resistance and friction ratio, in Figure 22, along with the recommended tip normalization exponents (c) from Figure 21.

Figure 22 thus shows the recommended normalization for both tip and sleeve resistances. These are not identical to each

other, but it should be noted that they appear to be sufficiently similar that “normalized” friction ratio  $[R_{f,1} = (f_{s,1} / q_{c,1}) * 100]$  is very similar to non-normalized friction ratio  $[R_f = (f_s / q_c) * 100]$ . Limited iteration is necessary to make the recommended adjustment of  $q_c$  to  $q_{c,1}$ , because  $R_f$  and  $R_{f,1}$  vary only slightly.

### 3.3.3 Thin Layer Corrections

A second source of potential uncertainty is the adjustment of measured CPT tip resistances for finite stiff layers. The effects of initial penetration into a stronger (e.g., less cohesive, potentially liquefiable) layer prior to achieving sufficient penetration into the layer to develop a “fully developed” tip resistance can result in a reduced tip resistance reading, with a similar reduction occurring as the cone approaches and exits the bottom of a stronger layer (“sensing” the approach of the softer underlying layer before actually reaching it).

Several approaches have been proposed for adjustment of measured tip resistances in “thin” layers (e.g.; Robertson and

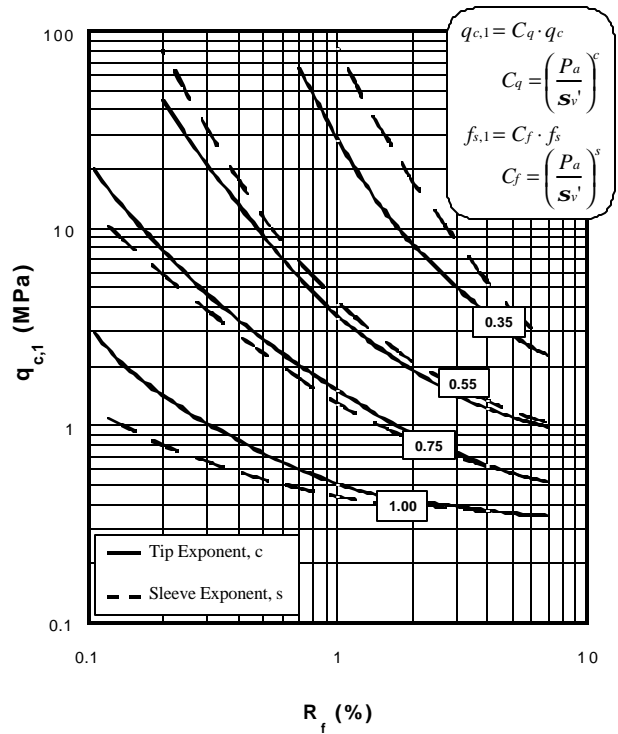


**Fig. 22: Recommended CPT Tip and Sleeve Normalization Exponents**

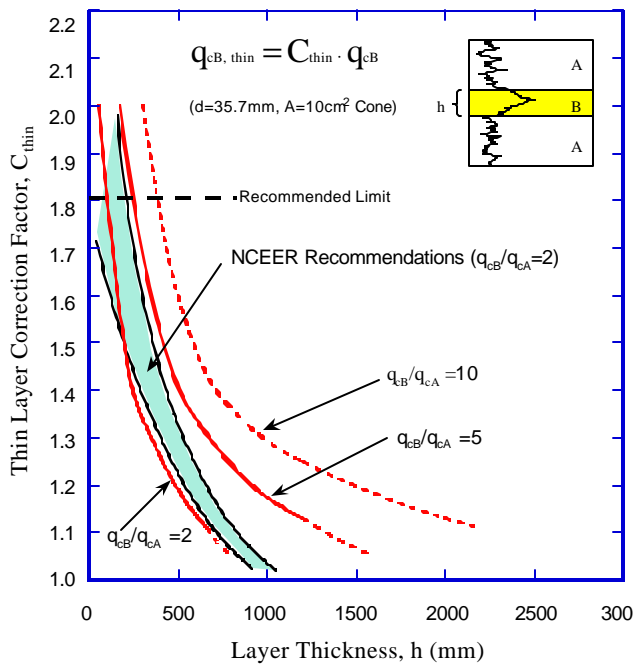


**Fig 23: Recommended Thin Layer Correction for CPT Tip Resistance, and Earlier NCEER Working Group Recommendations**

Wride, 1997; Youd et al., 2001). In this current effort, the elastic solution for “thin layer effects” proposed by Vreugdenhil et al. (1995) was calibrated against both available laboratory calibration chamber test data as well as field data (Moss, 2003), and the resulting recommended correction of CPT tip resistances for thin layer effects is presented in Figure 23. Also shown, for comparison, are the earlier recommendations of the NCEER Working Group (Youd et al., 2001). The new recommendations are largely compatible with the NCEER Working Group’s recommendations, but serve to extend the approach to higher contrasts in measured tip resistances between the (stiffer) “thin” layer and the (softer) overlying and underlying layers. In this procedure, the ratio of the final, corrected CPT tip resistance in the “thin” layer ( $q_{cA}$ ), relative to the average tip resistance of the softer overlying and underlying layers ( $q_{cB}$ ) serves as a proxy for the ratio of the stiffnesses of these layers. It should be noted that field cases with ratios of  $q_{cB}/q_{cA}$  of greater than about 5 are relatively uncommon.

The correction of CPT tip resistances for “thin layer effects” is then

$$q_{cB,corrected} = q_{cB,thin} = C_{thin} \cdot q_{cB} \quad (\text{Eq. 18})$$

where  $C_{thin}$  is as shown in Figure 23.

Given the intrinsic uncertainty involved in this type of “thin layer” adjustment, it is recommended that adjustment factors ( $C_{thin}$ ) of greater than 1.8 not be used for engineering

applications. A more severe limit was employed in back analyses of field case histories for liquefaction correlation development. Only a small number of cases incorporated in development of the final correlations required any thin layer adjustments, and none required an adjustment factor of greater than 1.5.

### 3.3.4 Field Performance Case Histories

A total of more than 600 field performance case histories were acquired and evaluated as a part of these studies. Some of these had been used by previous researchers in similar efforts, but many are new. This is, to date, the largest set of CPT-based field cases assessed for purposes of development of liquefaction triggering hazard correlations. The cases considered were from the 1964 Niigata (Japan), 1968 Inangahua (New Zealand), 1975 Haicheng (China), 1976 Tangshan (China), 1977 Vrancea (Romania), 1978 Izu-Oshima-Kinkai (Japan), 1979 Imperial Valley (USA), 1980 Mexicali (Mexico), 1981 Westmorland (USA), 1983 Borah Peak (USA), 1983 Nihonkai-Chubu (Japan), 1987 Edgecumbe (New Zealand), 1989 Loma Prieta (USA), 1994 Northridge (USA), 1995 Hyogoken-Nambu (Japan), 1995 Dinar (Turkey), 1999 Kocaeli (Turkey), 1999 Duzce (Turkey), and 1999 Chi-Chi (Taiwan) Earthquakes.

Length constraints do not permit a full treatment of the details involved in back-analyses and processing of these case histories, but evaluation methods used were similar to those employed by Cetin (2000) and Seed et al. (2003) for SPT-based studies. At each site, only the single most critical stratum was considered. Cyclic stress ratios (CSR) were evaluated using the recently proposed  $r_d$  relationships by Cetin and Seed (2000), except in cases where site-specific site response analyses could be performed. These new  $r_d$  relationships represent an improved basis for estimation of CSR, and are statistically unbiased with respect to site-specific response analyses. It should be noted that the earlier  $r_d$  recommendations of Seed and Idriss (1971) cannot be used with the new correlations proposed herein, as these earlier  $r_d$  recommendations provide generally higher estimates of CSR than do site-specific response analyses (or the new  $r_d$  recommendations of Cetin et al.) for strong levels of shaking, and are thus not compatible with the new correlations proposed herein.

For each field case history, the variances or uncertainties in both the critical loading and in-situ soil and index parameters were evaluated, and the cases were systematically rated for overall quality on the basis of uncertainty of key parameters. Only the most highly rated cases were then used for development of the new correlations; cases of lesser quality (with unacceptably high uncertainty or poorly defined parameters) were deleted from further consideration. At this time, a total of 201 cases were selected for incorporation in the correlations presented herein. This is the largest number of high quality cases (based on unusually high screening standards) used to date in development of these types of CPT-

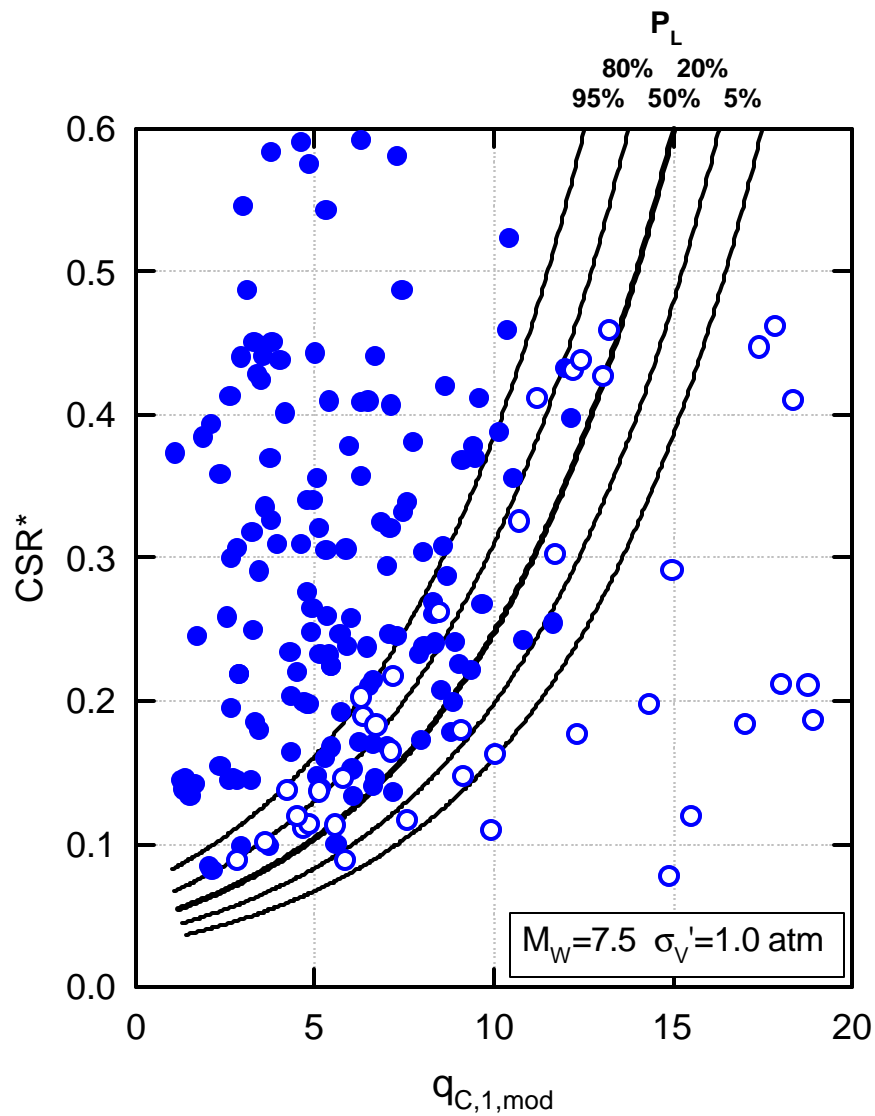


Fig. 24: Contours of 5%, 20%, 50%, 80% and 95% Probability of Liquefaction as a Function of Equivalent Uniform Cyclic Stress Ratio and Fines-Modified CPT Tip Resistance ( $M_w = 7.5$ ,  $\sigma'_v = 1\text{atm.}$ )

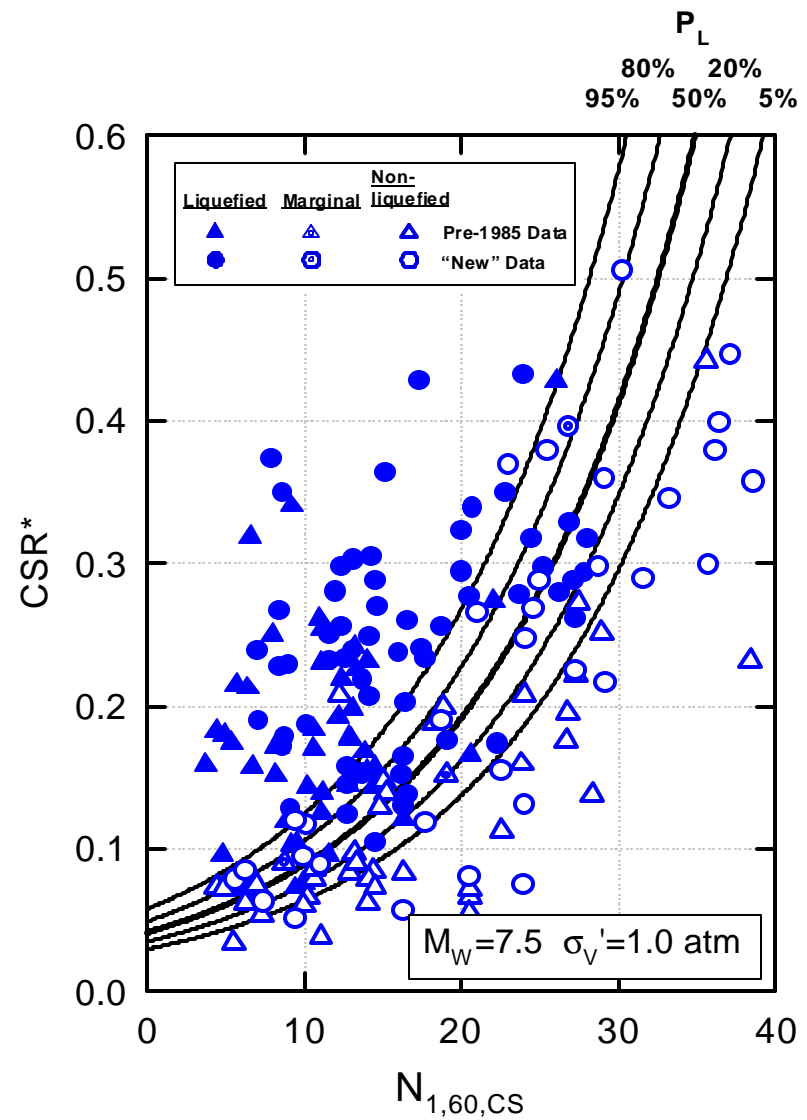


Fig. 25: Contours of 5%, 20%, 50%, 80% and 95% Probability of Liquefaction for  $\dot{q}' = 1\text{ atm.}$  and Duration Associated with  $M_w = 7.5$  As a Function of Fines Corrected SPT Penetration Resistance (Seed et al., 2001)

based correlations. As with the largely parallel SPT-based efforts, the back-analyses, processing, and selection of these cases was subjected to iterative review by an accomplished group of international experts with excellent prior experience in this area, in order to establish consensus evaluations of critical parameters.

### 3.3.5 Correlation Development

Length constraints again do not permit a full discussion of all details involved in development of the new recommended CPT-based probabilistic soil liquefaction triggering correlations. The details are largely parallel to those described by Cetin (2000) and Seed et al. (2001) in development of SPT-based correlations. A Bayesian updating methodology was employed to develop probabilistic correlations. This is essentially a high order probabilistic regression method well suited to this problem, and capable of dealing with the various types of contributing sources of aleatory and epistemic uncertainty involved. A discussion of development of a (similar) Bayesian treatment of the SPT-based correlations was presented by Cetin et al. (2002).

Figure 24 presents one view of the new recommended correlation, in this case a plot of contours of probability of liquefaction (for  $P_L = 5\%, 20\%, 50\%, 80\%$  and  $95\%$ ) as a function of equivalent uniform cyclic stress ratio (CSR<sub>eq</sub>) and modified normalized CPT tip resistance ( $q_{c,1,mod}$ ). In this figure, equivalent uniform CSR has been corrected for duration effects based on the magnitude-correlated duration weighting factor (DWF<sub>M</sub>) proposed in Seed et al. (2001) for SPT-based correlations, as the regression for this CPT-based correlation resulted in essentially equivalent magnitude-correlated duration scaling. This results in an expression of the correlation appropriate for events of  $M_w = 7.5$ . The correlation in Figure 24 is also normalized to an effective overburden stress of  $\sigma'_v = 1$ atmosphere.

In Figure 24, the solid dots represent the centroids of probabilistic distributions of the individual case histories for cases wherein liquefaction was judged to have been “triggered”, and open circles represent centroids of distributions of field cases wherein liquefaction did not occur. These distributions quantify each individual field case history and its distributed variance in both the horizontal and vertical axes. The CPT tip resistances of Figure 24 are adjusted for effects of fines (fines content and plasticity) to values of  $q_{c,1,mod}$  as described subsequently.

Figure 25, presented adjacent to Figure 24 for comparison purposes, represents a similar view of the corollary new recommended SPT-based relationship, also with contours for probabilities of liquefaction of  $P_L = 5\%, 20\%, 50\%, 80\%$  and  $95\%$ , also normalized for  $M_w = 7.5$ ,  $\sigma'_v = 1$ atm., and with  $N$  values corrected for fines content to  $N_{1,60,cs}$ .

The horizontal axis of Figure 24 represents modification of normalized CPT tip resistances ( $q_{c,1}$  values) for the frictional

effects of apparent fines content and character. Values of  $q_{c,1}$  are adjusted as

$$q_{c,1,mod} = q_{c,1} + \ddot{A}q_c \quad (\text{Eq. 19})$$

where  $\ddot{A}q_c$  is a function of  $q_{c,1}$ ,  $R_f$  and  $c$ , as shown in Figure 26. Figure 27 repeats the recommended fines adjustment of Figure 26, and also shows for comparison the “fines correction” factors recommended by Robertson and Wride (1997). Robertson and Wride recommended adjustment by a multiplicative factor ( $K_C$ ) as presented previously in Equation 15, where  $K_C$  is a function of both tip resistance and friction ratio as shown in Figure 27. Robertson and Wride also recommended, however, that  $K_C$  be taken as 1.0 (a null adjustment of  $q_{c,1}$ ) in the shaded region of Figure 27. It is interesting to note that the new recommended correction contours for fines content and character proposed herein also reflect a null adjustment in this shaded zone, yet provide a smoother variation of the adjustment ( $\ddot{A}q_c$ ) as it transitions to other areas of Figure 27. (The Robertson and Wride recommendations jump very sharply at the base and right edge of the shaded “null correction” zone.) The new contours also provide for much smaller overall adjustments of  $q_{c,1}$  for fines content and character than did the earlier curves proposed by Robertson and Wride, suggesting that these earlier recommendations were unconservative at high fines contents.

Figure 28 presents an alternate view of the new correlation, in this case contours of 15% probability of liquefaction triggering, but for three different values of  $\ddot{A}q_c$  spanning the full available range of  $\ddot{A}q_c$ .  $P_L = 15\%$  represents the new recommended “deterministic” threshold, analogous to the “deterministic” recommendations of most prior relationships. The adjacent Figure 29 similarly presents a view of the new SPT-based correlation, with 15% probability of liquefaction contours shown for three different levels of percent fines (fines content) spanning the full available range of fines corrections for the SPT-based relationship. The similarity between the relationships shown in Figures 28 and 29 is both interesting and important, as it represents strong mutual support between the new proposed SPT- and CPT-based correlations.

Finally, Figure 30 provides a comparison between the new proposed CPT-based correlation, and the previous correlations proposed by Robertson and Wride (1997) and Suzuki et al. (1995). The new correlation is represented in this figure by contours of 15% probability of liquefaction, as that is the level of probability recommended by the authors herein for use as a reasonable “deterministic” threshold. The correlations of Robertson and Wride, and Suzuki et al., are “deterministic” correlations, as they do not explicitly address probability (or uncertainty).

As shown in Figure 30, the “clean sand” ( $\ddot{A}q_c = 0$ ) line for the new correlation falls between the similarly based “clean sand” ( $R_f < 0.5\%$ ) line proposed by Suzuki et al., and the “clean sand” ( $K_C = 1.0$ ) line proposed by Robertson and Wride. The range of fines-corrected lines for the new correlation,

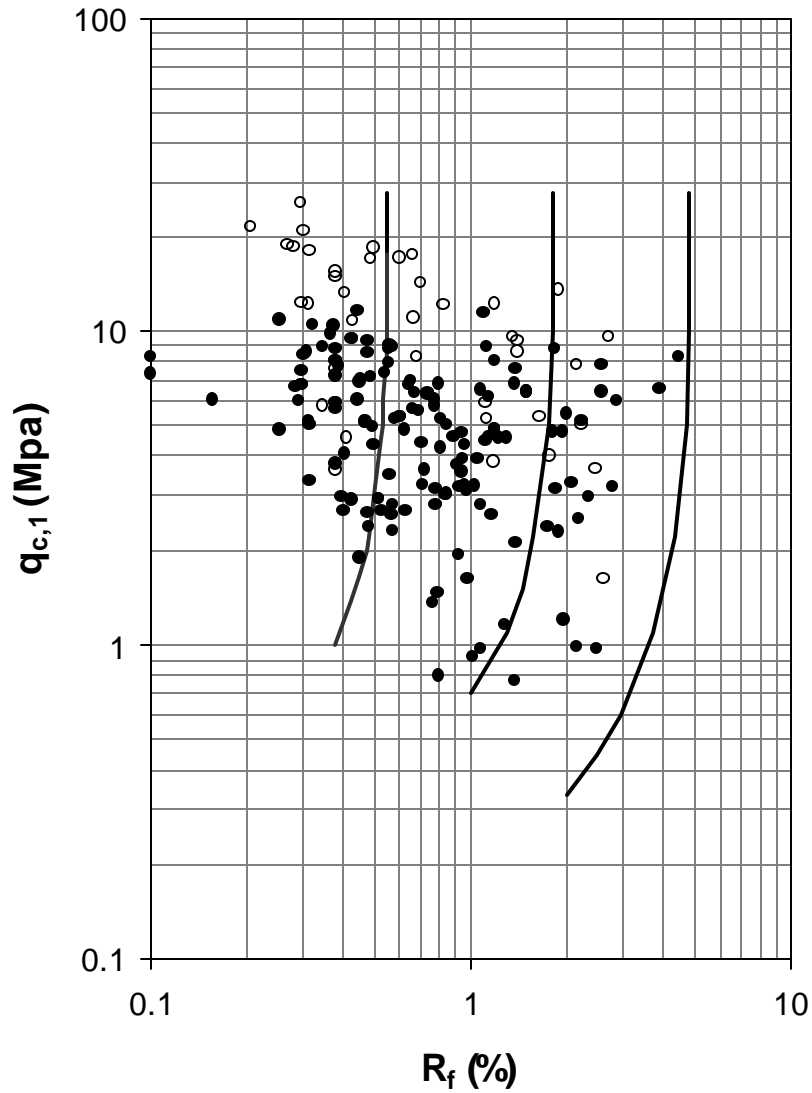


Fig 26: Recommended CPT Tip Resistance Modification for “Fines Content and Character” as a Function of  $q_{c,1}$  and  $R_f$

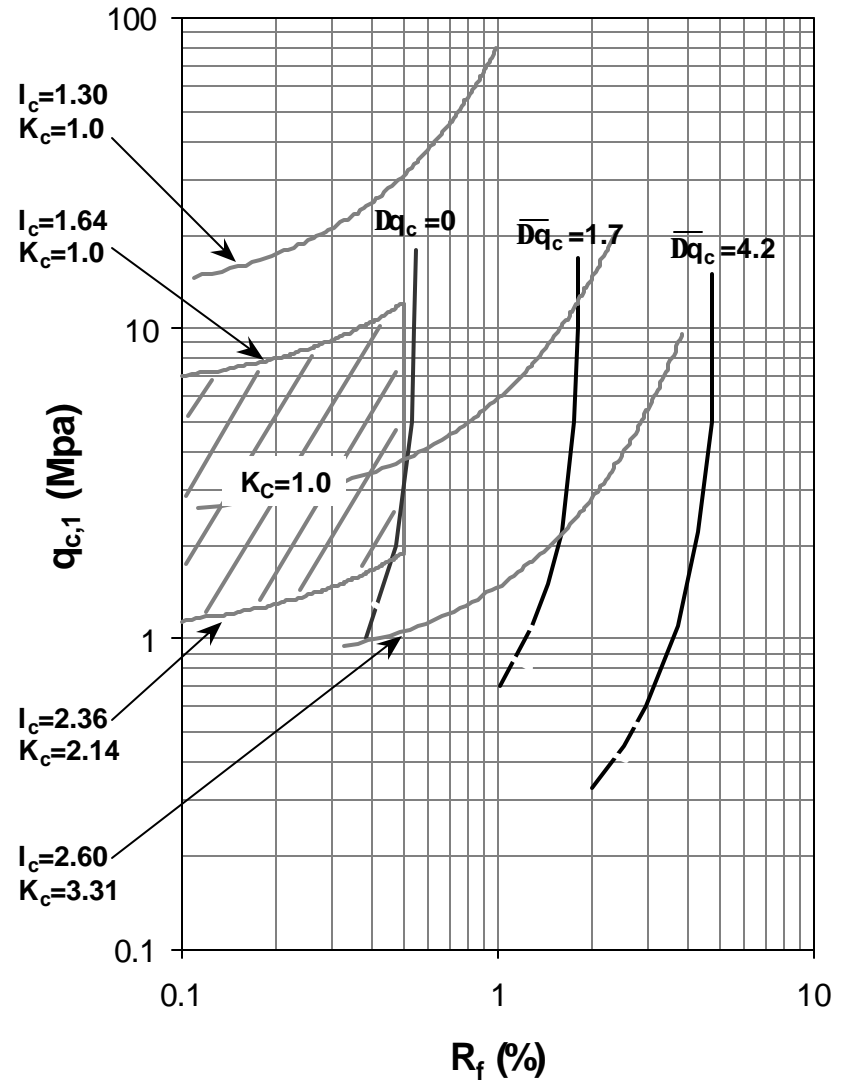


Fig 27: Recommended CPT Tip Resistance Modification for “Fines Content and Character” as a Function of  $q_{c,1}$  and  $R_f$ , Compared with the Earlier Recommendations of Robertson and Wride (1997)

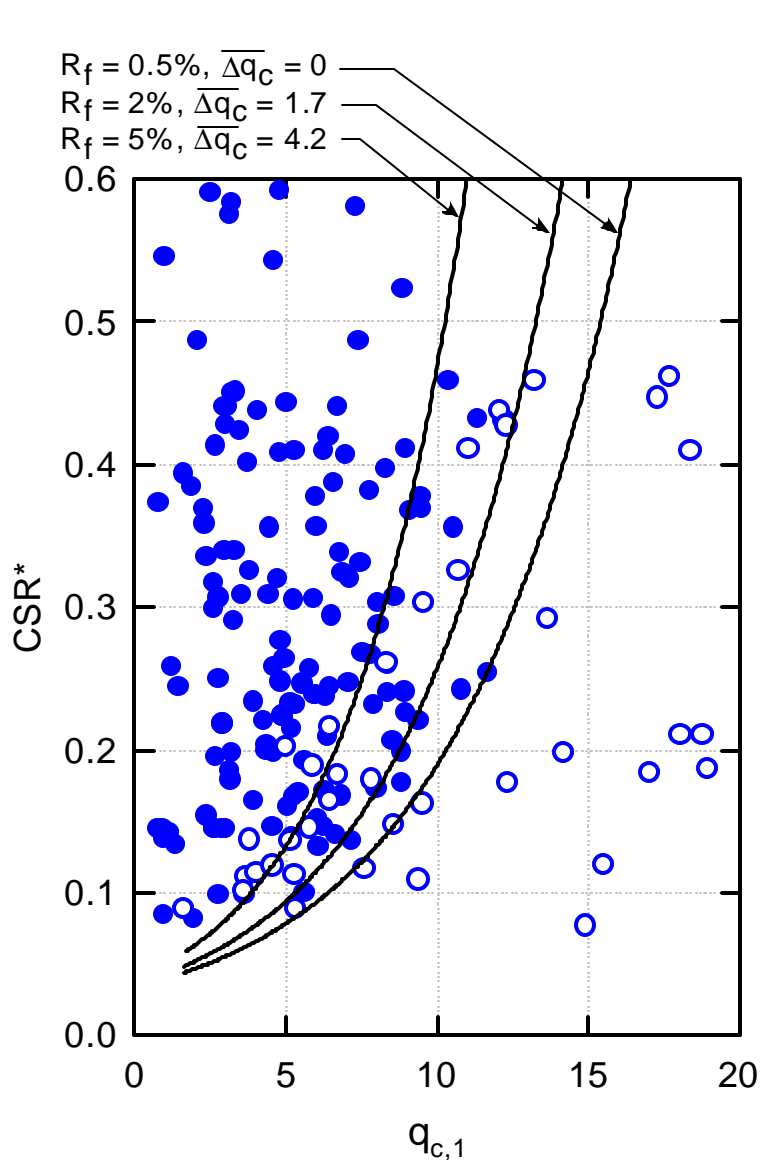


Fig. 28: Contours of 15% Probability of Triggering of Liquefaction for “Clean Sands” and Two Higher Levels of Required Fines Adjustment of CPT Tip Resistance (Spanning the Full Range of Fines Adjustments)

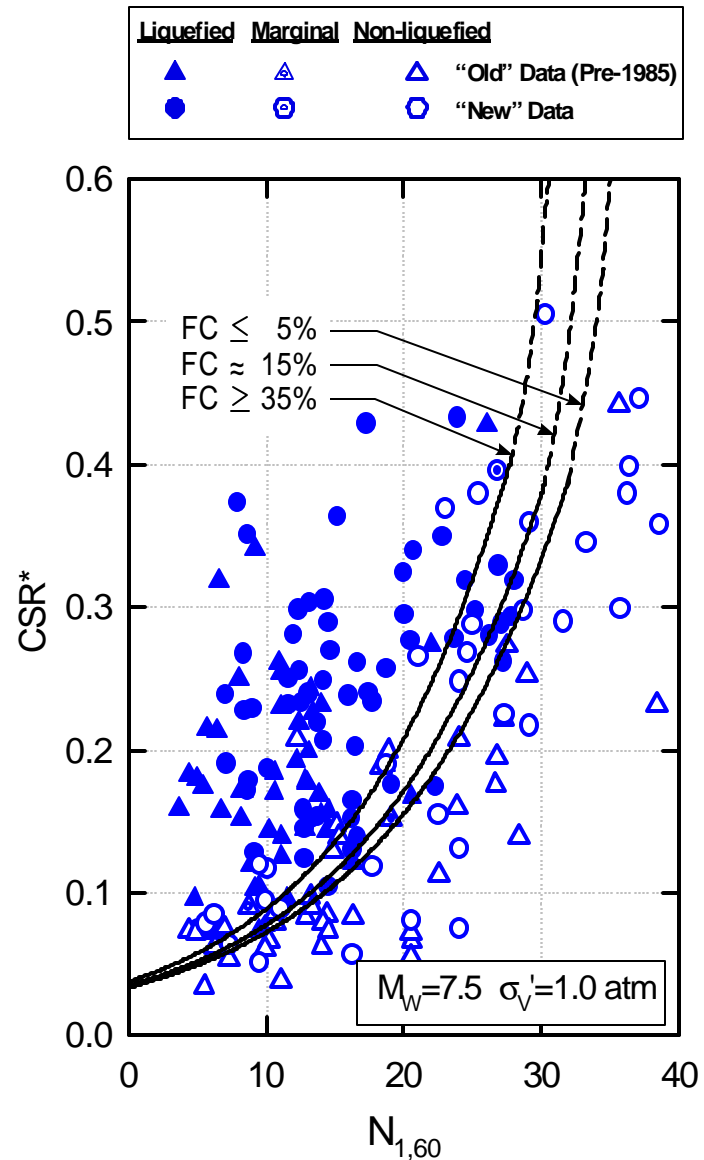
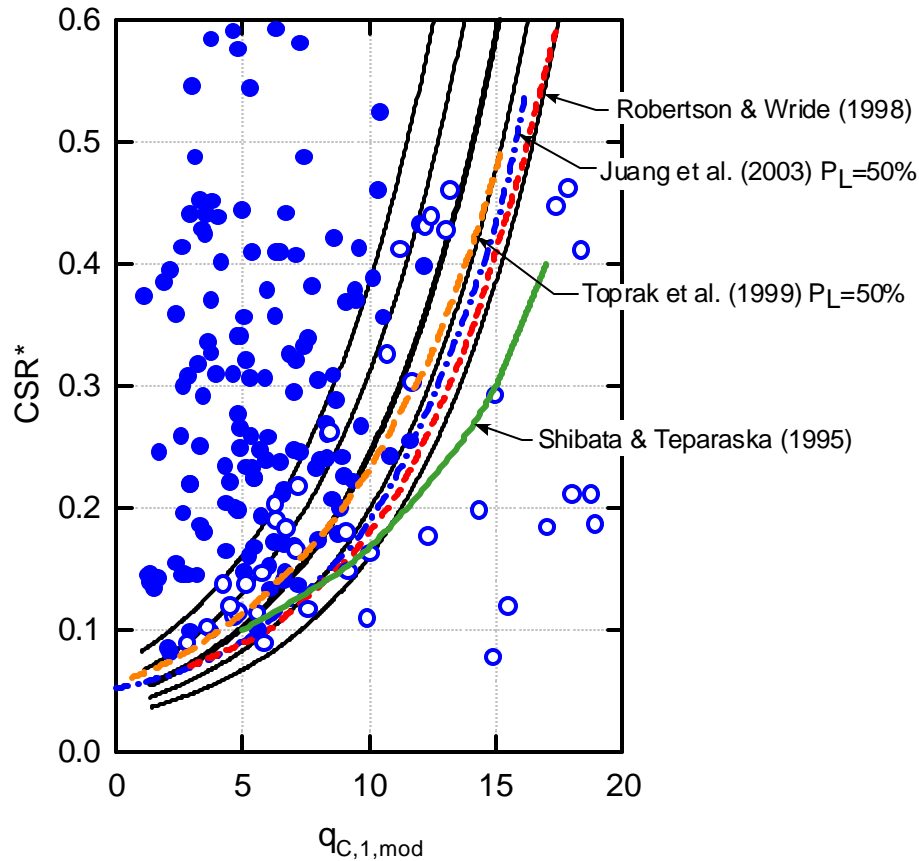


Fig. 29: Contours of 15% Probability of Triggering of Liquefaction for “Clean Sands” and Two Higher Levels of Required “Fines Correction” of SPT N-values (Spanning the Full Range of Fines Corrections) (Seed et al., 2001)



**Fig. 30: Comparison Between the Recommended New CPT-Based Correlation and Previous “Clean Sand” Boundary Curves from Relationships Proposed by Shibata and Teparaska (1995), Robertson and Wride (1998), Toprak et al. (1999), and Juang et al. (2003) ( $M_w=7.5$ ,  $s_v'=1$  atm.)**

however, represent much smaller adjustments for fines than the relationship proposed by Robertson and Wride, suggesting that the fines adjustment of the older relationship was unconservative. The fines adjustment proposed by Suzuki et al. (1995) was also smaller than that proposed previously by Robertson and Wride, but did not extend to high friction sleeve ratios ( $R_f > 1.0$ ).

### 3.3.6 Summary and Conclusions

The new CPT-based correlation presented herein represents a significant advance over previously available CPT-based correlations for assessment of seismically induced soil liquefaction hazard. These correlations are probabilistically posed, and a “deterministic” correlation based on  $P_L = 15\%$  is also recommended.

The new correlations employ a much larger database of high quality field performance case histories than was available to previous researchers, and the processing of these cases involved resolution of issues that had historically added to overall uncertainty including (1) normalization of CPT tip and sleeve resistances for effective overburden stress effects, and (2) development of improved “thin layer” corrections.

Overall, the new correlations are in very good overall agreement with previous, similar CPT-based efforts with regard to “clean sands”. The earlier “clean sand” liquefaction boundary curve proposed by Robertson and Wride (1997) is only slightly unconservative relative to the new relationship, and the “clean sand” boundary curve proposed by Suzuki et al. (1995) is slightly more conservative than the recommended new relationship.

It is principally when dealing with silt and silty, sandy, clayey soils that the new correlations differ significantly from earlier and widely used CPT-based correlations. The new relationships reflect a much smaller adjustment (increase) in modified CPT tip resistance ( $q_{c,1,mod}$ ) as apparent fines content and plasticity increase than the earlier relationship of Robertson and Wride (1997), suggesting that the earlier relationship can be significantly unconservative for these soils. The fines adjustment of Suzuki et al. (1995) is in closer agreement with the new relationship proposed, but does not extend to high friction ratios and so is incomplete.

Overall, the new CPT-based relationships appears to be largely compatible with the similarly improved SPT-based relationships proposed by Seed et al. (2001), and the new CPT-based relationship appears to have similar levels (only

marginally higher) of uncertainty (or variance) associated with assessment of liquefaction triggering potential as the new SPT-based relationship. This does not mean that the SPT-based relationships are intrinsically “better”; the use of CPT offers important advantages with regard to continuity of penetration data, and also the ability to discern and characterize thinner strata, than SPT (while the SPT offers increased certainty as to soil type and character, especially invariably stratified soils.) Accordingly, both methods have significant relative advantages, and both are likely to be of continued significant value to working engineers.

### 3.4 $V_S$ -Based Triggering Correlations:

Liquefaction triggering correlations based on measurements of in situ shear wave velocity ( $V_S$ -based correlations) are very attractive because: (1)  $V_S$  can be measured with non-intrusive methods (e.g. Spectral Analysis of Surface Waves (SASW)), and (2)  $V_S$  can be measured in coarse soils (gravelly soils and coarser) in which SPT and CPT can be obstructed by interference with coarse soil particles.  $V_S$ -based correlations can provide both a potentially rapid screening method, and a method for assessment of coarse, gravelly soils which cannot be reliably penetrated or reliably characterized with small diameter penetrometers (SPT and CPT).

At this time, the best  $V_S$ -based correlation available is that of Andrus and Stokoe (2000). Figure 32 presents the core of this correlation, which is based on overburden stress-corrected  $V_{S,1}$  vs. magnitude-correlated equivalent uniform CSR. This  $V_S$ -based correlation is well described in the NCEER Workshop summary papers (NCEER, 1997; Youd et al., 2001.) Although it is certainly the best of its type, this correlation is less well-defined (more approximate) than either SPT- or CPT-based correlations. This is not due only to lack of data (though the  $V_S$ -based field case history database is considerably smaller than that available for SPT and CPT correlation development). It is also because  $V_S$  does not correlate as reliably with liquefaction resistance as does penetration resistance because  $V_S$  is a very small-strain measurement and correlates poorly with a much “larger-strain” phenomenon (liquefaction). Small amounts of “ageing” and cementation of interparticle contacts can cause  $V_S$  to increase more rapidly than the corollary increase in liquefaction resistance. Accordingly, the relationship between  $V_S$  and the CSR required to induce liquefaction varies significantly with the geologic age of the deposits in question. An additional problem with  $V_S$ -based correlations is uncertainty regarding appropriate normalization of  $V_S$  for effects of effective overburden stress. In view of these uncertainties, current  $V_S$ -based correlations for resistance to

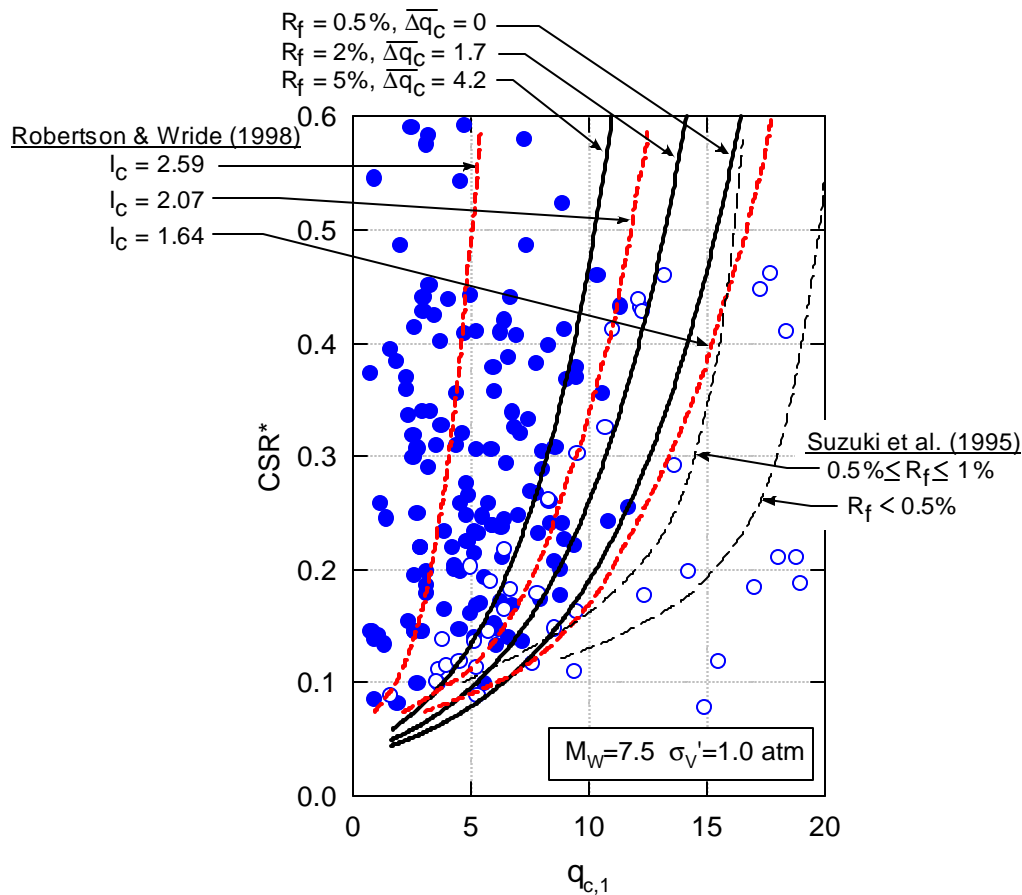


**Fig. 31: Comparison Between the Recommended New CPT-Based Correlation and Previous Relationships Proposed by Suzuki et al. (1995) and Robertson and Wride (1998)**

[ $M_w=7.5, \sigma_v'=1 \text{ atm.}$ ]

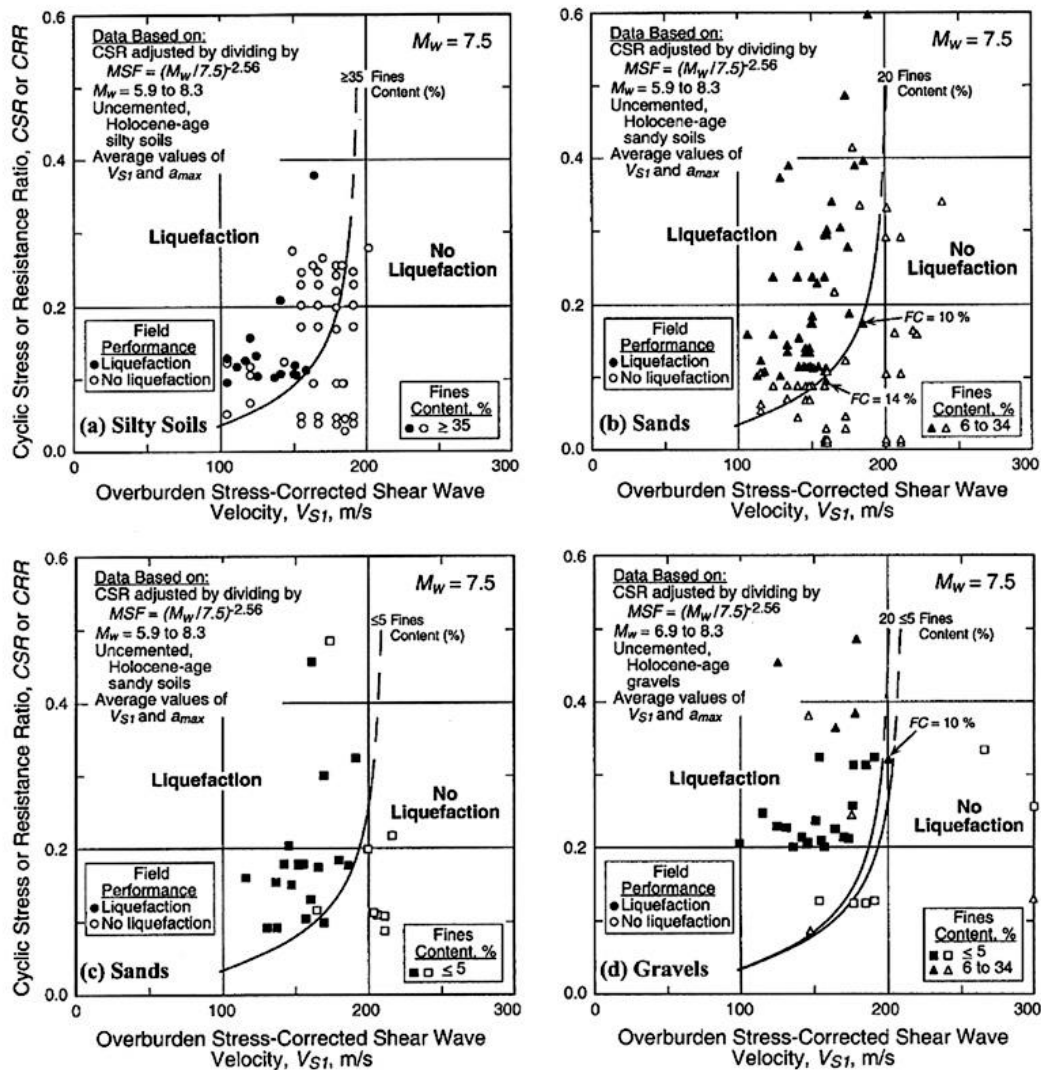


Fig. 32:  $V_s$ -Based Liquefaction Triggering Correlation (Andrus & Stokoe, 2000)

“triggering” of liquefaction are best employed either conservatively, or as preliminary (and approximate) screening tools to be supplemented by other methods.

Efforts are underway to improve the resolution and reliability of  $V_s$ -based correlations. Dr. Rob Kayen of the U.S. Geological Survey recently spent a year travelling through Asia and making  $V_s$  measurements (by means of SASW) at many of the field performance case history sites employed in the new SPT- and CPT-based correlations. This augments recent  $V_s$  measurements at U.S. case history sites, and has resulted in a tremendous increase in the number of  $V_s$ -based case histories now available, and at sites where the critical soil stratum can be cross-identified by SPT- and/or CPT-based methods. This new data, along with previously available  $V_s$ -based data, is currently being processed and back-analyzed, and new  $V_s$ -based correlations are under development using these data (using largely the same types of procedures as those used to develop the new SPT- and CPT-based correlations.)

In the interim, the relationship of Andrus and Stokoe is the best available, and should be used conservatively and with understanding of the considerable uncertainties involved.

### 3.5 Evaluation of Liquefaction Potential in Coarse, Gravelly Soils:

Coarse, gravelly soils can be especially problematic with regard to evaluation of resistance to “triggering” of liquefaction, as large particles (gravel-sized and larger) can impede the penetration of both SPT and CPT penetrometers. As large-scale frozen sampling and testing are too expensive for conventional projects, engineers faced with the problem of coarse, gravelly soils generally have three options available here.

One option is to employ  $V_s$ -based correlations.  $V_s$  measurements can be made in coarse soils, either with surface methods (e.g. SASW, etc.) or via borings (cross-hole  $V_s$ ,

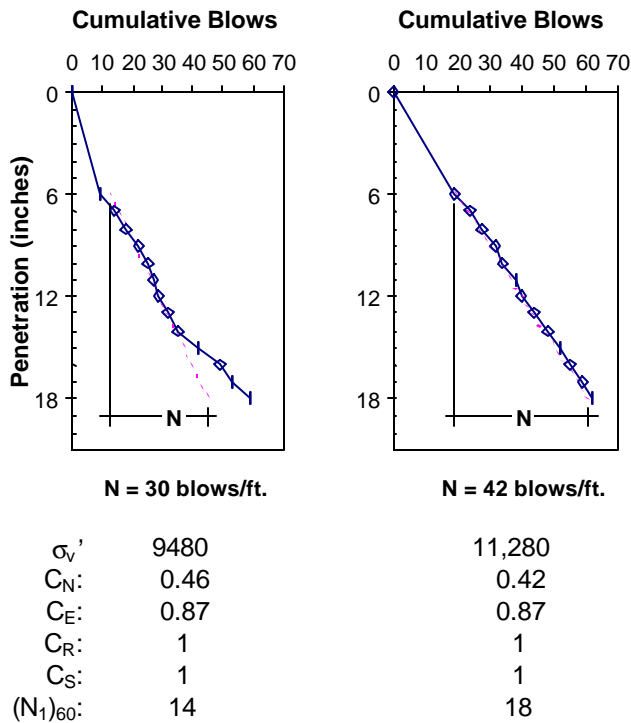


**Fig. 33: Adjustment of Short-Interval SPT for Effects of Coarse Particles**  
(Olivia Chen Consultants, 2003)

down-hole  $V_S$ , or “OYO Method”  $V_S$  (suspension logger). As discussed in the previous section,  $V_S$ -based correlations are somewhat approximate, however, and so should be considered to provide conclusive results only for deposits/strata that are clearly “safe” or clearly likely to liquefy.

### 3.5.1 Short-Interval SPT

A second option is to attempt “short-interval” SPT testing. This can be effective when the non-gravel (finer than about 0.25-inch diameter) fraction of the soil represents greater than about half of the overall soil mix/gradation. (Note that it is approximately the  $D_{30}$  and finer particle size range that controls the liquefaction behavior of such soils.)

Short-interval SPT involves performing the SPT in largely the standard manner, but counting the blow count (penetration resistance) in 1-inch increments rather than 6-inch increments. When penetration is more than 1-inch for a single blow, a fractional blow count of less than 1 blow/inch is credited. The resulting history of penetration (in blows/inch) is then plotted for each successive inch (of the 12-inches of the test). When values (per inch) transition “significantly” from low to high, it is assumed that a coarse particle was encountered and impeded the penetrometer. High values (rapid increases in blowcount) are discarded, and the low values are summed, and then scaled to represent the equivalent number of blows per 12-inches. (e.g.: If it is judged that 7 of the inches of penetration can be

“counted”, but that 5 of the inches must be discarded as unrepresentatively high, then the sum of the blows per the 7 inches is multiplied by 12/7 to derive the estimated overall blow count as blows/12 inches.)

Figure 32 illustrates this approach. This figure shows “correction” of two of the more than 400 SPT performed as part of the investigation of seismic stability of Calaveras Dam in California (Olivia Chen Consultants and Geomatrix Consultants, 2003). Large portions of the embankment dam fill were comprised of hydraulically placed excavated colluvium, and so represented an unusually complex and heterogeneous mix of weathered silty and clayey fines, sands, and variably high fractions of coarse (gravel-sized and coarser) particles.

Figure 32(a) shows an example in which the SPT apparently encountered significantly increased resistance after about the 8<sup>th</sup> inch of the 12-inch interval (neglecting the sacrificial first 6-inch interval which drives to test depth). For this test, the slope of the unimpeded drive was extrapolated to develop the estimated “corrected” blowcount of 30 blows/ft. Figure 32(b) shows the cumulative blowcount for a second SPT at the same site. In this case, the blowcounts increased a bit towards the end of the test, but were judged not to have exhibited a sudden increase, and the blowcount was therefore simply summed over the 12-inch driving interval in the conventional manner. (It should be noted that blowcount can often tend to increase slightly, but not suddenly, as penetration progresses. In these cases, judgement is required as to whether or not to impose a “correction” to the measured full 12-inch blowcount.)

This approach has been shown to correlate well with  $N_{BPT}$  values from the larger-scale Becker Penetrometer for soils with gravel-plus sized fractions of less than about 40 to 50%. It is noted, however, that the corrected short-interval SPT blowcounts can still be biased to the high side due to unnoticed/undetected influence of coarse particles on some of the penetration increments used, so that it can be appropriate to use lower than typical enveloping of the resulting blowcounts to develop estimates of “representative” N-values for a given stratum (e.g.: 25 to 40-percentile values, rather than 35 to 50-percentile values as might have been used with regular SPT in soils without significant coarse particles).

### 3.5.2 The Becker Penetrometer Test

When neither  $V_S$ -based correlations nor short-interval SPT can sufficiently reliably characterize the liquefaction resistance of coarse soils, the third method available for coarse soils is the use of the large-scale Becker Penetrometer. As illustrated schematically in Figure 34, the Becker Penetrometer is essentially a large-diameter steel pipe pile driven by a diesel pile hammer (while retrieving cuttings pneumatically up through the hollow pipe.) The Becker Penetrometer Test (BPT) resistance can be correlated with SPT to develop “equivalent” N-values ( $N_{BPT}$ ). Care is required in continually monitoring the performance of the BPT during driving, as corrections must be made for driving hammer bounce chamber

pressures, etc. (see Harder, 1997 and Youd et al., 2001). The best current BPT correlation (with SPT) for purposes of liquefaction engineering applications is described by Harder (1997), NCEER (1997), and Youd et al. (2001), and is presented in Figure 35 (based on energy-corrected BPT resistance.)

BPT has been performed successfully for liquefaction evaluations in soils with maximum particles sizes ( $D_{100}$ ) of up to 1 m. and more, and to depths of up to 80 m. The BPT is a large and very noisy piece of equipment, however, and both cost and site access issues can be problematic.

Another problem with the BPT is the question of “casing friction”. The cross-correlation between BPT resistance and equivalent N-values ( $N_{BPT}$ ) is based largely on relatively shallow data. As the Becker penetrometer drives the pipe “pile” (penetrometer) to progressively greater depths, there is progressively more side wall area available upon which side wall friction and adhesion can act to impede penetration (in addition to the resistance at the penetrating tip.) It is primarily tip resistance that we seek to measure.

Three approaches have been taken to deal with this issue. The simplest is to note that there was at least some casing drag in the data used to establish the correlation between Becker blowcounts and equivalent  $N_{BPT}$ , and then to simply neglect potential casing drag. This involves further noting that casing drag is minimized by driving relatively continuously (without prolonged pauses or breaks) so that the casing does not “set up”.

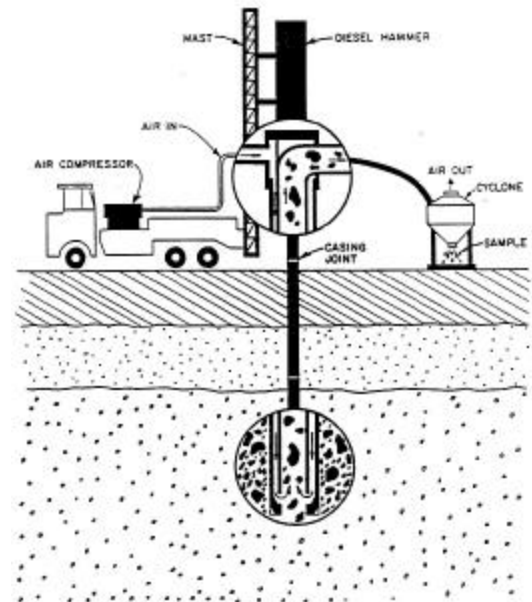


Fig. 34: Schematic Illustration of the Becker Penetrometer (Harder, 1997)

The second approach was proposed by Sy et al. (1997) and involves the use of instrumented driving, and then application of dynamic wave equation analysis (as for regular pile driving) to attempt to analytically separate tip and side wall resistances. This approach suffers the same problem as does dynamic pile driving analysis; the analysis is very sensitive to the “J-factor”

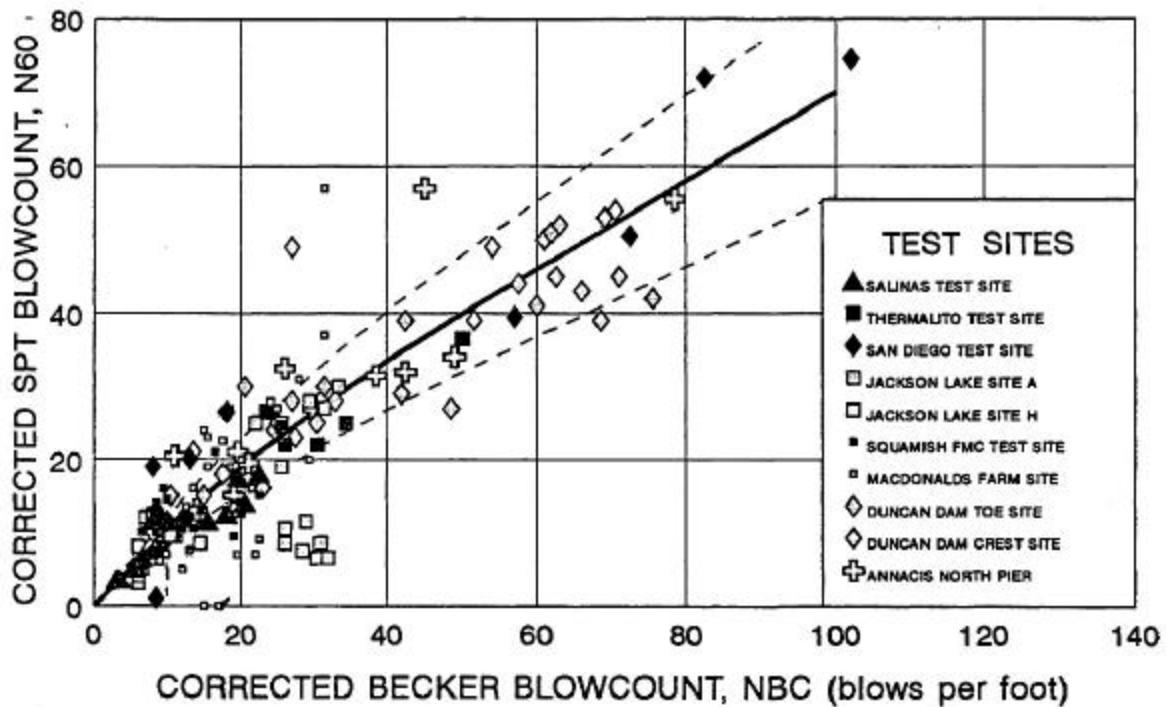
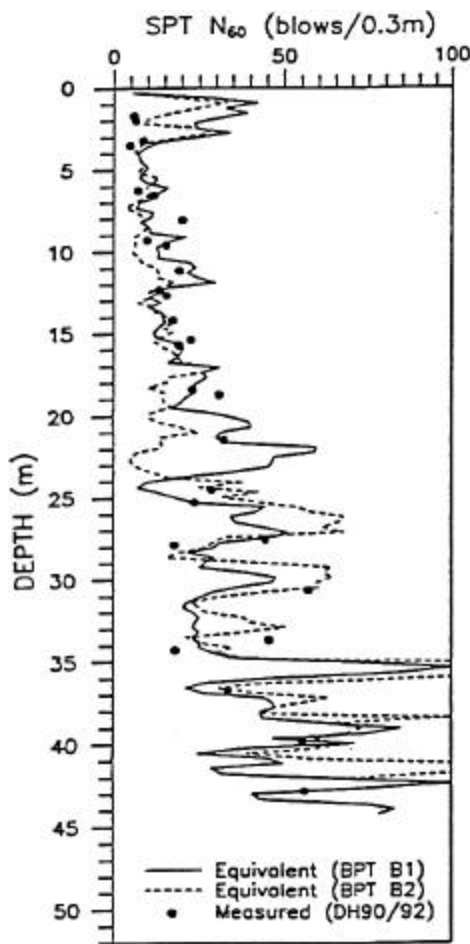


Fig. 35: Cross-correlation Between Becker Penetrometer Blowcounts and Equivalent SPT Blowcounts (Harder, 1997)

used to represent damping along the exterior casing surface, and this factor cannot be readily determined. The result is a volatility in the analysis; high BPT blowcounts can tend to go a bit higher, and low blowcounts can tend to go a bit lower, after correction by this approach.

Figure 36 illustrates typical results. This figure shows BPT resistance vs. depth as measured in a deep glacial till in western Canada. The soil being penetrated is a coarse, gravelly fill underlain by a deep deposit of glacial till. The till is highly variable, but can be generally characterized as very broadly well-graded, with variable fines content and coarser particles ranging up to 1m. and more in size. As shown in this figure, the tip resistance after correction (the solid dots) using the method of Sy et al. ranges both slightly higher and slightly lower than the uncorrected resistance (the solid and dashed lines), and follows approximately the same mean trend.

In view of the uncertainties involved in either neglecting casing drag, or analytical adjustment by dynamic wave equation analysis, a third approach has also been developed. This involves attempting to directly measure “casing drag”, and then correcting BPT driving resistance for this effect.



**Fig. 36: Comparison Between Uncorrected BPT Driving Resistances and Corrected Tip Resistances Based on Dynamic Wave Equation Analysis**

This approach was used in investigations at the Calaveras Dam in California. The Dam was initially constructed mainly by hydraulic placement of colluvial fill, an unusual mix of materials and methods that resulted in unusually complex sub-stratification, and an unusually challenging mix of variable soils ranging from low to very high fines contents, and with coarse, gravelly fractions ranging from a few percent to well over 50%. The initial embankment failed during construction in 1918, and was subsequently completed using both dumped and rolled fill sections. Figures 37(a) and (b) illustrate some of the complexity of the resulting internal embankment and foundation zonation and geometry. The final result was lower elevation fills and underlying alluvium that required investigation, topped by more competent rolled fills that were potentially obstructions (with regard to casing drag) to the planned use of BPT to investigate the variably coarse lower soils.

Both BPT and short-interval SPT were used in this investigation. Seventeen rotary wash borings, with more than 400 short-interval SPT, were performed, and for zones and strata considered to be of potentially liquefaction-susceptible soil “type” the short-interval SPT were processed as in Section 3.5.1 to develop “corrected” SPT N-values. In addition, eleven Becker penetrometer probes were performed (a total of more than 1600 feet of BPT). The Becker probes were driven in 10-foot continuous lengths, and were then halted and withdrawn 5 feet, and then re-driven 5 feet. The first foot of re-driving was taken as “re-seating” of the penetrometer, and material ravelled and/or squeezed into the hole during re-driving, so that the last 2 or 3 feet had significant tip resistance as well as casing drag. The second foot of re-drive was, however, taken as representing almost entirely casing drag. The casing drag from the 2<sup>nd</sup> foot of re-driving was then used as a basis for “correcting” the total driving resistance to account for casing drag.

Casing drag was found to typically represent between 5% to 45% of the total measured BPT resistance, with an average of about 19%.

Because of the complex geometry, and the complex internal sub-stratification within apparent “zones” (see Figure 37) an unusually large number of sub-zones and sub-strata were evaluated with regard to liquefaction resistance. Without specifically identifying these, Table 2 presents a summary of the characterization of these various zones using both “corrected” short-interval SPT and casing-corrected BPT based on subtraction of averaged casing drag measurements as described above. Large numbers of both types of data were available in most of the zones of interest, and both median and 35-percentile resultant “corrected” equivalent clean sand blowcounts ( $N_{1,60,cs}$ -values) were developed by both approaches. As shown in Table, there is a generally good level of agreement between the results of the short-interval SPT and the corrected  $N_{BPT}$  data, suggesting that these two methods can both be used in variable soils of these types with some reliability.



**Table 2: Selection of Representative  $(N_1)_{60,CS}$  Values for Embankment and Foundation Zones and Subzones, Calaveras Dam and Foundation**

Zone	Zone Description	Subzone	30 <sup>th</sup> Percentile $(N_1)_{60}$ SPT	30 <sup>th</sup> Percentile $(N_1)_{60}$ BPT	50 <sup>th</sup> Percentile $(N_1)_{60}$ SPT	50 <sup>th</sup> Percentile $(N_1)_{60}$ BPT	Representative Fines Content	$\Delta N_{CS}$ (for fines)
I	Rock Berm (Placed In The 1970s)		N/D	22	N/D	29	15 (F)	N/A
II	Dumped Weathered Rock Fill	II(M) II(TD) II(US)	17 9 23	19 (B) 8 21	21 12 22	23 8 20	14 7 10	1.5 1 1
III	Cobbly Gravel Fill		/ND	7	N/D	8	20 (F)	1.5
IV	Rolled Fill	IV IV(R)	17 24	23 (L) 12 (L)	22 (L) 32 (L)	25 16	48 12 (F)	N/A 1
V	Mixed Dumped and Sedimented Hydraulic Fill	V V(F) V(G)	13 12 17	19 17 17	16 17 20	23 23 22	20 15 (F) 19	1.5 1.5 1.5
V(R)	Mixed Hydraulic and Rolled Fill		21	14 (L)	24	18	15 (F)	1.5
VI	Disturbed and Mixed Hydraulic, Dumped, and Rock Fill	VI VI(F) VI(G)-Res VI(G)-Emb VI(R)	10 11 7 27 12 (L)	N/D 22 (L) N/D 22 N/D	17 18 8 40 12 (L)	N/D 36 (L) N/D 31 N/D	11 59 11 11 15	1 N/A 1 1 1.5
VII	Sedimented Hydraulic Fill		10	N/D	13	N/D	62	N/A
VIII	Base Alluvium		19	20	30	26	8	1
X	Mixed Fill		12	17	13	26	19 (F)	1.5
XI	Rocky Colluvium		32	36	34	43	N/D	0

(L): Limited penetration data available

(B): Based on data at bottom of zone

(F): Calibrated field-estimated fines contents were also considered

N/A: Not Applicable (High CL content)

N/D: Not Determined

### 3.6 Non-Zero Static “Driving” Shear Stresses:

An additional consideration in evaluation of the liquefaction potential of saturated soils is the presence of non-zero static “driving” shear stresses. These are shear stresses induced by gravity loading (and geometry) that are present both before and during the earthquake. Because they are gravity-induced, they are essentially “following” loads and continue to act during seismic (cyclic) excitation.

Figure 38 presents the “classic” representation of static, driving shear stresses (After Seed, 1979). Figure 38(a) illustrates the effective normal and shear stresses acting on horizontal and vertical planes in an element of soil at some

depth below a level ground surface. There is a non-zero shear stress within the element, as the vertical effective stress and the “At-Rest” horizontal effective stress are not equal, but the soil element is kinematically constrained and has no strong intrinsic desire to deform in shear. The shear stress on the horizontal planes is zero, and the “driving” shear stresses are taken as zero for this case.

Figure 38(b) illustrates a second element of soil, this time at some depth below a sloping ground surface. At this point within (or beneath) a slope, the shear stress acting on the horizontal planes is not zero, and the element has non-zero “driving” static shear stresses, and a resultant desire to deform

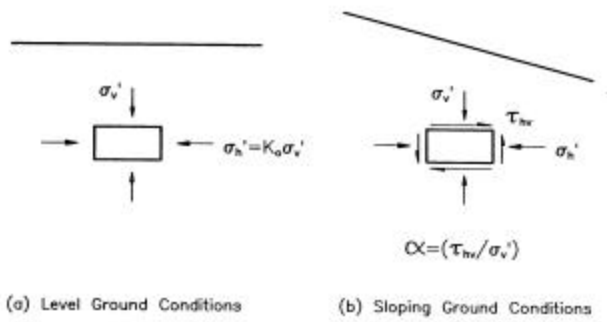


**Fig. 38: Stress Conditions on Horizontal Planes beneath Level and Sloping Ground Surfaces**  
(Seed et al., 1979)

in shear in a downslope direction. The measure of the relative importance of these non-zero driving shear stresses is routinely expressed as the ratio ( $\hat{a}$ ) of “static, driving” shear stress acting on a horizontal plane divided by (normalized by) the effective vertical stress acting on that plane as

$$\hat{a} = \hat{\sigma}_{hv} / \hat{\sigma}'_v \quad [\text{Eq. 20}]$$

Increasing levels of static driving shear stresses can have an increasing effect on the vulnerability of the soil to cyclic generation of pore pressures and triggering or initiation of liquefaction. For very loose soils (soils that are contractive under monotonic shearing), the presence of initial static driving shear stresses ( $\hat{a} > 0$ ) significantly increases vulnerability to liquefaction, as initial cyclic pore pressure induced softening leads to monotonic accumulation of shear deformations, and these, in turn, lead to further pore pressure increases.

For very dense soils (soils that are dilatant under monotonic shearing), however, the presence of non-zero initial static driving shear stresses can lead to reduction in the rate of generation of pore pressures during cyclic loading. As each cycle of loading produces an incremental increase in pore pressure, and some resultant reduction in strength and stiffness, the driving shear stresses then act to produce shear deformations that cause dilation of the soil, in turn reducing pore pressures.

Figure 39 presents one of the best “simplified” representations of the effects of non-zero static driving shear stresses on the vulnerability of soils to “triggering” of liquefaction under cyclic loading (after Harder and Boulanger, 1997). This figure presents an adjustment factor ( $K_a$ ) that represents the relative increase in liquefaction due to the presence of non-zero driving shear stresses. This factor is usually applied to scale the equivalent uniform cyclic shear stress ratio required to “trigger” liquefaction as

$$CSR_{liq,\hat{a}>0} = CSR_{liq,\hat{a}=0} K_a \quad [\text{Eq. 21}]$$

As shown in Figure 39, the CSR required to induce liquefaction increases with increasing  $\hat{a}$  for high SPT N-values, and Decreases with increasing  $\hat{a}$  for low N-values.

It should be noted that Figure 39 is appropriate only for soils at an initial effective overburden stress of less than or equal to approximately 3 atmospheres. At higher initial effective overburden stresses, the high effective stresses suppress dilation of dense soils, and exacerbate contraction of loose soils, so that the  $K_a$  values of Figure would rotate clock-wise (in an adverse manner.) There is currently no widely accepted guidance as to the degree or rate of this rotation with increased effective stress, but work is in progress (by several research teams) and improved guidance here can be expected in the next year and two.

It should be noted that the  $K_a$  values do not have to be applied as a multiplier of the CSR required to trigger liquefaction (they do not have to be applied to the “resistance” term.) They can, instead, be applied as inverse multipliers of the loading term by scaling the earthquake-induced CSR as

$$CSR_{eq,\hat{a}>0} = CSR_{eq,\hat{a}=0} / K_a \quad [\text{Eq. 22}]$$

This has significant potential advantages with regard to prediction of liquefaction-induced displacements and deformations, as discussed later in parts of Section 5.

Finally, it should be noted that “slopes” are not the only source of non-zero static driving shear stresses. Non-zero  $\hat{a}$

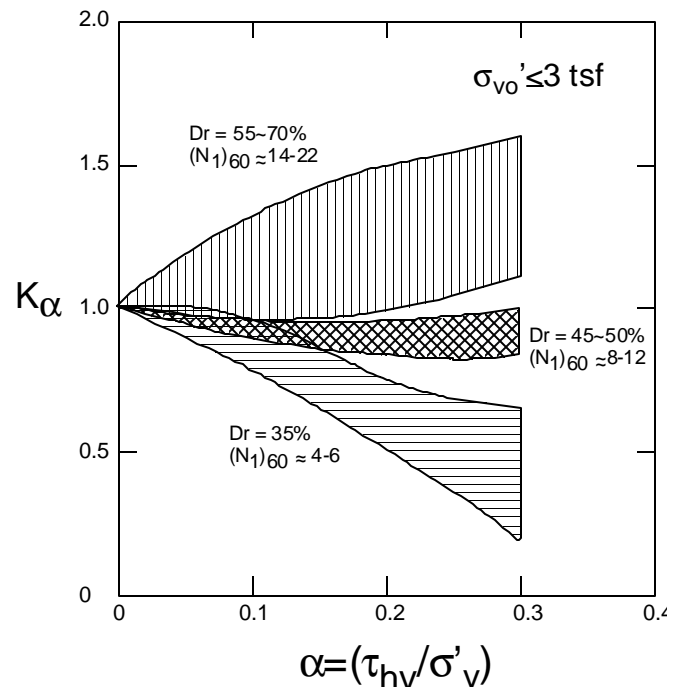


**Fig. 39: Recommended Values of  $K_a$  as a Function of SPT N-Values for Effective Vertical Stresses of Less Than 3 atmospheres**  
(After Harder and Boulanger, 1997)

conditions can also arise due to bearing loads of shallow foundations, due to loading of piles and other deep foundation elements, due to “free” faces of excavations, due to grade changes constrained by walls, etc. It has largely been conventional to neglect the non-zero  $\sigma'$  conditions near the edges of shallow-founded structures in performing liquefaction triggering assessments, and this will be examined a bit further in Section 5.4.2.

#### 4.0 ASSESSMENT OF POST-LIQUEFACTION OVERALL STABILITY

Once it has been determined that initiation or “triggering” of liquefaction is likely to occur, the next step in most liquefaction studies is to assess “post-liquefaction” global stability. This entails evaluation of post-liquefaction strengths available, and comparison between these strengths and the driving shear stresses imposed by (simple, non-seismic) gravity loading. Both overall site stability, and stability of structures/facilities in bearing capacity, must be evaluated. If post-liquefaction stability under simple gravity loading is not assured, then “large” displacements and/or site deformations can ensue, as geometric rearrangement is necessary to re-establish stability (equilibrium) under static conditions.

The key issue here is the evaluation of post-liquefaction strengths. There has been considerable research on this issue over the past two decades (e.g.: Jong and Seed, 1988; Riemer, 1992; Ishihara, 1993; etc.). Two general types of approaches are available for this. The first is use of sampling and laboratory testing, and the second is correlation of post-liquefaction strength behavior from field case histories with in-situ index tests.

Laboratory testing has been invaluable in shedding light on key aspects of post-liquefaction strength behavior. The available laboratory methods have also, however, been shown to provide a generally unconservative basis for assessment of in-situ post-liquefaction strengths. The “steady-state” method proposed by Poulos, Castro and France (1985), which used both reconstituted samples as well as high-quality “slightly” disturbed samples, and which provided a systematic basis for correction of post-liquefaction “steady-state” strengths for inevitable disturbance and densification that occurred during sampling and re-consolidation prior to undrained shearing, provided an invaluable incentive for researchers. The method was eventually found to produce post-liquefaction strengths that were much higher than those back-calculated from field failure case histories (e.g.: Von Thun, 1986; Seed et al., 1989).

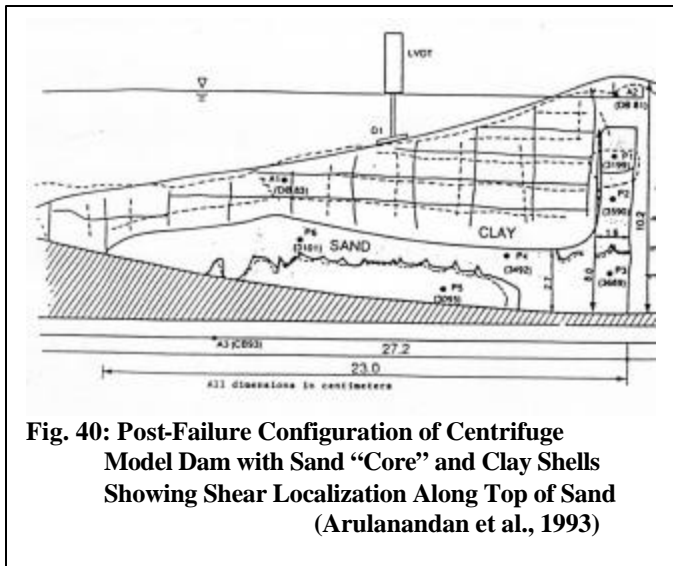
Reasons for this included: (1) the very large corrections required to account for sampling and reconsolidation densification prior to undrained shearing, (2) sensitivity to the assumption that the steady-state line (defining the relationship between post-liquefaction strength,  $S_{u,r}$  vs. void ratio,  $e$ ) which was evaluated based on testing of fully remolded (reconstituted) samples provides a basis for “parallel” correction for this unavoidable sample densification, (3) use of C-U triaxial tests, rather than simple shear tests, for field

situations largely dominated by simple shear, (4) reconsolidation of samples to higher than in-situ initial effective stresses, and (5) the failure of laboratory testing of finite samples to account for the potentially important effects of void redistribution during “undrained” shearing in the field.

It has now been well-established that both simple shear and triaxial extension testing provide much lower undrained residual strengths than does triaxial compression (e.g.: Riemer, 1992; Vaid et al., 1990; Ishihara, 1993; etc.), often by factors of 2 to 5, and simple shear tends to be the predominant mode of deformation of concern for most field cases. Similarly, it is well-established that samples consolidated to higher initial effective stresses exhibit higher “residual” undrained strengths at moderate strains (strains of on the order of 15 to 30%), and this range of strains represents the limit of accurate measurements for most testing systems.

These issues can be handled by performing laboratory tests at field in-situ initial effective stress levels, and by performing undrained tests in either simple shear or torsional shear. The remaining unresolved issues that continue to preclude the reliable use of laboratory testing as a basis for assessment of in-situ (field) post-liquefaction strengths are two-fold. The first of these is the difficulty in establishing a fully reliable basis for correction of laboratory test values of  $S_{u,r}$  for inevitable densification during both sampling and laboratory reconsolidation prior to undrained shearing. The correction factors required, for loose to medium dense samples, are routinely on the order of 3 to 20, and there is no proven reliable basis for these very large corrections. Use of frozen samples does not fully mitigate this problem, as volumetric densification due to reconsolidation upon thawing (prior to undrained shearing) continues to require large corrections here.

The second problem is intrinsic to the use of any laboratory testing of finite samples for the purpose of assessment of in-situ (field) post-liquefaction strengths, and that is the very important issue of void redistribution. Field deposits of soils of liquefiable type, both natural deposits and fills, are inevitably sub-stratified based on local variability of permeability. This produces “layers” of higher and lower permeability, and this layering is present in even the most apparently homogenous deposits. During the “globally undrained” cyclic shearing that occurs (rapidly) during an earthquake, a finite sublayer “encapsulated” by an overlying layer of at least slightly lower permeability can be largely isolated and may perform in a virtually undrained manner, remaining essentially at constant volume. Although the sublayer loses no volume, however, there is a progressive rearrangement of the solids and pore fluid within the sublayer as the soils cyclically soften and/or liquefy. This progressive rearrangement, which causes the solid particles to settle slightly and thus increase the density in the lower portion of the sub-layer, while simultaneously reducing the density of the top of the sublayer, is “localized void redistribution” during globally undrained shearing.



Owing to the very sensitive relationship between post-liquefaction strength ( $S_{u,r}$ ) and void ratio ( $e$ ) for loose to medium density soils, even apparently minor amounts of increase in void space (reduction in dry density) at the top of a sub-layer can result in large reductions in  $S_{u,r}$ . In extreme cases, water attempting to escape from the sublayer can be temporarily trapped by the overlying, less pervious layer, and can form a “film” or water-filled “blister” at the interface between the two layers (in which case the shear strength,  $S_{u,r}$ , is reduced fully to zero along this interface.)

An interesting early example of this behavior was produced in a centrifuge test performed by Arulanandan et al. (1993), as illustrated in Figure 40. In this experiment, an embankment was constructed with a sand “core” and a surrounding clay “shell” to prevent drainage during cyclic loading. The sand core was marked with layers of black sand so that localized changes in volume (and density) could be tracked during globally undrained shearing. When subjected to a model earthquake, cyclic pore pressure generation within the sand occurred, and the embankment suffered a stability failure. During the “undrained” earthquake loading, the overall volume of the saturated sand “core” remained constant, satisfying the definition of globally undrained loading. Locally, however, the lower portions of the sand “core” became denser, and the upper portions suffered corollary loosening. The top of the sand layer suffered the greatest loosening, and it was along the top of this zone of significantly reduced strength that the slope failure occurred.

Given the propensity for occurrence of localized void redistribution during seismic loading, and the ability of Nature to selectively push failure surfaces preferentially through the resulting weakened zones at the tops of localized sub-strata (and water blisters in worst-cases), the overall post-liquefaction strength available is a complex function of not only initial (pre-earthquake) soil conditions (e.g. density, etc.), but also the scale of localized sub-layering, and the relative

orientations and permeabilities of sub-strata. These are not qualities that can be reliably characterized, at this time, by laboratory testing of soil samples (or “elements”) of finite dimensions.

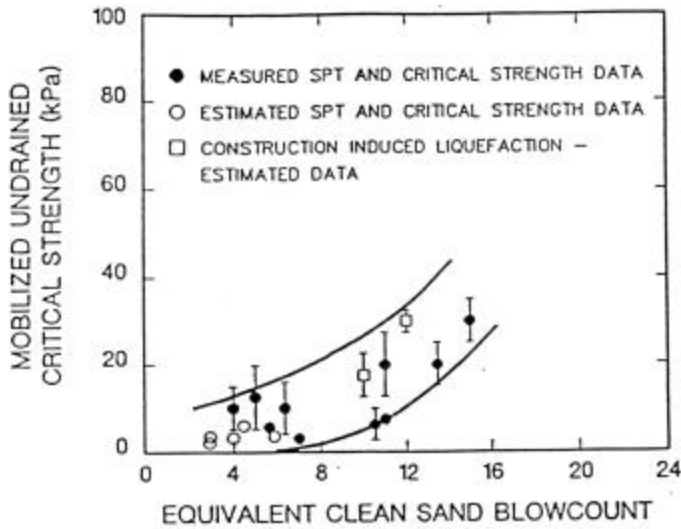
Accordingly, at this time, the best basis for evaluation of post-liquefaction strengths is by development of correlations between in-situ index tests vs. post-liquefaction strengths back-calculated from field case histories. These failure case histories necessarily embody the global issues of localized void redistribution, and so provide the best indication available at this time regarding post-liquefaction strength for engineering projects.

Figure 41 presents a plot of post-liquefaction residual strength ( $S_{u,r}$ ) vs. equivalent clean sand SPT blow count ( $N_{1,60,cs}$ ). This was developed by careful back analyses of a suite of liquefaction failures, and it should be noted that these types of back analyses require considerable judgement as they are sensitive to assumptions required for treatment of momentum and inertia effects. The difficulties in dealing with these momentum/inertia effects (which are not an issue in conventional “static” stability analyses) are an important distinction between the efforts of various investigators to perform back-analyses of these types of failures. In this figure, the original correction for fines used to develop  $N_{1,60,cs}$  is sufficiently close to that of Equations 6 and 7, that Equations 6 and 7 can be used for this purpose.

Stark and Mesri (1992), noting the influence of initial effective stress on  $S_{u,r}$ , proposed an alternate formulation and proposed a correlation between the ratio of  $S_{u,r}/P$  and  $N_{1,60,cs}$ , as shown in Figure 42, where  $P$  is the initial major principal effective stress ( $\sigma'_{1,i}$ ). This proposed relationship overstates the dependence of  $S_{u,r}$  on  $\sigma'_{1,i}$ , and so is overconservative at shallow depths ( $\sigma'_{1,i} < 1$  atmosphere) and is somewhat unconservative at very high initial effective stresses ( $\sigma'_{1,i} > 3$  atmospheres).

It is also true, however, that the relationship of Figure 41 understates the influence of  $\sigma'_{1,i}$  on  $S_{u,r}$ . Figure 43 shows an excellent example of this. Figure 43(a) shows the stress paths for a suite of four IC-U triaxial tests performed on samples of Monterey #30 sand, all at precisely the same density, but initially consolidated to different effective stresses prior to undrained shearing. (The sample void ratios shown are post-consolidation void ratios.) As shown in this figure, the samples initially consolidated to higher effective stresses exhibited higher undrained residual strengths ( $S_{u,r}$ ). The ratio between  $S_{u,r}$  and  $P$  was far from constant, however, as shown in Figure 43(b).

The influence of  $\sigma'_{1,i}$  on  $S_{u,r}$  (and on the ratio of  $S_{u,r}/P$ ) is a function of both density and soil character. Very loose soils, and soils with higher fines contents, exhibit  $S_{u,r}$  behavior that is more significantly influenced by  $\sigma'_{1,i}$  than soils at higher densities and/or with lower fines content. At this time, the authors recommend that the relationship of Figure 41 (Seed & Harder, 1990) be used as the principal basis for evaluation of



**Fig. 41: Recommended Relationship Between  $S_{u,r}$  and  $N_{1,60,CS}$  (Seed and Harder, 1990)**

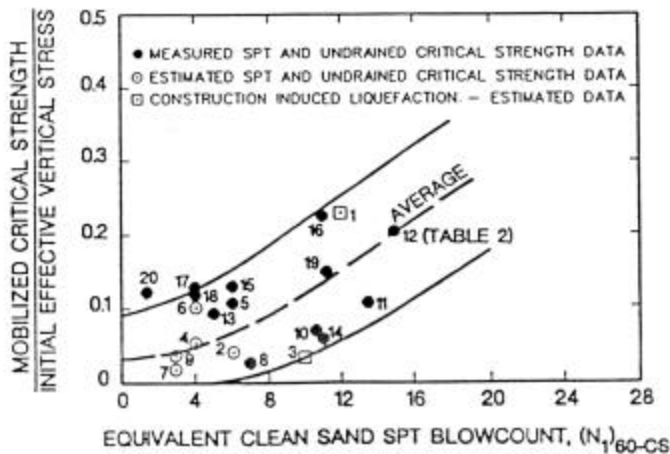


**Fig. 42: Relationship Between  $S_{u,r}/P$  vs.  $N_{1,60,CS}$  as Proposed by Stark and Mesri (1992)**

in-situ  $S_{u,r}$  for “relatively clean” sandy soils (Fines Content < 12%). For these soils it is recommended that both relationships of Figures 41 and 42 be used, but that a 5:1 weighting be employed in favor of the values from Figure 41. Similarly, a more nearly intermediate basis (averaging the results of each method, with 3:1 weighting between the relationships of Figures 41 and 42) is recommended for very silty soils (Fines Content > 30%). For fines contents between 12% and 30%, a linear transition in weighting between the two proposed relationships can be used.

It must be noted that engineering judgement is still required in selection of appropriate post-liquefaction strengths for specific project cases. Consideration of layering and sub-layering, permeability/drainage, and potential void redistribution, and the potential for confluence of alignment of layering interfaces with shear surfaces must all be considered. For most “typical” cases, use of  $S_{u,r}$  values in the lower halves of the ranges

shown in Figures 41 and 42 (with due consideration for weighting of these) appears to represent a suitably prudent range for most engineering purposes at this time, but lower overall average post-liquefaction strengths can be realized when layering and void redistribution combine unusually adversely with potentially critical failure modes.

Finally, a common question is “what happens at  $N_{1,60,CS}$  values greater than about 15 blows/ft.?” The answer is that the relationships of Figures 41 and 42 should be concave upwards (to the right), so that extrapolation at constant slope to the right of  $N_{1,60,CS}=15$  blows/ft should provide a conservative basis for assessment of  $S_{u,r}$  in this range. As these projected values represent relatively good strength behavior, this linear extrapolation tends to be sufficient for most projects. It should be noted, however, that values of  $S_{u,r}$  should generally not be taken as higher than the maximum drained shear strength. Values of  $S_{u,r}$  higher than the fully-drained shear strength would suggest significant dilation. Dilation of this sort tends to rapidly localize the shear zone (or shear band), and so reduces the drain path length across which water must be drawn to satisfy the dilational “suction”. As these distances can be small, rapid satisfaction of this dilational demand is possible, and “undrained” (dilational) shear strengths higher than the drained strength can persist only briefly. Accordingly, for most engineering analyses the use of the fully drained shear strength as a maximum or limiting value is prudent. Similarly, the maximum shear strength cannot exceed the shear strength which would be mobilized at the effective stress corresponding to “cavitation” of the pore water (as it reaches a pore pressure of  $-1$  atmosphere). The above limit (to not more than the fully-drained strength) is a stronger or more limiting constraint, however, and so usually handles this problem as well.

## 5.0 EVALUATION OF ANTICIPATED LIQUEFACTION-INDUCED DEFORMATIONS AND DISPLACEMENTS

### 5.1 Introduction:

Engineering assessment of the deformations and displacements likely to occur as a result of liquefaction or pore-pressure-induced ground softening is a difficult and very challenging step in most projects, and this is an area where further advances are needed.

### 5.2 Assessment of “Large” Liquefaction-Induced Displacements:

For situations in which the post-liquefaction strengths are judged to be less than the “static” driving shear stresses, deformations and displacements can be expected to be “large”; generally greater than about 1m., and sometimes much greater. Figure 44 shows examples of global site instability corresponding to situations wherein post-liquefaction strengths are less than gravity-induced driving shear stresses. These are schematic illustrations only, and are not to scale.

For most engineering projects, the “large” deformations associated with post-liquefaction “static instability” are unacceptably large, and engineering mitigation is thus warranted. It is often, therefore, not necessary to attempt to make quantified estimates of the magnitudes of these “large” deformations. Exceptions can include dams and embankments, which are sometimes engineered to safely withstand liquefaction-induced displacements of more than 1m.

Estimates of the “large” deformations likely to occur for these types of cases can often be made with fair accuracy (within a factor of about  $\pm 2$ ). “Large” liquefaction-induced displacements/deformations ( $> 1m.$ ) are usually principally the result of gravity-induced “slumping”, as geometric

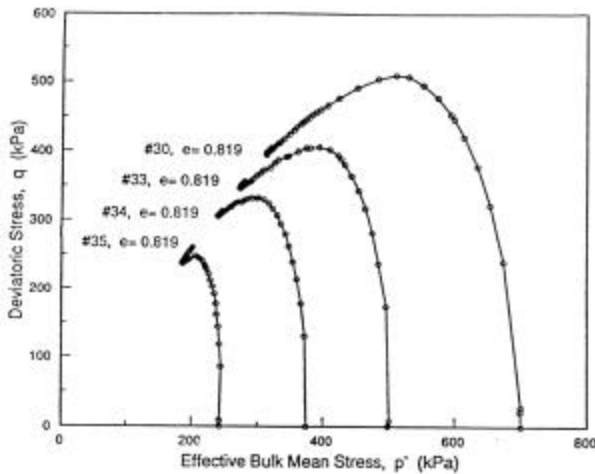
rearrangement of the driving soil and/or structural masses is required to re-establish static equilibrium. A majority of the deformations, for these cases, usually occur after strong shaking has ceased so that cyclic inertial forces are not very important in “driving” the deformations (though they are very important in “triggering” the liquefaction-induced ground softening.)

Three general types of approaches can be used to estimate expected “large” liquefaction-induced ground deformations, and these are: (1) fully nonlinear, time-domain finite element or finite difference analyses (e.g.: Finn et al., 1986; Beaty et al., 1998; France et al., 2000; etc.), (2) statistically-derived empirical methods based on back-analyses of field earthquake case histories (e.g.: Hamada et al, 1986; Youd et al., 2002; etc.), and (3) simple static limit equilibrium analyses coupled with engineering judgement. When applied with good engineering judgement, and when the critical deformation/displacement modes are correctly identified and suitable post-liquefaction strengths are selected, all three methods can provide reasonable estimates of the magnitudes of expected displacements.

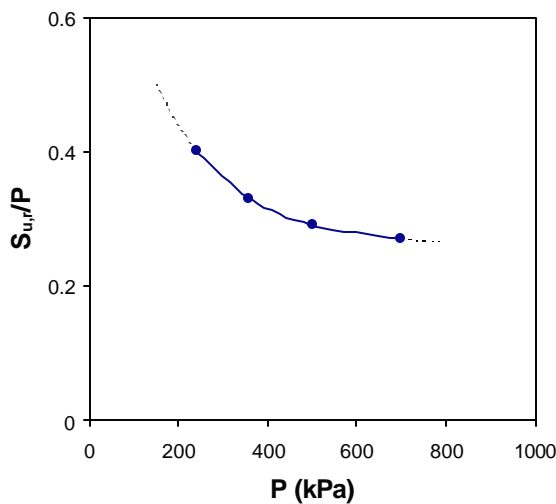
Finite element and finite difference analyses are the most complex of the three approaches, and we cannot reasonably discuss these in detail within the confines of this paper. These methods have, to date, principally been employed mainly for relatively critical (and well-budgeted) studies, but growing comfort with these methods (coupled with decreasing computing costs) can be expected to bring these types of analyses more into the mainstream. The principal difficulty associated with these methods is the difficulty of evaluating the model “input” parameters necessary for the relatively complex behavioral and/or constitutive models used. These models are usually “sensitive” to relatively minor variations in one or more parameters, and assessment of this type of parameter sensitivity is a vital element of such studies. (A slightly more extensive discussion of these methods is presented in Section 5.5.)

The second type of methods available are the “Hamada-type” empirical methods for estimation of lateral displacements due to liquefaction-induced lateral spreading. These methods are based on back-analyses of lateral spreading case histories, and involve probabilistically and/or statistically derived empirical equations for estimation of expected lateral spreading displacements. Currently, the most widely used such method in the western U.S. is that of Bartlett and Youd (1995), as recently updated by Youd et al. (2002). This method addresses two types of cases: cases where there is a “free face” towards which lateral spreading can occur (e.g.: Figures 44(a) and 44(b)), and cases without a free face but with a sloping ground surface (e.g.: Figures 44(c) and 44(d)). Two different empirical equations are provided, one for each of these two situations.

Figure 45 shows the results of this approach (both equations, as applicable.) Figure 45(a) shows a plot of predicted displacement magnitude vs. the actual observed displacement



(a) Stress Paths



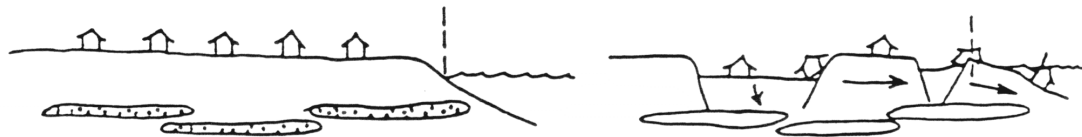
(b) Ratio of  $S_{u,r}/P$  vs.  $P$

**Fig. 43: Results of IC-U Triaxial Tests on Monterey #30/0 Sand (After Riemer, 1992)**

☐ - Liquefied zone with low residual undrained strength



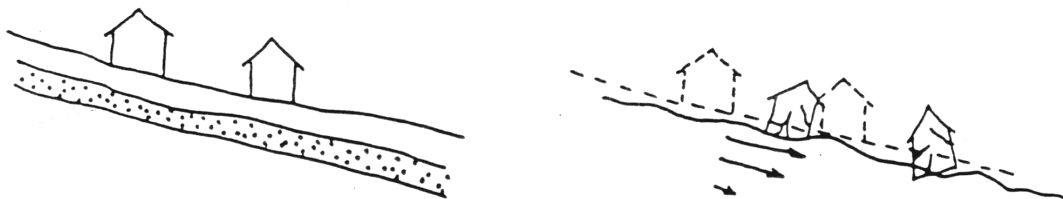
(a) Edge Failure/Lateral Spreading by Flow



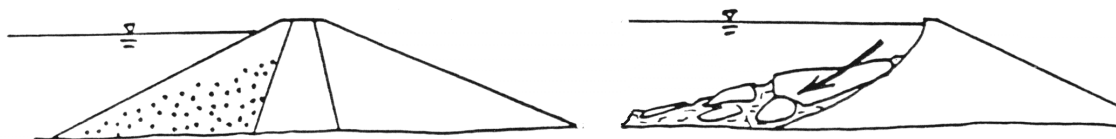
(b) Edge Failure/Lateral Spreading by Translation



(c) Flow Failure



(d) Translational Displacement



(e) Rotational and/or Translational Sliding

**Fig. 44: Schematic Examples of Liquefaction-Induced Global Site Instability and/or “Large” Displacement Lateral Spreading**

for the case histories studied. For (measured) displacements greater than approximately 1.5m., the ratio of predicted:measured displacements was generally in the range of 0.5:1 to 2:1, and this is a reasonable band of accuracy for engineering purposes in this range of displacements.

For displacements of less than about 1m, however, the predictive accuracy is much poorer, reflecting the difficulty of predicting displacements and deformations in this “small to moderate” displacement range within which cyclic shearing and cyclic shear stress reversal, as well as dilatent strength with each reversal of cyclic load, gives rise to very complex stress-strain and cyclic pore pressure behaviors.

The third method for estimation of expected “large” liquefaction-induced displacements is based on evaluation of the deformations/displacements required to re-establish static equilibrium. This requires careful assessment of the most critical mode of failure/deformation. An important issue in this approach is the progressive acceleration and then deceleration of the displacing soil (and/or structural) mass. The deformations are not arrested when the geometry is sufficiently rearranged as to produce a “static” Factor of Safety of 1.0 (based on post-liquefaction strengths, as appropriate.). Instead, shear strength must be employed to overcome the momentum progressively accumulated during acceleration of the displacing mass, so that the deforming mass comes to rest at a “static” Factor of Safety of greater than 1.0 (FS  $\cong$  1.05 to 1.25 is common, depending on the maximum velocity/momentum achieved before deceleration).

For many problems, simply estimating the degree of geometry rearrangement necessary to produce this level of Factor of Safety (under “static” conditions, but with post-liquefaction strengths) can produce fair estimates of likely displacements. Alternatively, incremental calculations of (1) overall stability (excess driving shear stresses), (2) acceleration (and then deceleration) of the displacing mass due to shear stress imbalance (vs. shear strength), (3) accrual and dissipation of velocity (and momentum), and (4) associated geometry rearrangement, can produce reasonable estimates of likely ranges of displacements for many cases (Moriwaki et al., 1998).

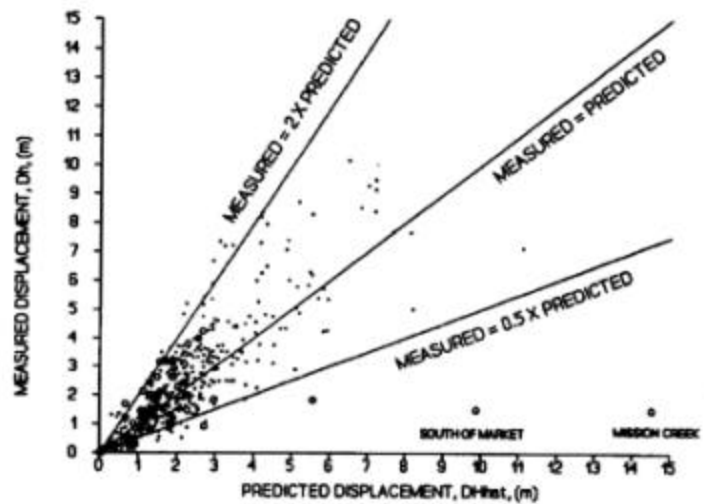
Finally, it should be noted that these three types of approaches for estimation of expected “large” liquefaction-induced displacements and deformations can be used to cross-check each other. For example, it is prudent to check the final geometry “predicted” by the results of finite element or finite difference analyses for its “static” Factor of Safety (with post-liquefaction strengths.)

### 5.3 Assessment of “Small to Moderate” Liquefaction-Induced Displacements:

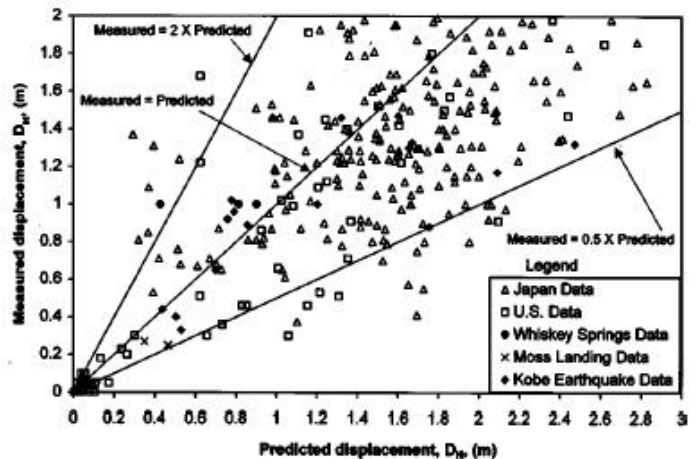
Although it is feasible to make reasonably accurate estimates of post-liquefaction deformations and displacements for cases of “large” displacements, we currently do not have tools for accurate and reliable estimation of “small to moderate”

liquefaction-induced displacements (displacements/deformations of less than about 0.75m). Unfortunately, it is this “small to moderate” range of 0 to 0.75m. that is most important for most conventional buildings and engineered facilities.

Unlike the case of “large” liquefaction-induced displacements, which are dominated by displacements “driven” principally by gravity forces after the cessation of strong shaking, “small to moderate” displacements are very strongly affected by cyclic inertial forces produced by strong shaking. In addition, “small to moderate” displacements are usually controlled in large part by complicated cyclic, pore pressure-induced softening followed by dilation and corollary reduction in pore pressures (and consequent re-establishment of strength and stiffness).



(a) All case histories



(b) Cases of less than 2m. displacement

**Fig. 45: Predicted vs. Measured Displacements from Lateral Spreading Case Histories (Youd et al., 2002)**

This softening and re-stiffening behavior is relatively complex and difficult to predict with good accuracy and reliability.

Figures 46 through 48 illustrate the complicated types of mechanical behaviors that control cyclic deformations in this “small to moderate” displacement range. Figure 46 presents the results of an undrained cyclic simple shear test of Monterey #0/30 sand at a relative density of  $D_r = 50\%$ , and an initial vertical effective stress of  $\sigma'_{v,i} = 85$  kPa. These conditions correspond roughly to a soil with an  $N_{1,60,cs}$  value of about 10 blows/ft. In this figure, (a) the bottom left figure presents evolution of cyclically-induced pore pressures (expressed as reduction in  $\sigma'_{v,i}$ ), (b) the bottom right figure shows increasing shear strains with increasing numbers of cycles, (c) the top right figure shows shear stress vs. shear strain behavior, and (d) the top left figure presents the effective stress path followed during this test. All four sub-figures are scaled so that the axes of the figures to the side and/or above and below each share commonly scaled axes.

As shown in Figure 46, shear strains are relatively small for the first 25 cycles, until significant cyclically-induced pore pressures have been generated. At that point (after about 25 cycles), there is a rapid increase in cyclic shear strains, representing “triggering” of liquefaction. Examining the stress path plots (and also the stress-strain and cyclic pore pressure generation plots) shows clearly that pore pressures are generated upon initial reversal of cyclic shear stresses during each half-cycle of loading, but that dilation ensues later in each cycle as shear strains begin to increase in the new direction of loading. This process of cyclic softening and then re-stiffening during each cycle is now well understood, but remains difficult to model reliably for non-uniform (irregular) cyclic loading, as in earthquakes.

Figure 47 similarly shows the same suite of plots for an undrained cyclic simple shear test on a sample of the same sand, but this time at an initial relative density of  $D_r = 75\%$ . This corresponds roughly to an in situ  $N_{1,60,cs}$  value of about 25 to 30 blows/ft. Denser soils in this range exhibit very different behavior than the looser sample of Figure 46.

The cyclic stress ratio of the test presented in Figure 47 is 1.8 times higher than that of the previous figure. The denser sample (Figure 47) is more strongly dilatant with each half-cycle of loading, and instead of relatively “suddenly” beginning a rapid rate of increase of shear strains (as in the previous test), this denser sample exhibits a more moderate (and less dramatically accelerating) rate of increase of cyclic shear strains. Indeed, as there is no sudden transition in behaviors, it is difficult to identify a singular point at which “triggering” of liquefaction can be said to occur. At this time, it is recommended that “triggering” or initiation of liquefaction be considered to have occurred when a soil has experienced significant cyclic pore pressure generation (and attendant softening and loss of strength), and has reached a cyclic shear strain (in either single direction) of  $\gamma \cong 3\%$ . At this level of shear strain, subsequent performance (including “post-liquefaction” strength and stress-deformation behavior)

will be controlled largely by the soil’s contractive or dilatant behaviors.

Further complicating the issue of prediction of liquefaction-induced deformations is the fact that, for most cases of engineering interest, there is a directionally preferential “driving” shear stress due to gravity loading (in addition to cyclic inertial stresses induced by the earthquake). Figure 48 presents the results of an undrained cyclic simple shear test with these initial “driving” shear stresses. In this test, the “driving” shear stresses are aligned in the same direction as the (reversing) cyclic shear stress loading, and the initial (constant) driving shear stresses are equal to 0.08 times the initial vertical effective stress (of 85 kPa). In addition to the types of cyclic softening and dilatant re-stiffening shown in the two previous figures, this test (Figure 48) also exhibits cyclic “ratcheting” or progressive accumulation of shear strains in the direction of the driving shear force. It is this type of complex “ratcheting” behavior that usually principally controls “small to moderate” liquefaction-induced deformations and displacements (displacements in the range of about 2 to 75 cm. for field cases.)

This problem is further complicated in field cases by the occurrence of cyclic shear stresses “transverse” (not parallel to) the direction of the (static) driving shear stresses. Boulanger et al. (1995) clearly demonstrated that cyclic shear stresses transverse to driving shear forces can, in many cases, represent a more severe type of loading for “triggering” of liquefaction than cyclic shear stresses aligned “parallel” with driving forces. It is only in the last few years, however, that high quality laboratory data with “transverse” as well as “parallel” cyclic simple shear loading (and driving shear stresses) has begun to be available (e.g.: Kammerer, 2002; Wu, 2003; etc.), and development and calibration of improved analytical and constitutive models for this type of behavior are currently still under development. Additional complications involved in attempting to predict “small to moderate” liquefaction-induced deformations and displacements include: (1) the irregular and multi-directional loading involved in field situations, representing a complex and multi-directional seismic response problem, and (2) the many types and “modes” of deformations and displacements that can occur.

Figures 49 and 50 illustrate a number of “modes” or mechanisms that can result in “small to moderate” lateral and vertical displacements, respectively. These figures are schematic and for illustrative purposes only; they are not to scale.

Figure 49 illustrates three examples of modes of deformation that can produce “small to moderate” liquefaction-induced lateral displacements (of less than about 1m.) It should be noted that these can also produce much larger deformations, if the liquefiable soils are very loose, and geometry is sufficiently adverse. Figure 49(a) shows an example of limited lateral spreading towards a free face, and Figure 49(b) shows an example of limited lateral spreading downslope or downgrade. These modes can also give rise to large

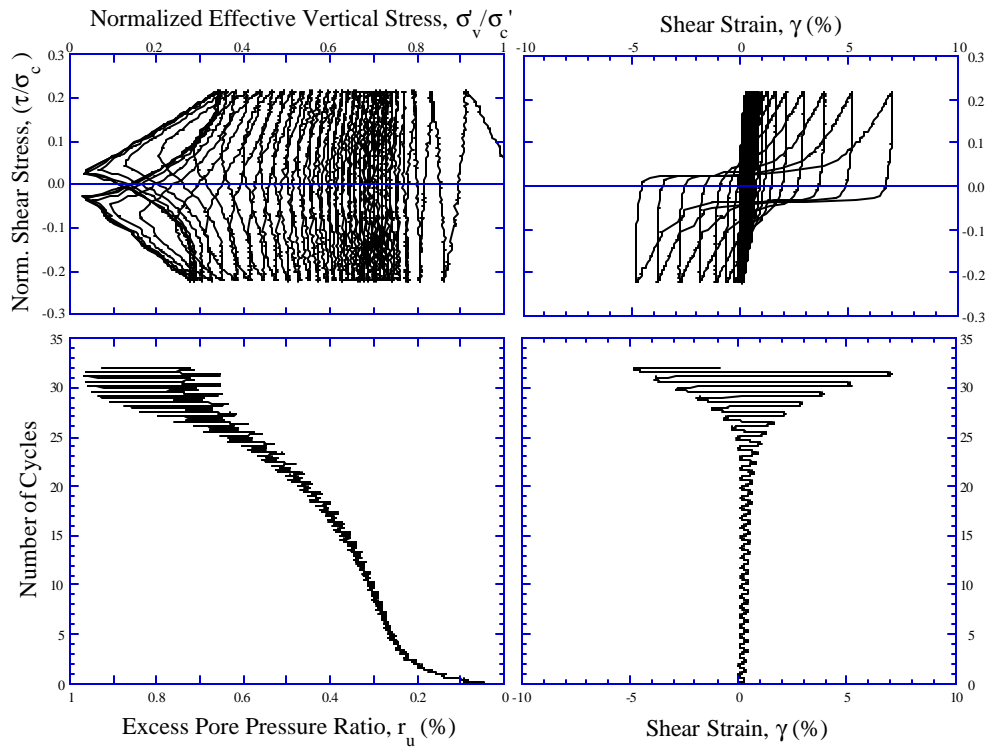


**Fig. 46: Undrained Cyclic Simple Shear Test on Monterey #30/0 Sand (Test No. Ms15j)**  
 $D_r=50\%$ ,  $s_{vj}'=85$  kPa,  $CSR=0.22$ ,  $a=0$

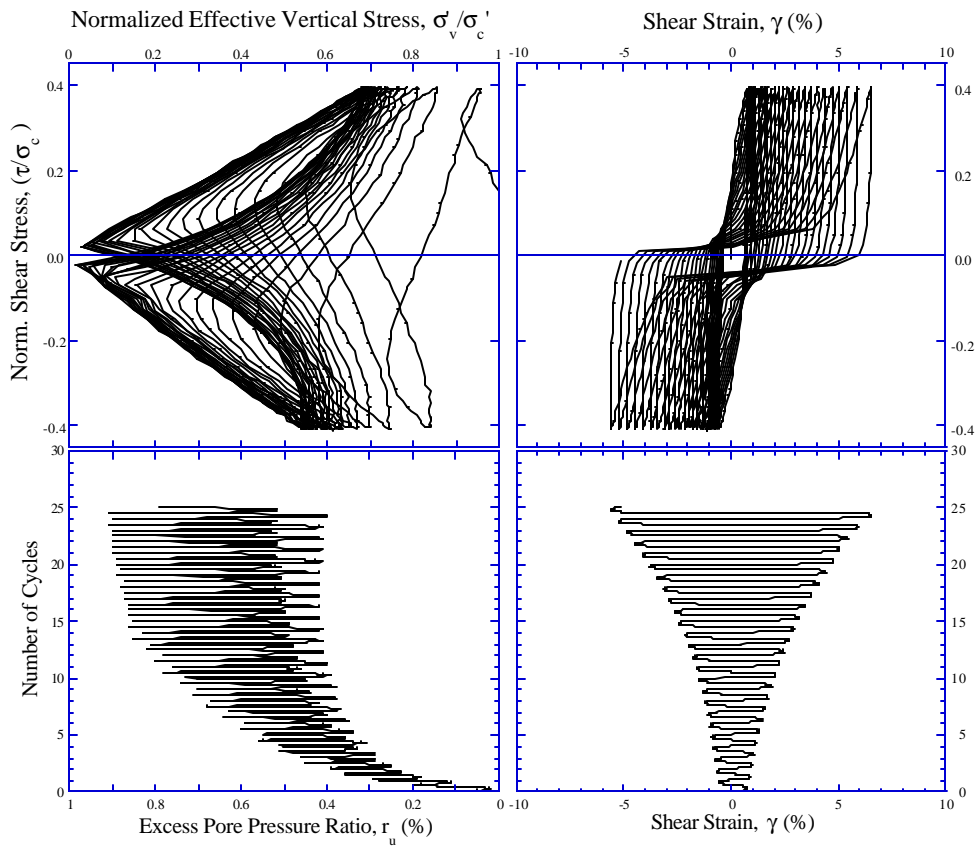


**Fig. 47: Undrained Cyclic Simple Shear Test on Monterey #30/0 Sand (Test No. Ms30j)**  
 $D_r=75\%$ ,  $s_{vj}'=85$  kPa,  $CSR=0.4$ ,  $a=0$

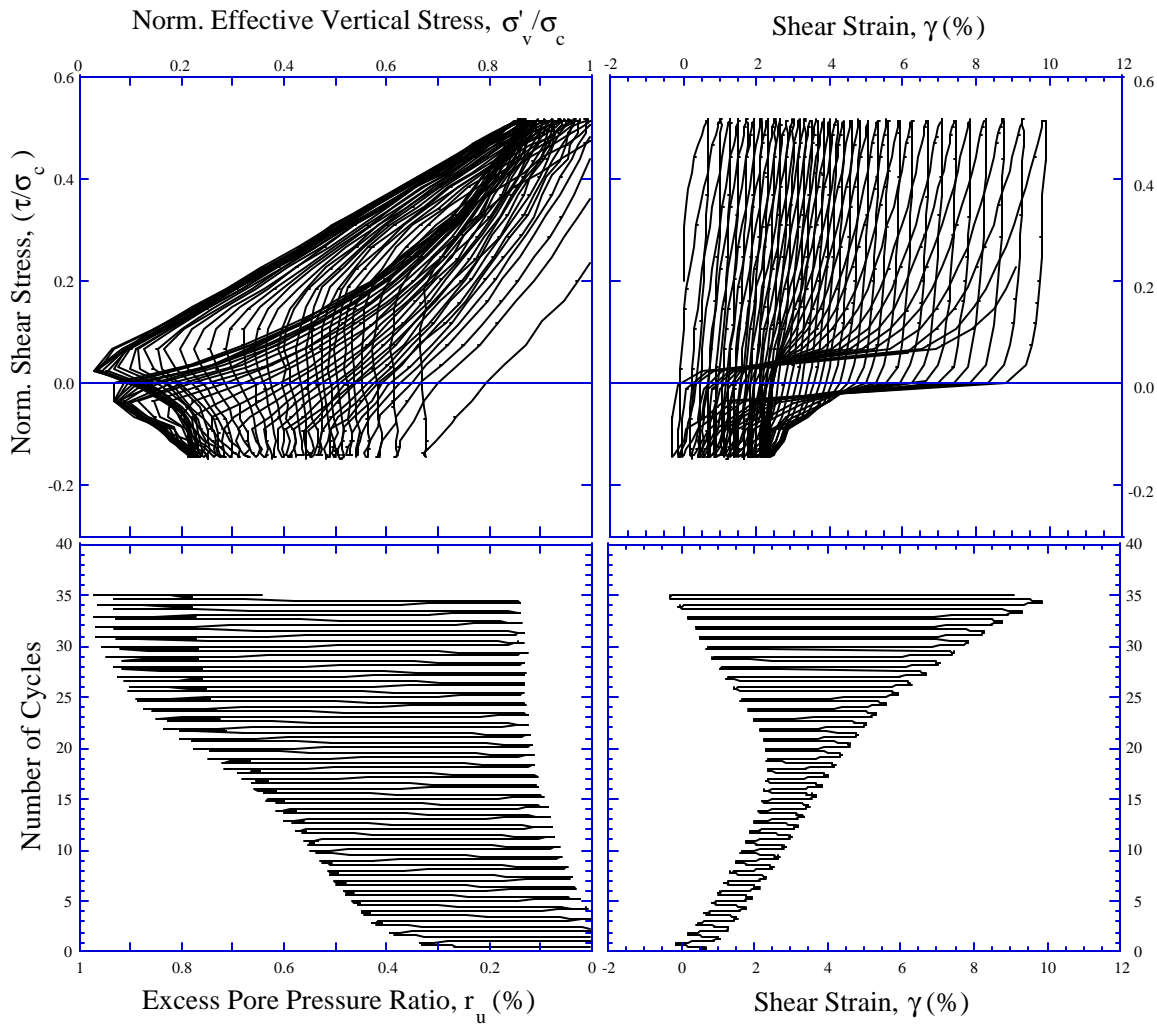


**Fig. 48: Undrained Cyclic Simple Shear Test on Monterey #30/0 Sand (Test No. Ms10k)**  
 $D_r=55\%$ ,  $s_{v,i}'=85$  kPa,  $CSR=0.33$ ,  $a=0.18$

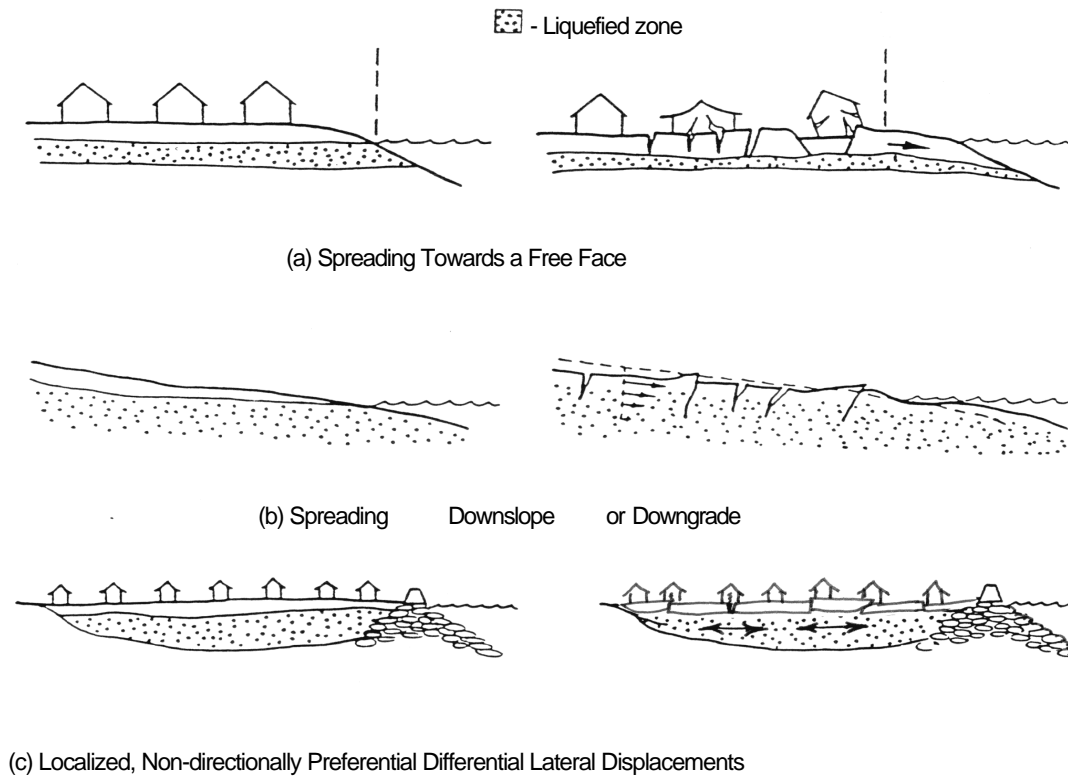
displacements, but when the liquefiable soils have limited shear strain potential (the shear strain required for dilatant re-stiffening), then displacements are limited.

Figure 52 (Shamoto, Zhang and Tokimatsu, 1998) presents engineering estimates of limiting (post-liquefaction) shear strains, as a function of SPT N-values. As shown previously in Figures 46 through 48, the shear strain required for dilatant re-stiffening decreases with increased initial density (or increased Nvalue). Although there is not yet a well-established (or well-defined) basis for selection of the precise shear strain corresponding to the “limiting” shear strain (see for examples, Figures 46 through 48), the types of values presented in Figure 52 represent suitable approximate values for many engineering purposes. An updated set of recommendations of this type will be presented and discussed in Section 5.4.

These “limiting” shear strains are not, by themselves, an upper bound to displacement potential; rather they are a basis for

estimation of resistance to shear deformations. In field cases in which significant and adverse static “driving” shear stresses occur (e.g. slopes, free faces, etc.) actual deformations can be as much as twice the values of these “limiting” shear strains, and even more when post-liquefaction residual strength is low relative to the static driving shear stresses.

The two general types of lateral spreading deformations illustrated in Figures 49(a) and (b) correspond to the two types of lateral spreading addressed by the empirical correlation proposed by Youd et al. (2002). As shown in Figure 45(a), this approach provided reasonable estimates of expected displacements for cases with displacements of greater than about 1.5m. However, as shown in Figure 45(b) (which is an enlarged view of part of Figure 45(a)), this approach does not provide accurate or reliable estimates of lateral displacements for cases where measured displacements are less than about 1m. (the range within which complex cyclic inertial loading and cyclic softening and dilatant re-stiffening largely control displacements). There are, at present, no well-calibrated and



**Fig. 49: Schematic Examples of Modes of “Limited” Liquefaction-Induced Lateral Translation**

verified engineering tools for accurate and reliable estimation of lateral displacements in this range. This is an area of urgent need for further advances, and research to fill this gap is underway in several countries.

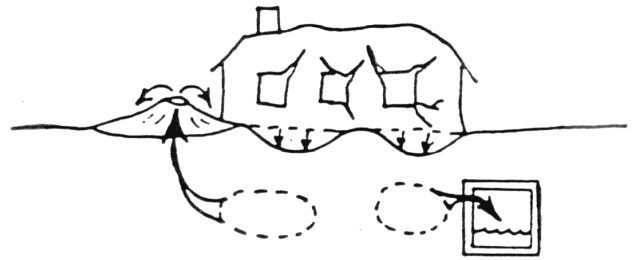
Figure 45(c) shows another mechanism which can produce “limited” lateral displacements; in this case, liquefaction of soils beneath a non-liquefied surface “crust”, and laterally constrained against large lateral spreading towards a free face. When the surface “crust” is thin relative to the thickness of the underlying layer, and when the liquefied soils have low density (low  $N_{60,cs}$  values), the “crust” can separate into distinct sections or “blocks”, and these crustal sections can move differentially with respect to each other. This can produce shearing, compression and tensile separations at the edges of surface blocks. This, in turn, can be damaging to structures and/or utilities that are unfortunate enough to straddle the block boundaries.

There are no good means to predict where the inter-block boundaries will occur, and there are no reliable methods at

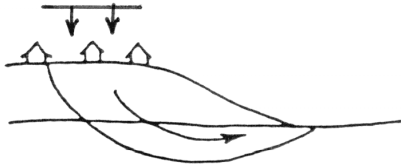
present to predict the magnitudes of localized differential block displacements that are likely to occur. Ishihara (1985) provides some insight into this “pie crust” problem, as shown in Figure 52. Ishihara suggests, based on empirical observations from a number of Japanese earthquakes, that surface manifestations of liquefaction will not be significant if (1) the site is relatively level, (2) the edges are constrained so that lateral spreading towards a free face is prevented, and (3) the ratio of the thickness of the non-liquefied surface “crust” ( $H_1$ ) to the thickness of the liquefied underlying soils ( $H_2$ ) is greater than the values indicated in Figure 52 (as a function of peak ground surface acceleration, as shown.) It should be noted, however, that these recommendations are useful only up to surface peak accelerations of up to 0.4 to 0.5g, and that these have not been verified in many earthquakes as yet. Preliminary field data from the recent 1999 Kocaeli (Turkey) and 1999 Chi-Chi (Taiwan) Earthquakes suggests that these criteria may not always provide fully satisfactory performance.



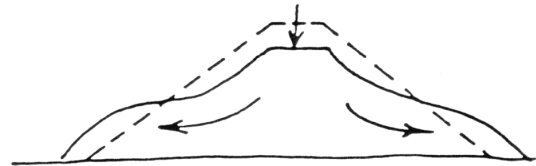
(a) Ground Loss Due to Cyclic Densification and/or Volumetric Reconsolidation



(b) Secondary Ground Loss Due to Erosion of "Boil" Ejecta



(c) Global Rotational or Translational Site Displacement



(d) "Slumping" or Limited Shear Deformations



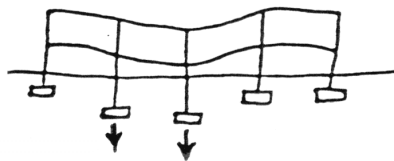
(e) Lateral Spreading and Resultant Pull-Apart Grabens



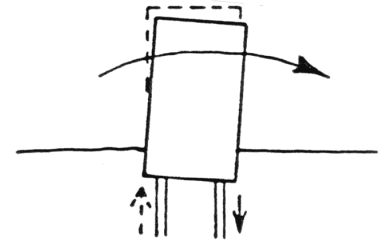
(f) Localized Lateral Soil Movement



(g) Full Bearing Failure



(h) Partial Bearing Failure or Limited "Punching"



(i) Foundation Settlements Due to Ground Softening Exacerbated by Inertial "Rocking"

**Fig. 50: Schematic Illustration of Selected Modes of Liquefaction-Induced Vertical Displacements**

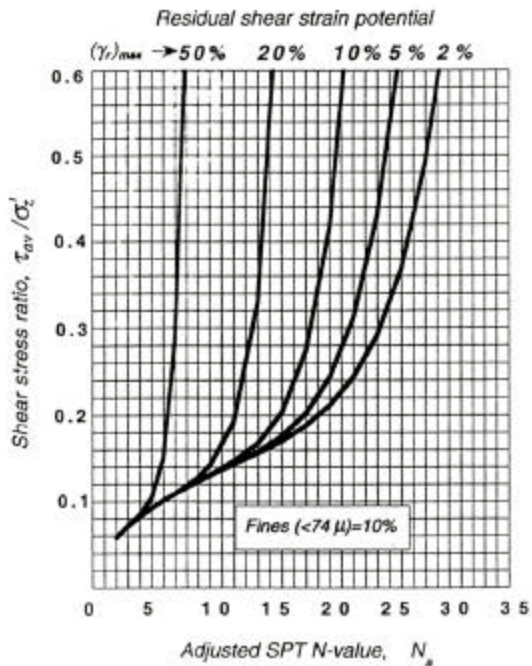


**Fig. 51: Estimates of Limiting Shear Strains for Sandy Soils with ~ 10% Fines (Shamoto et al., 1998)**

Given the potential risk associated with localized differential movements at crustal block boundaries, it is recommended herein that these criteria should, at a minimum, always be supplemented by well-reinforced and laterally continuous foundations to constrain lateral differential displacements and to reduce differential vertical displacements at the bases of structures at such sites, especially when the liquefied layer contains soils with low equivalent  $N_{1,60,cs}$  values ( $N_{1,60,cs} \leq 15$ ), or when the ratios of  $H_1/H_2$  are near the boundaries of Figure 52. Shallow-founded structures and facilities should always be checked for bearing capacity (with post-liquefaction strengths) at such sites, and the possibility of lateral site translations (lateral spreading) should also be checked.

In addition to differential lateral displacements, engineers must also deal with the hazard associated with both total and differential potential vertical displacements. There are a number of mechanisms that can produce vertical displacements of sites and/or structures and other engineered facilities. Figure 50 presents schematic illustrations of a number of these. Again, this figure is schematic and for illustrative purposes only; it is not to scale. The modes of vertical displacement illustrated in Figure 50 can be grouped into three general categories. Figures 50(a) and (b) illustrate settlements due to reduction or loss of soil volume. Figures 50(c) through (f) illustrate modes of settlement due to deviatoric ground movements. Figures 50(g) through (i) illustrate structural settlements due to full or partial bearing failures.

Figure 50(a) shows “ground loss” or settlement due to cyclic densification of non-saturated soils and/or due to volumetric reconsolidation of liquefied (or partially liquefied) soils as cyclically-induced pore pressures escape by drainage. The overall magnitude of these types of settlements can be reasonably well predicted by several methods (e.g.: Tokimatsu and Seed, 1987; Ishihara and Yoshimine, 1992), but these methods cannot reliably predict the magnitude and distribution of locally differential settlements. Overall settlement estimates are generally accurate within  $\pm$  a factor of about 2 to 3, so long as suitable adjustments are made for fines content (as both methods are for “clean” sands.) The fines adjustment recommended here is that of Equations 6 and 7. Section 5.4.1 will present a recommended improved procedure for estimation of these types of “post-liquefaction reconsolidation” ground settlements.

Figure 50(b) illustrates a second mechanism of ground loss; secondary ground loss as a result of erosion of soil particles carried by water escaping through cracks and fissures (often referred to as “sand boils”) as excess pore pressures are dissipated. Boil ejecta (transported soils) can be carried to the ground surface, or they can be carried to accessible buried voids (e.g.: basements, buried culverts and sewers, etc.) Secondary ground loss due to erosion of boil ejecta is usually localized, and so can be locally differential. It is also essentially impossible to predict. The best defense here is usually to ensure sufficient lateral continuity of foundations as to be able to “bridge” or cantilever over localized subsidences. Another alternative is deep foundation support (piles or piers) extending beneath the depth of potential ground loss.

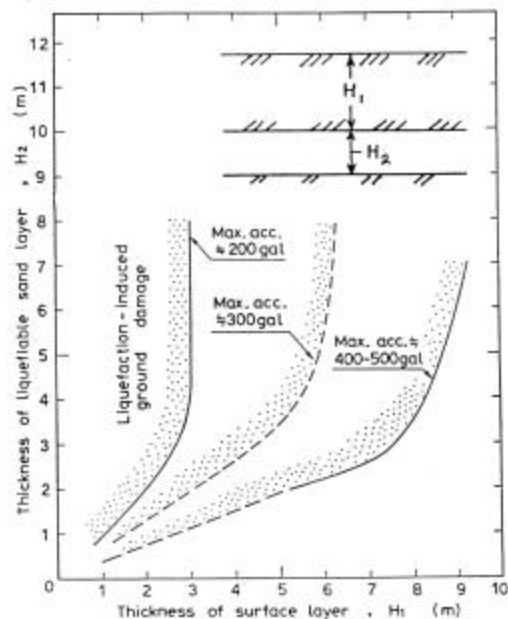


**Fig. 52: Proposed Boundary Curves for Site Identification of Liquefaction-Induced (Surface) Damage (After Ishihara, 1985)**

Figures 50(c) and (d) illustrate rotational and “slumping” (distributed shear) types of ground movements that produce settlements at the crests or heels of the slopes or embankments. Although these types of potential liquefaction-induced deformations and displacements are relatively amenable to engineering prediction when they are “large” (>1m.), there are at present no accurate and reliable (or well-calibrated) methods for estimation of expected displacements when displacements will be small to moderate ( $D \cong 0.05$  to 0.75m.) Accordingly, significant judgement is currently required to assess the likely deformations, and their impact on structures and other engineered facilities. The lack of reliable and well-calibrated analysis tools here often results in the need for conservative assumptions, and often leads to implementation of conservative hazard mitigation measures.

Figures 50(e) and (f) illustrate closely related mechanisms that can produce surface settlements. Figure 50(e) illustrates lateral spreading producing grabens, or settlements, in zones of locally differential extension (pull-apart zones). Figure 50(f) illustrates localized lateral soil movement producing both heaving and settlement as overall soil volume is largely conserved. These types of potential movements are also difficult to predict, and again conservative assumptions and/or conservative steps to mitigate this type of hazard are often called for when these types of movements are judged to represent potentially serious hazards for a site, structure, or other engineered facility.

Finally, in addition to liquefaction-induced soil (or site) displacements, another class of potential concerns are those associated with potential differential movements of structures relative to the ground. Figures 50(g) through (i) illustrate several subsets of these types of movements.

Figure 50(g) represents the case in which liquefaction-induced loss of strength and stiffness is sufficiently severe that full bearing failure occurs. This type of full bearing failure occurs when overall bearing capacity, based on post-liquefaction strengths ( $S_{u,r}$ ) as appropriate, is insufficient for static equilibrium under gravity loading. This can produce very large “punching” settlements (many tens of centimeters or more), and can even lead to toppling of structures when they are narrow relative to their height.

Figure 50(h) represents partial bearing failure or limited “punching” settlements. These limited punching types of settlements can occur at isolated footings, or can occur with mat and raft foundations (especially at corners and edges.) Limited punching settlements are generally associated with situations in which post-liquefaction strengths are sufficient to prevent full bearing failure, and they are the result of cyclic softening and attendant deformations required to generate sufficient dilational re-stiffening as to arrest movements.

Estimation of these “limited” punching/bearing settlements can be further complicated by the interaction of increased cyclic vertical loads due to inertial “rocking” of structures with cyclic softening (and cyclic dilational re-stiffening), as

illustrated schematically in Figure 50(i). There are, at present, no reliable and well-calibrated engineering/analytical tools for estimation of likely limited punching settlements. This is a major gap in practice, as it is limited punching settlements (in the range of about 0.05 to 0.75 m.) that represent one of the principal liquefaction-related hazards for many buildings and engineered structures. Preliminary results of studies to develop, and to field calibrate such analytical methods, will be presented and discussed briefly in Section 5.4.2.

Widespread liquefaction in the city of Adapazari in the recent 1999 Kocaeli (Turkey) Earthquake and in the city of Duzce in the 1999 Duzce (Turkey) Earthquake produced differential foundation/soil punching types of settlements in this range for hundreds of buildings, and many additional buildings suffered similar ranges of settlements in the cities of Wu Feng, Nantou, and Yuan Lin during the 1999 Chi-Chi (Taiwan) Earthquake. These two events thus provided both strong incentive, as well as large numbers of potential field case histories, and as a result considerable research efforts are currently underway to develop methods for estimation of these types of “limited” punching/bearing displacements.

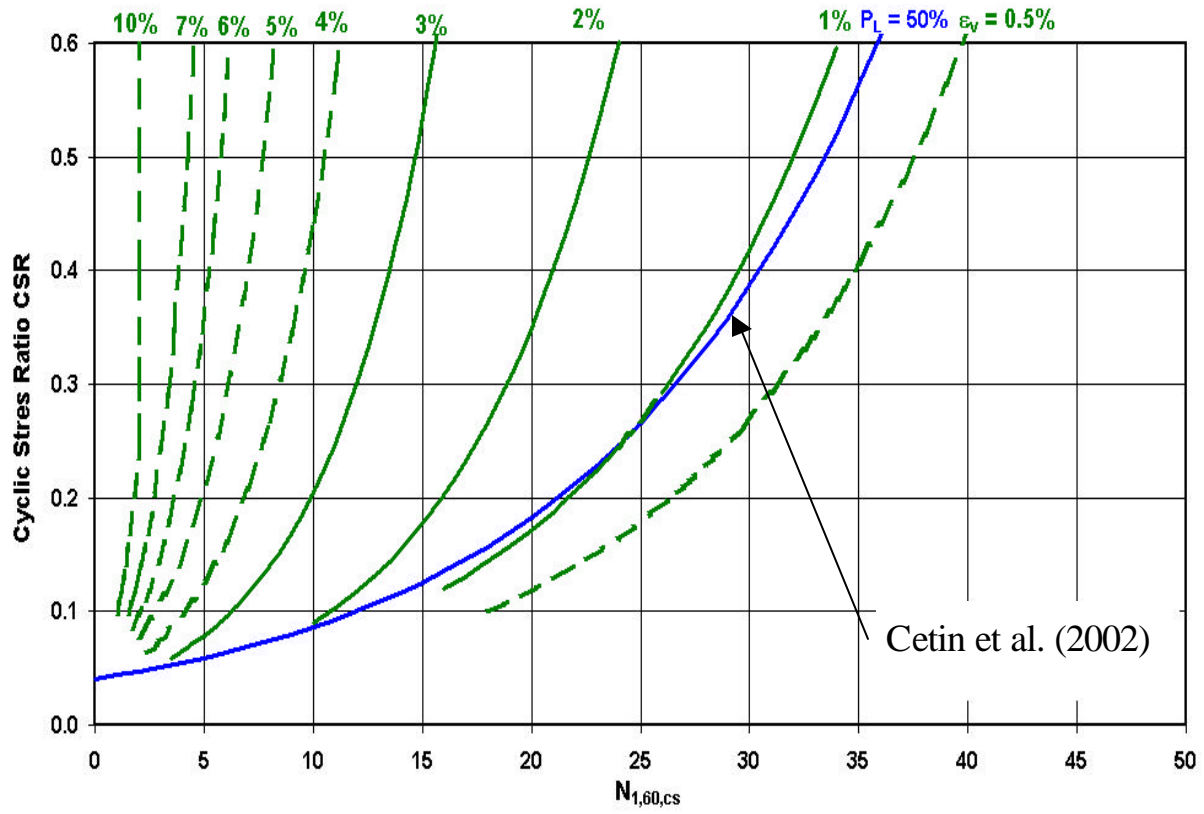
#### 5.4 Engineering Assessment of Small to Moderate Liquefaction-Induced Displacements (Selected Modes):

There is a need for improved “simplified” analytical methods for engineering assessment of expected liquefaction-induced deformations and displacements. For most civil projects, the engineer needs a basis for estimation of likely resulting lateral and vertical displacements of the ground and/or the base of the structure or other engineered facility. These methods need to be both adequately accurate and reliable, and thus must be well-calibrated against field performance case histories. Significant research efforts are underway, by multiple teams of researchers and in several countries, to develop improved analysis tools for these purposes. This section will briefly comment on some of these evolving methods.

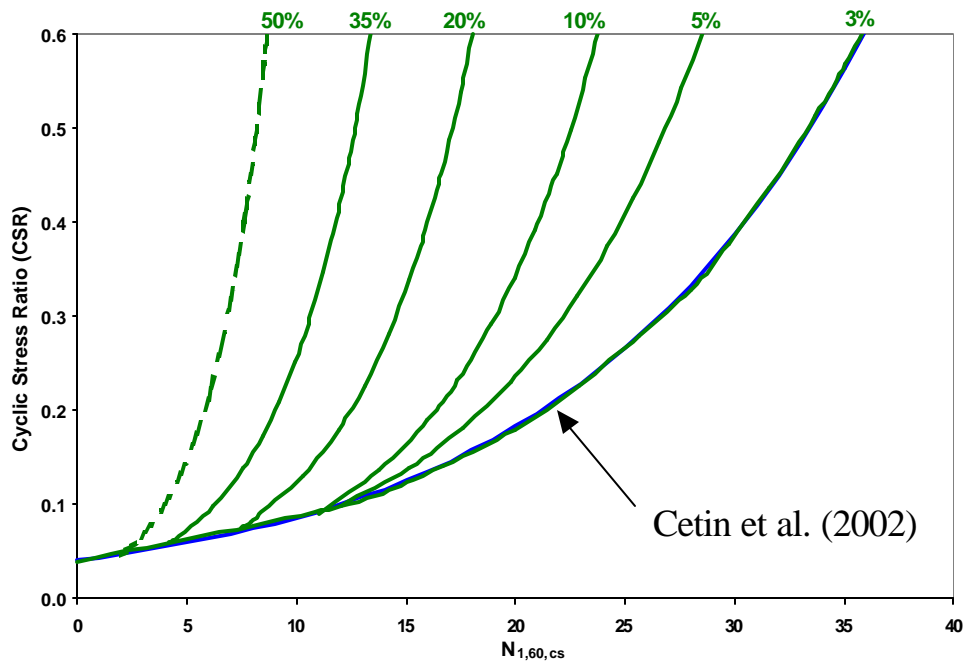
##### 5.4.1 Site Settlements Due to Post-Liquefaction Volumetric Reconsolidation

Estimation of expected site settlements due to post-liquefaction volumetric reconsolidation (as cyclically generated excess pore pressures are dissipated by expulsion of water; see Figures 50(a) and (b)) is the simplest of the vertical displacement mechanisms to analyze, and several good methods already exist for this (Tokimatsu and Seed, 1987; Ishihara and Yoshimine, 1992; Shamoto et al., 1998). All of these methods produce reasonably good predictions of actual field case history observations of post-liquefaction site settlements for sites where lateral site displacements were small.

Figure 53(a) presents new recommendations regarding expected volumetric reconsolidation strains after liquefaction, or after at least significant cyclically-induced pore pressure



(a) Volumetric Reconsolidation Strains



(b) Shear Strain Potential Index

**Fig. 53: Recommended Relationships for (a) Volumetric Reconsolidation Strains and (b) Shear Strain Potential Index as a Function of Equivalent Uniform Cyclic Stress Ratio and  $N_{1,60,CS}$  for  $M_w = 7.5$  (Wu, 2003)**

generation. The solid line in this figure is the “triggering” boundary for  $R_L = 50\%$  from Figure 16, and represents the approximate boundary for “triggering” of liquefaction. The strain contours represent expected values of volumetric strain due to post-earthquake dissipation of cyclically generated excess pore pressures. This is based on recent laboratory cyclic simple shear testing data, as well as previously available laboratory and field data from other researchers (Wu, 2003).

The horizontal axis of Figure 53(a) represents fines-adjusted, normalized SPT penetration resistance, using the same fines corrections that were employed previously in the new “triggering” relationships presented in Section 3.1 (Equations 6 and 7). The vertical axis represents equivalent uniform cyclic stress ratio adjusted for: (1) magnitude-correlated duration weighting ( $DWF_M$ ), and (2) effective overburden stress ( $K_0$ ). In using this figure, the earthquake-induced  $CSReq$  must be scaled by both  $DWF_M$  and  $K_0$ , using Equations 13 and 14.

To estimate expected site settlements due to volumetric reconsolidation, the recommended procedure is to simply divide the subsurface soils into a series of sub-layers, and then to characterize each sub-layer using SPT data. Volumetric contraction (vertical strain in “at-rest” or  $K_0$  conditions) for each sub-layer is then simply summed to result in total site settlements.

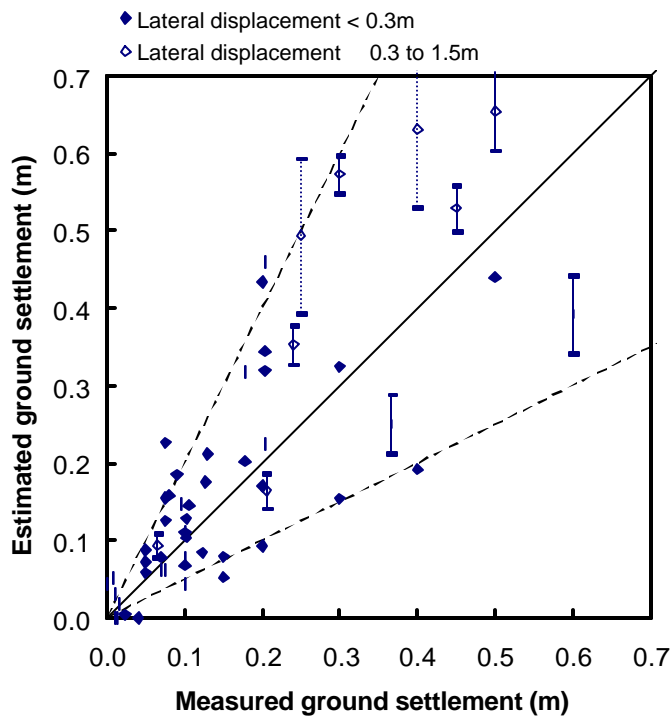


Fig. 54: Predicted vs. Actually Observed Liquefaction-Induced Ground Settlements (Wu, 2003)

Figure 54 presents a summary of the results of application of this procedure to back-analysis of field performance case histories during a number of earthquakes (Wu, 2003). As shown in this Figure, predicted settlements are typically within a factor of  $\pm 2$  relative to those actually observed. All of the sites represented in Figure 54 experienced lateral site displacements of less than 1.5 m. Sites that experienced lateral displacements of less than 0.3 m are represented by solid symbols, and sites that experienced maximum lateral displacements of between 0.3 to 1.5m are represented with open symbols.

For sites experiencing “small to moderate” lateral site displacements (displacements of between 0.3 to 1.5 m), the vertical site settlement estimated based on summation of the volumetric reconsolidation strains of Figure 52(a) were increased by an additional term representing 10% to 20% of the lateral site translation (with a mean of 15%). The vertical bars of Figure 54 represent this 10% to 20% augmented range. For sites expected to experience maximum lateral translations of greater than about 1.5m, these types of “simplified” predictions of vertical settlements should not be considered reliable.

It should be noted that non-saturated soils (above the water table) can also suffer volumetric contraction during strong shaking (“shake down”). This volumetric contraction is usually significantly less severe than that experienced by saturated soils generating significant cyclically-induced pore pressures (typically on the order of less than 0.5% volumetric strain in all but the loosest of soils), but when significant depths of non-saturated soils with low to moderate SPT penetration resistance are present, it is advisable to also add prediction of non-saturated “shake-down” to estimates of site settlements. The best published method for prediction of non-saturated shake-down for “liquefiable” types of soils is that of Tokimatsu and Seed (1987), and non-saturated shake-down predictions by their method are included in the predictions presented in Figure 54. These were only significant (greater than about 10% of the total predicted settlements) at 5 of the case sites studied; at several sites with very low ground water tables and thus significant depths of non-saturated alluvial soils with relatively low blowcounts, non-saturated shake-down accounted for up to 20% to 30% of the total predicted settlements.

Finally, it should be noted that deposits of cohesionless soils, and low plasticity cohesive (“silty”) soils, can be notoriously heterogeneous in nature. As a result, interpretation of the results of predictions of expected site settlements due to volumetric reconsolidation should be leavened by an understanding of the variance or uncertainty (which appears to be a factor of about  $\pm 2$ ), as well as by the understanding that these are “average” settlements, and that local differential settlements can be expected.

5.4.2 Engineering Assessment of Liquefaction-Induced Settlements of Shallow-Founded Structures

The quest for relatively “simple” and reliable methods for prediction of liquefaction-induced settlements of shallow-founded structures has been one of the most important and elusive objectives of research to fill “holes” in our analytical repertoire. Numerous research efforts are currently underway, by diverse teams of researchers in at least several different countries, many inspired by the widespread damages resulting from differential or “partial punching” settlements of many hundreds of structures in the recent 1991 Luzon (Phillipines), 1999 Kocaeli (Turkey), 1999 Duzce (Turkey), and 1999 Chi-Chi (Taiwan) Earthquakes.

One approach under development by the authors (as well as a very talented team of research students at Middle East Technical University in Ankara, Turkey, working with Prof. Onder Cetin) is nearing completion, and is showing very promising results when predictions are compared with observed field performance. This “simplified” method is not all that simple, and space limitations do not permit a full treatment of this approach in this paper. (Besides, it is still under development; expected to be completed within the

calendar year.) Instead, a brief description of the approach, and of the results to date, will be presented.

This method is being developed and field-calibrated using field performance case histories selected for study from among the many hundreds of structures that suffered liquefaction-induced settlements and/or partial punching failures in the city of Adapazari, Turkey during the 1999 Kocaeli Earthquake, and in the city of Duzce, Turkey, during the 1999 Duzce Earthquake.

Figure 55 illustrates typical conditions considered. In both of these cities, relatively stiff, monolithic reinforced concrete buildings of 2 to 6 stories were routinely founded at shallow depths (usually on thick mat foundations) over potentially liquefiable soils and with a shallow ground water table. Performance varied from relatively minor foundation settlements of less than 10cm (relative to the adjacent ground), to measured settlements of more than 1m. Several buildings (of tall, narrow aspect ratio) in Adapazari suffered sufficient partial bearing failures that they toppled over.

The approach under development involves first assessing post-liquefaction stability (bearing capacity relative to post-

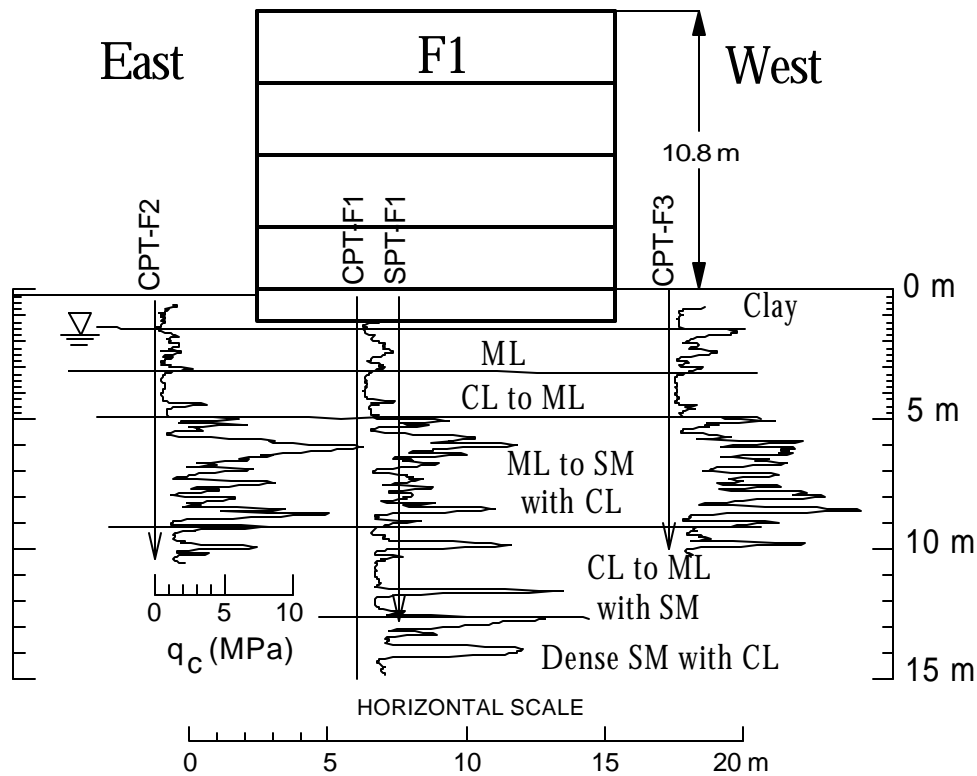


Fig. 55: Example of Foundation Soil Conditions for a Four-Story Reinforced Concrete Structure in Adapazari, Turkey (After Bray et al., 2003)

liquefaction residual strengths). All of the field cases studies “passed” this screening (as, apparently, did all but a few of the structures in these two cities), and consideration next progressed to assessment of expected structural settlements.

Settlements of the structures had two principal contributing source mechanisms; “volumetric” settlements arising principally from volumetric reconsolidation, and “deviatoric” settlements arising from cyclic bading in combination with static “driving” shear stresses due to foundation bearing loads. Total settlement,  $\ddot{A}Z_{total}$ , at either the corner or the edge of a shallow-founded structure was then estimated as

$$\ddot{A}Z_{total} = \ddot{A}Z_{volumetric} + \ddot{A}Z_{deviatoric} \quad [\text{Eq. 23}]$$

In this equation,  $\ddot{A}Z_{volumetric}$  can be calculated in much the same manner as was described in the previous section, except that the cyclic loading (and the resultant CSR) in each sub-layer beneath the building foundation is exacerbated by soil/structure interaction (SSI) which induces additional cyclic loading of the ground near the edges due to both differential lateral inertial forces between the structure and the ground (“hockey-puck-like” kinematic and inertial interaction) and vertical loading pulses due to “rocking” forces from the structure.

These increased (SSI-induced) cyclic loadings have been analyzed by means of extensive 3-dimensional, nonlinear dynamic SSI analyses, and one of the great challenges in development of “simplified” methods is boiling down all the results of these SSI analyses to develop simplified estimates of exacerbated CSR in layers near and below the foundations.

An additional, and relatively minor, issue is the increase in vertical effective stress beneath the foundations (relative to the adjacent free field ground) which produces a minor and adverse  $K\sigma$  effect.

With regard to  $\ddot{A}Z_{volumetric}$ , the result of SSI-exacerbated CSR (and of  $K\sigma$  effects) is some minor increase in settlements relative to the adjacent “free field” ground, but these were relatively minor; typically on the order of 5 to 10 cm. As the adjacent free field ground also experienced some non-zero  $\ddot{A}Z_{volumetric}$ , and as the “Observed Settlements” of the cases presented in Figure 56 represent differential settlement of the structure relative to the adjacent free filed ground surface, the contribution of  $\ddot{A}Z_{volumetric}$  to the “Estimated (predicted) Settlements” in Figure 56 was relatively minor.

The second term of Equation 23 ( $\ddot{A}Z_{deviatoric}$ ) is more complicated, and was the principal contributor to observed building settlements in the two cities studied.  $\ddot{A}Z_{deviatoric}$  represents shear deformations in the general direction of “partial bearing failure” though often with much smaller displacements) and is a function of: (1) the SSI-exacerbated cyclic loading (CSR) in each soil sub-layer beneath the foundation, and (2) the static “driving” shear stresses due to the bearing loads of the foundation.

## Total Building Settlement

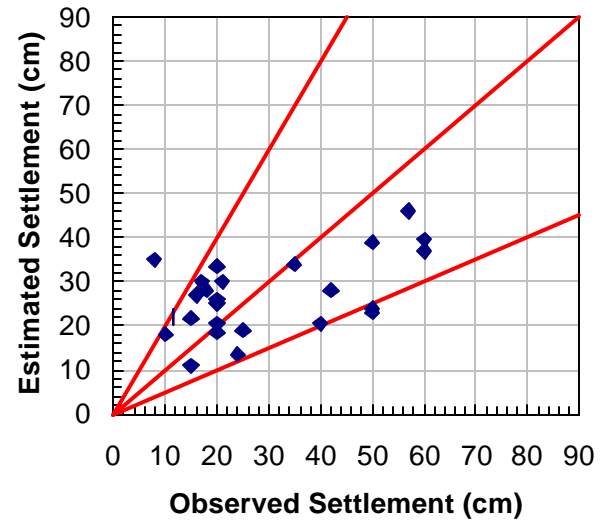


**Fig. 56: Predicted vs. Actually Observed Liquefaction-Induced Building Settlements in Duzce and Adapazari (Cetin, et al., work in progress)**

Figure 53(b) presents recommended values of Shear Strain Potential Index (SPI). SPI is the maximum shear strain developed in 15 cycles of uniform cyclic loading, without significant static “driving” shear forces ( $\dot{a} = 0$  conditions.) The limiting shear strain indices of Figure 53(b) were used as the principal index of resistance to shear deformations.

These are only an “index” as the actual shear strains developed are a function of the interaction of CSR with static “driving” shear stresses. As these driving shear stresses are very significant near the bases of the edges of the structures, the complex interaction of these driving loads with the earthquake-induced cyclic loads is a critical issue. There is some insight that can be gleaned from laboratory cyclic testing data, but in the end the final characterization of the interaction between CSR and  $\dot{a}$  was developed by regression of field case histories. The form of the calculation of  $\ddot{A}Z_{deviatoric}$  is to perform analyses of each soil sub-layer beneath the corner or edge of the structure as in Equation 24, and then sum the settlements. For each sub-layer

$$\ddot{A}Z_{deviatoric} = f(\text{CSR}_{\text{free-field}}, \text{CSR}_{\text{SSI}}, \text{SPI}, \dot{a}, K_{\dot{a},\dot{a}}) \quad [\text{Eq. 24}]$$

where  $K_{\dot{a},\dot{a}}$  is a strain-based factor that characterizes the effects of non-zero driving shear stresses on the accumulation of shaer strain in the driven direction. (This is somewhat analogous to the  $K_{\dot{a}}$  factor discussed earlier in Section 3 for “triggering” evaluations, but is not at all the same.)

Figure 56 presents a comparison between predicted liquefaction-induced building settlements and those actually observed for 26 buildings in the cities of Adapazari and Duzce. Both “Estimated” and “Observed” settlements in this figure represent settlements of the building relative to the adjacent “free field” ground.

Most of the cases presented in Figure 56 are from the city of Duzce, as many of the cases studied in Adapazari are complicated by the presence of cohesive soils from “Zone B” of Figure 3; soils that are vulnerable to cyclic strain softening (especially when  $\dot{\alpha}$  is non-zero). These cohesive soils appear to have contributed significantly to overall building settlements in many of these cases, but the analytical methods described above are applicable only to soils of Zone A of Figure 4.

Additional cases are being studied and analyzed, and these analytical tools are still being refined. It is hoped that this work will be completed by late Summer or early Fall, and more complete presentations of this method, as well as its development and calibration against an increasing number of field case histories, should be available soon.

#### 5.4.3 Engineering Assessment of “Small to Moderate” Lateral Site Displacements

A number of researchers have investigated the phenomenon of permanent deformation due to liquefaction-induced lateral spreading, beginning with the seminal early work of Hamada et al. (1986). Hamada et al. began by assembling a database of case histories, consisting of sites where lateral spreading occurred during three earthquakes (the 1964 Niigata, 1983 Nihonkai-Chubu, and 1971 San Fernando Earthquakes). The case histories were divided into three main types based on topographic conditions, which are illustrated in Figure 57: (A) slightly inclined ground conditions (“gently sloping”), (B) horizontal ground surface with a vertical discontinuity (a “free-face”), and (C) horizontal ground surface and a liquefiable layer with an inclined lower boundary. Each case history consisted of a “segment” where the sliding could be regarded as one block. The geotechnical characteristics and measured displacements were then averaged across the segment. An empirical regression technique was applied to the database, the variable components of which were based on topographic and geologic descriptors (e.g. thickness of liquefiable layer,  $H$ , gradient of ground surface,  $\theta$ , etc.). The

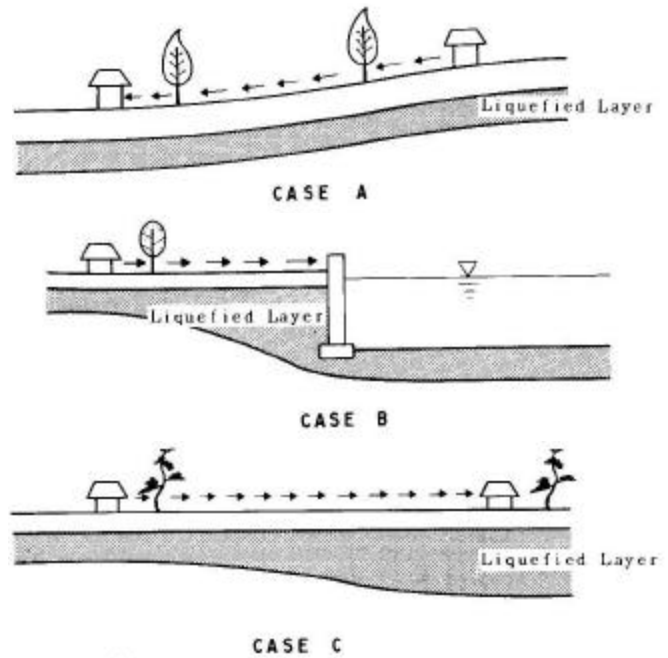


Fig. 57: Types of Permanent Lateral Ground Displacements (after Hamada et al., 1986)

result was a very simple predictive equation for lateral spread displacement as

$$D_H = 0.75 H^{0.5} \theta^{0.33} \quad [\text{Eq. 25}]$$

Bartlett and Youd (1992) built on Hamada’s empirical approach by: (1) adding additional case histories to the database, (2) changing the definition of a case history from the previously described “segments” to each individual measured displacement vector, and (3) adopting an expanded set of input variables into the predictive equation. Cases were divided into two types: (1) “gently sloping ground” cases, and (2) cases with a “free face”. Separate predictive equations for each of these two types of cases were then developed by multiple linear regression (MLR).

Youd et al. (2002), the most recent update to Youd’s body of work on lateral spread displacement prediction, corrects several errors in the original database and attempts to further optimize the variables used in the MLR predictive equations, as shown Equations 26(a) and 26(b).

(a) For free-face conditions:

$$\begin{aligned} \text{Log } D_H = & -16.713 + 1.532M - 1.406 \log R^* - 0.012R + 0.592 \log W \\ & + 0.540 \log T_{15} + 3.413 \log (100 - F_{15}) - 0.795 \log (D50_{15} + 0.1 \text{ mm}) \end{aligned} \quad [\text{Eq. 26(a)}]$$

(b) For gently sloping ground conditions:

$$\begin{aligned} \text{Log } D_H = & -16.213 + 1.532M - 1.406 \log R^* - 0.012R + 0.338 \log S + 0.540 \log T_{15} \\ & + 3.413 \log (100 - F_{15}) - 0.795 \log (D50_{15} + 0.1 \text{ mm}) \end{aligned} \quad [\text{Eq. 26(b)}]$$

For a description of the input variables, the reader is referred to Youd et al. (2002). Figure 45 shows the measured vs. predicted displacements from the revised Youd et al. work (using both equations, as appropriate to each individual case). Despite efforts to refine the MLR equations, the predictive capacity is largely within a factor of two for displacements of greater than about 1.5m., but is less accurate and reliable for smaller displacements. Because it is displacements of considerably less than 1m. that are of principal interest for most engineering applications, further developments are needed.

Bardet et al. (1999) built upon the Youd et al. corrected database, and used largely the same lateral spread case history database to develop a probabilistic model. This is a potentially valuable step because it casts the predictive equations in a probabilistic format, such that an analysis of lateral spreading could be folded into a probabilistic seismic hazard analysis framework. Bardet et al. also performed an additional regression on only that portion of Youd's database that represents displacements of less than two meters, reframing the problem of lateral spreading deformations to focus on "small to moderate" displacements.

Rauch and Martin (2000, 2001) took a good look at the phenomenon of liquefaction-induced lateral spreading, resulting in a fundamental step "backward" to the original Hamada work. Rauch and Martin built a new database of case histories where each lateral spread feature was represented as a single data point, characterized by a maximum and mean horizontal and vertical displacement, rather than using multiple individual displacement vectors at a single "feature" as independent data points. While this substantially reduces the number of case histories within the database, it is a fundamentally more sound approach, as adjacent displacement measurements are not statistically independent as simple statistical regression techniques would require.

Current research at UC Berkeley continues the advancement of the "Hamada"-type approach, i.e. empirical treatment of liquefaction-induced lateral spreading displacements. Building upon the viewpoint that a lateral spread is a single case, but internally addressing the variation of displacements across a given spreading feature, ongoing research at UC Berkeley breaks away from MLR statistical techniques and adopts the Bayesian methodology previously described in Section 3.1 (b) of this paper. This methodology allows for appropriate treatment of uncertainty and variability in the data, as well as in the modelling.

This research effort will also tailor the predictive equation form (an ability granted by the Bayesian methodology) to better account for principal factors affecting lateral spread displacements: (a) magnitude and duration, as represented by the magnitude-corrected duration-weighted cyclic shear ratio,  $CSR_{eq}$ , (b) distributed strain within the potentially liquefiable layer(s), as characterized and indexed to limiting shear strain potential index (SPI), and (c) cyclic strain accumulation attributed to interaction of cyclic loading with static driving

stress. Efforts will be made to combine the "free-face" and "gently sloping ground" conditions into one condition represented by a statically-induced shear strain normalized by effective overburden stress, similar to the treatment given to analyses of dams. The resulting model is expected to represent an improvement on several fronts through: (1) the utilization of engineering parameters that represent the principal factors affecting the problem of liquefaction-induced lateral spreading, (2) appropriate treatment of inherent variability and statistical/model uncertainty, and (3) sound calibration against field case histories of liquefaction-induced lateral spreading as represented by the case history database (estimated completion in about one year).

### 6.6.3 Finite Element and Finite Difference Analyses:

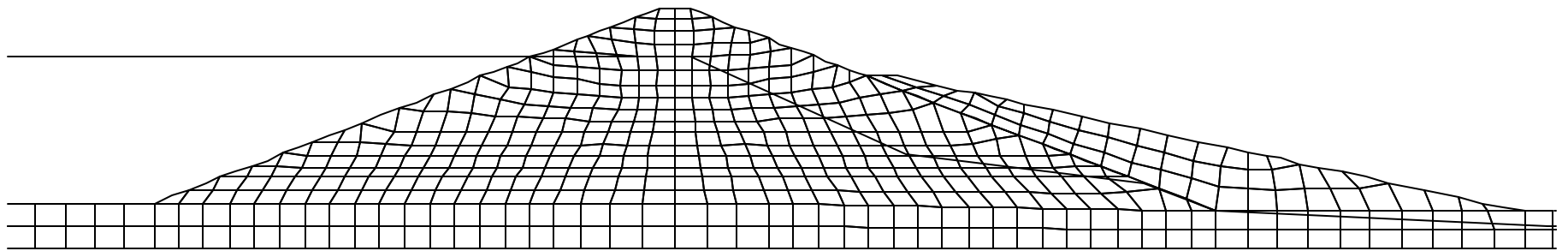
There are an increasing number of finite element (FEM) and finite difference (FDM) programs available, including both commercial and proprietary codes, for analysis of liquefaction-related problems. Both relatively simple, and more advanced and complex, constitutive and behavioral models continue to evolve for these applications. FEM and FDM analyses are increasingly being applied to significant projects including analyses of major earth and rockfill dams as well as complex soil/structure interaction problems including harbor frontages, quay wall systems, levees, bridge abutments and foundations, and pile and pier foundations in liquefiable ground.

As analytical models become more powerful and more complex, there is an increased need to "check" and calibrate these analyses against field case histories and against both simpler approximate analyses and engineering judgement on individual engineering projects.

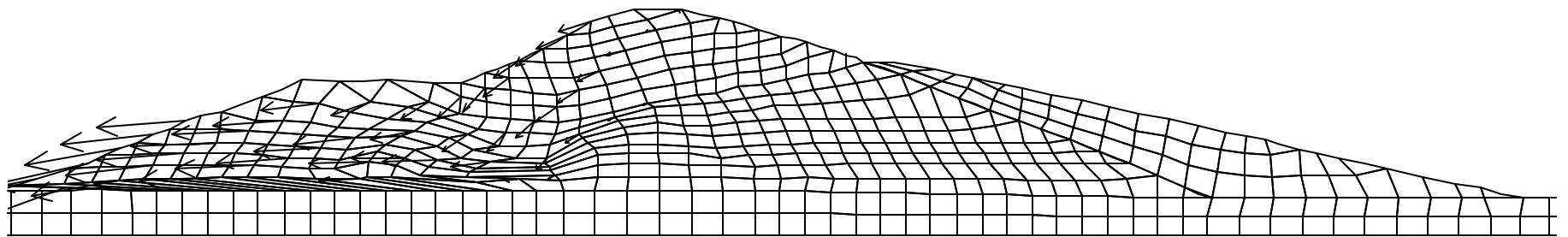
These types of analyses are typically "sensitive" to variations in one or more modelling parameters, and often to variations within the range of accuracy with which the key parameter(s) can be defined. It is important to check for these parameter sensitivities, and to account for the resulting range of analytical outcomes in engineering use of the results.

The San Fernando Dam case histories are a key suite of studies, and should be back-analyzed with any program intended for subsequent "forward" application to analyses of current dams. (These are also an important suite of case histories for calibration of more "simplified" analytical methods.) The San Fernando Dams essentially represent a suite of four case histories, as there are two dams (the Upper and Lower San Fernando Dams), and each dam has both an upstream and a downstream face. Performance of the dams in the earthquake is well-documented, and embankment and foundation soil conditions are also well-studied.

Figure 58 illustrates the use of finite difference analyses in back-analysis of the liquefaction-induced upstream slope stability failure of the Lower San Fernando Dam in the 1971 San Fernando Earthquake. The code used was a modified, proprietary version of the commercially available code FLAC

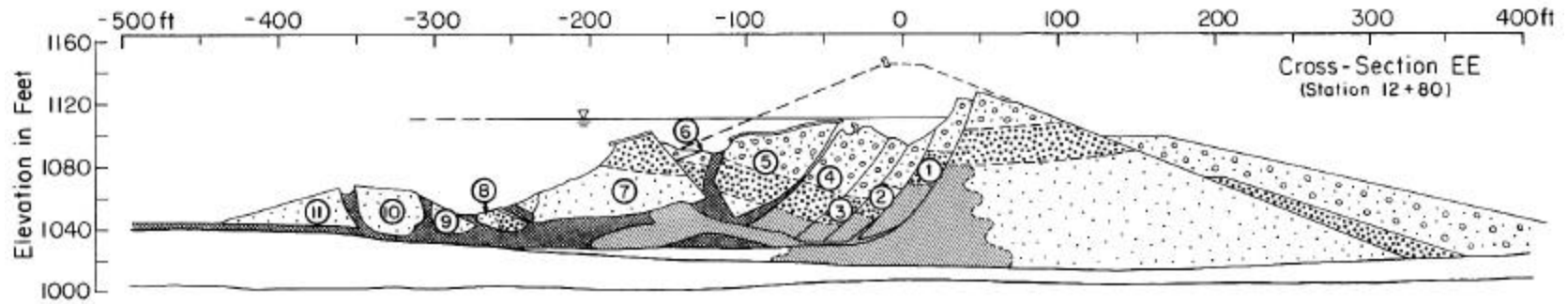


a) FLAC Mesh of Initial Conditions

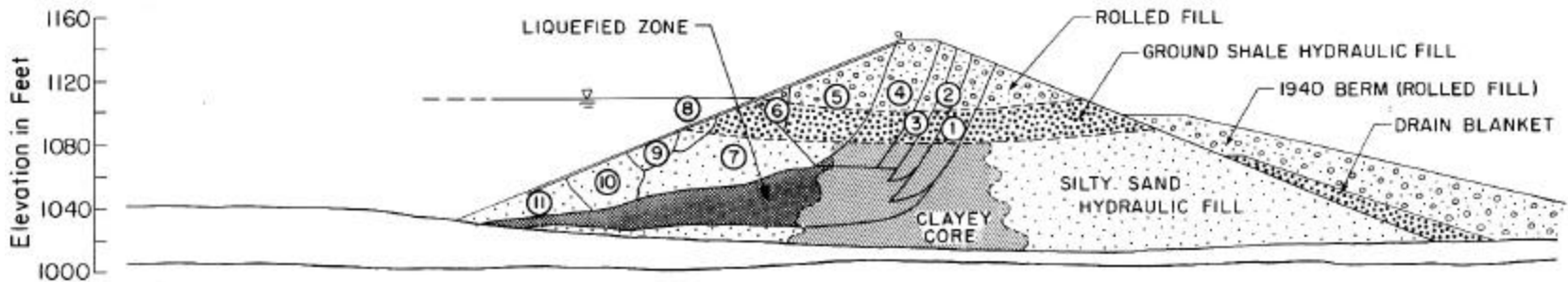


b) Final Configuration with Velocity Vectors

**Fig. 58: Finite Difference Analyses of the 1971 Liquefaction-Induced Upstream Slope Failure in the Lower San Fernando Dam (Beaty and Byrne: Beaty,2001)**



(a) Post-Failure Cross-Section



(b) Reconstruction of Conditions Prior to the Earthquake

Fig. 59: Cross-Sections Through the Lower San Fernando Dam Showing Conditions Before and After the Upslope Slope Failure (Seed et al., 1988)

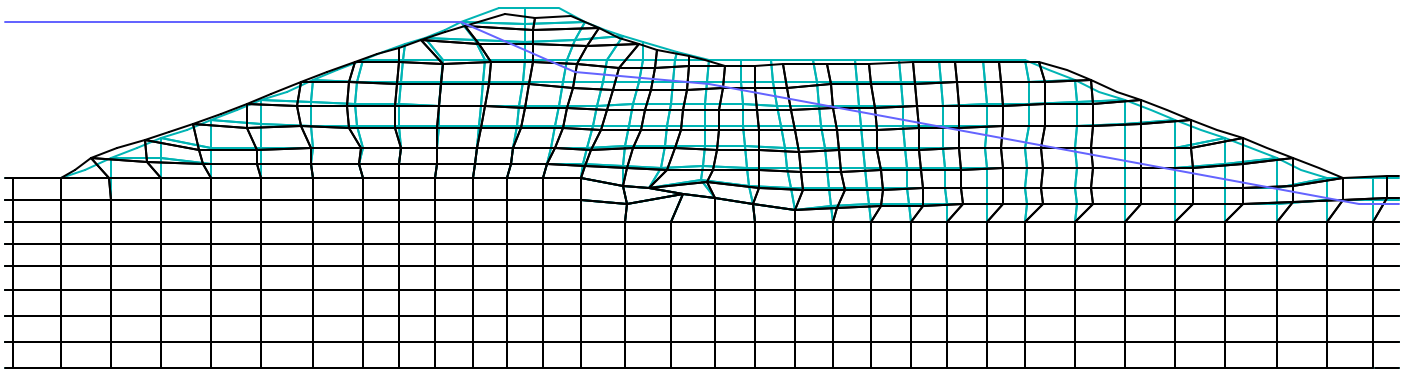


**Fig. 60: Finite Difference Mesh Showing Final Deformed Shape of Upper San Fernando Dam**

(Beatty and Byrne: Beatty, 2001)

(Beatty, 2001). The original code (Itasca Consulting Group, Inc., 2000) was modified to implement a new constitutive model and to facilitate improved treatment of post-liquefaction stress-deformation and residual strength behaviors.

The Lower San Fernando Dam was initially constructed by hydraulic fill methods, and was subsequently topped and buttresses by lesser rolled fill sections. Figure 59(a) shows a cross-section of soil conditions prior to the earthquake, and Figure 59(b) shows the deformed/displaced configuration after the upstream slope failure. It is well-known that the upstream face of the Lower Dam suffered a liquefaction-induced stability failure that resulted in large displacements (of up to 150 feet) back into the reservoir, and significant crest loss (~40 feet) as well.

Many analysis methods have successfully concluded that the upstream face would fail in this manner. What is more difficult, however, is to use the same analysis method to demonstrate that the downstream face does not fail at the same time. Differences between the soil properties and geometries of the upstream and downstream faces are relatively subtle, and many analyses either predict failure of both, or successful performance of both. The “correct” answer was a massive upstream failure, and limited movements of less than several feet on the downstream side.

Even more challenging, is to also use the same analytical tools to predict the performance of the Upper Dam as well. The Upper Dam was built with similar methods and materials, but with different geometry. The Upper Dam remained “stable”, suffering relatively minor lateral bulging at the lower faces on both the upstream and downstream sides, and attendant crest settlement of approximately 3 feet.

Figure 58(a) shows the original, pre-earthquake mesh used to back-analyze the performance of the Lower Dam. Figure 58(b) shows the deformed mesh, and displacement velocity vectors, at the point that the analysis was discontinued due to

excessive mesh distortion. These results indicate large deformations and displacements to the upstream side, and only limited displacements to the downstream side, in very good agreement with observed behavior.

It should be noted that the analysis of the Lower dam can be extended to larger total deformations by re-meshing, and then continuing the analysis. This can impose some degree of approximation in the analysis, but can also produce both useful and reasonable results.

Figure 60 shows analyses of the performance of the Upper Dam using the same FDM code and methods. The dashed lines show the pre-earthquake mesh configuration, and the solid lines show the final (post-earthquake) deformed mesh. Maximum movements in both the upstream and downstream directions, as well as the “predicted” crest slumping, were again in good general agreement with those actually observed.

When using these types of (FEM or FDM) procedures to analyze “expected” embankment deformations and displacements, it is important to recognize the strengths and shortcomings of these approaches, and also to cross-check the analyses against simpler analytical approaches. FEM and FDM analyses tend to be unable to adequately “localize” shear to a narrow shear band or slip surface in many cases of very large displacement. On the other hand, they can suitably model inertial and gravity “driving” forces as well as general strength/resistance to deformations, and can produce very reasonable predictions of the general magnitude and distribution of displacements. The details of shear displacements may be off, but these predictions can provide very useful engineering insight.

One important check of predictions of “large” liquefaction-induced displacements is to check the “static” factor of safety based on post-liquefaction undrained residual strengths (as discussed in Section 4.0). Because the slumping/deforming/sliding failure masses accumulate some velocity as they move,

the resultant accumulated momentum must be reversed as they are brought back to rest. As a result, these masses come to rest at an apparent “post-liquefaction” Factor of Safety of greater than 1.0, and values of FS = 1.05 to 1.2 are common for cases of large displacements. Checking the apparent “post-liquefaction” Factor of Safety of the final (predicted) deformed geometry can provide important insight regarding the reasonableness of the analytical results in such cases.

It should also be noted that even the most advanced FEM and FDM analysis methods cannot reliably predict the degree of local differential displacements of adjacent “blocks” along the embankment, and cannot therefore reliably serve to predict expected longitudinal and transverse cracking; these can be critical issues in evaluation of the ability of the embankment to safely retain the reservoir. Similarly, some judgement must also be applied in assessment of the likely height of the single lowest point of the crest after a design earthquake, as it is the single lowest point that defines available freeboard.

These same types of considerations apply to use of these methods for analysis of other types of problems and geometries, including soil/structure interaction applications. Limitations of the analytical models in terms of their accuracy and reliability, and their ability to model key details, must be assessed, and (1) the results need to be checked by simpler analytical approaches, and (2) significant judgement needs to be applied in evaluation and use of the results of advanced FEM or FDM analyses.

This paper cannot possibly go much deeper into this subject, so we will summarize by noting that the increased availability and power of FEM and FDM analysis tools does not reduce the importance of either (1) “simplified” analytical tools, or (2) engineering judgement. Instead, the power and complexity of these evolving analysis tools places an increased premium on judgement and cross-checking of the results of these more advanced analyses. Used with prudence and judgement, advanced (FEM and/or FDM) analysis tools can provide significant improved insight for many engineering problems.

## 7.0 MITIGATION OF LIQUEFACTION HAZARD

### 7.1 General:

When satisfactory performance of structures and/or other engineered facilities cannot adequately reliably be assured, engineered mitigation of the unacceptable liquefaction hazard is generally required. There are many methods, and variations on methods, currently available for this, and more are under development.

Table 3 presents a brief list of selected major mitigation methods available. It should be noted that these do not have to be employed singly; it can often be optimal to use two or more methods in combination.

It is not reasonable, within the constraints of this paper, to attempt a comprehensive discussion of all available mitigation

methods. Instead, limited comments will be offered regarding various aspects of some of these. It should be noted that mitigation of liquefaction hazard is an area subject to considerable controversy, and that our understanding of the efficacy of some of these methods is still evolving. It is suggested that key issues to be considered in selection and implementation of mitigation methods are: (1) applicability, (2) effectiveness, (3) the ability to verify the reliability of the mitigation achieved, (4) cost, and (5) other issues of potential concern (e.g.: environmental and regulatory issues, etc.). More comprehensive treatments of many of the mitigation methods listed in Table 3 are available in a number of references (e.g.: Mitchell et al., 1995; Hausmann, 1990).

The first class or category of methods listed in Table 3 involve surface compaction. When this is the case, potentially liquefiable soil types should be placed in layers and compacted, using vibratory compaction, to specifications requiring not less than 95% relative compaction based on the maximum dry density ( $\rho_{d,max}$ ) as determined by a Modified AASHTO Compaction Test (ASTM 1557D).

The second group of methods listed in Table 3 involves in-situ ground densification. It is recommended that these methods be coupled with a suitably comprehensive post-treatment verification program to assure that suitable mitigation has been achieved. CPT testing is particularly useful here, as it is rapid and continuous. When CPT is to be used for post-densification verification, it is a very good idea to establish pre-densification CPT data, and to develop site-specific cross-correlation between SPT and CPT data.

In addition, it should be noted that ageing effects (including establishment of microbonding and even cementation at particle contacts) is disrupted by in situ densification. These ageing effects increase both resistance to liquefaction, and also resistance to penetration (as measured by SPT, CPT, etc.) Immediately after in-situ densification, despite increased overall density of the soils, it is not unusual to find that penetration resistances have not increased nearly as much as expected, and in some cases they have even been observed to decrease slightly. Over subsequent weeks and months, however, as ageing effects re-establish themselves, penetration resistances generally continue to increase. A large fraction of ageing effects usually occur over the first 6 to 12 weeks after treatment, and penetration tests performed sooner than this can be expected to provide conservatively biased results.

In-situ vibrodensification, or compaction by means of vibratory probes, has been employed to depths of 70m. Difficulties in penetrating to depth through dense and/or coarse soils, and failure to deliver sufficient vibrational energy as to achieve adequate densification in the face of high overburden stresses, can limit the efficacy of these methods at the deepest of these depths. Vibroflotation, using vibroflots whose vibrational source is at the lower tip of the vibrating probe (within the ground), can generally deliver higher vibrational energy to greater depths than most other vibratory probe systems.

**Table 3: List of Selected Methods for Mitigation of Seismic Soil Liquefaction Hazard**

General Category	Mitigation Methods	Notes
I. Excavation and/or compaction	(a) Excavation and disposal of liquefiable soils (b) Excavation and recompaction (c) Compaction (for new fill)	
II. In-situ ground densification	(a) Compaction with vibratory probes (e.g.: Vibroflotation, Terraprobe, etc.) (b) Dynamic consolidation (Heavy tamping) (c) Compaction piles (d) Deep densification by blasting (e) Compaction grouting	-Can be coupled with installation of gravel columns  -Can also provide reinforcement
III. Selected other types of ground treatment	(a) Permeation grouting (b) Jet grouting (c) Deep mixing (d) Drains - Gravel drains - Sand drains - Pre-fabricated strip drains (e) Surcharge pre-loading (f) Structural fills	-Many drain installation processes also provide in-situ densification.
IV. Berms, dikes, sea walls, and other edge containment structures/systems	(a) Structures and/or earth structures built to provide edge containment and thus to prevent large lateral spreading	
V. Deep foundations	(a) Piles (installed by driving or vibration) (b) Piers (installed by drilling or excavation)	-Can also provide ground densification
VI. Reinforced shallow foundations	(a) Grade beams (b) Reinforced mat (c) Well-reinforced and/or post-tensioned mat (d) "Rigid" raft	

Vibrodensification is generally very effective in soils with less than about 5% clay fines, but can be ineffective in soils with larger fractions of clay fines. It had long been thought that the difficulty in vibrodensification of soils with high fines contents was related to the inability of water to escape, and indeed some improvement in densification of soils with high fines contents has been observed with the use of pre-installed wick drains to assist in allowing egress of water. It is noted, however, that the clay contents at which vibrodensification begins to be ineffective are at least somewhat similar to the

clay contents at which classic cyclically-induced liquefaction ceases to occur (see Figures 2 and 3). It appears likely that, as vibrodensification essentially works by liquefying and densifying the soils, the limit of "treatable" soil types is at least somewhat coincident with the types of soils that are "liquefiable", and thus in need of treatment.

Some of the vibrodensification methods also result in installation of dense gravel columns through the treated ground (vibro-replacement). It has been suggested that these

dense gravel columns, which have high shear moduli relative to the surrounding (treated) soils, will attract a large share of the earthquake-induced cyclic shear stresses propagating through the composite treated ground, and thus partially shield the softer surrounding soils from cyclic loading. This, in turn, would produce the added benefit of reducing the cyclic shear stress ratios (CSR) to which the treated soils would be subjected during an earthquake.

Estimates of the level of shear stresses borne by the dense gravel columns are sometimes computed by estimating the contributions of the stiffer columns and the softer surrounding soil, based on an assumption of a simple shear mode of deformation, and using contributory areas of the dense gravel columns and the surrounding soils and their respective shear moduli. Unfortunately, for column height to diameter ratios of greater than about three, the deformations of the gravel columns are dominated by flexure, rather than simple shear, and this renders them much “softer” than the above-described analyses would suggest. Indeed, the gravel columns generally provide relatively little “shielding” of the surrounding soils, and this hypothesized shielding effect can usually best be conservatively neglected.

Vibrodensification-installed gravel columns are also sometimes credited as serving as “drains” to rapidly dissipate seismically-induced excess pore pressures. This will be discussed a bit later under “Drains”.

Dynamic consolidation (or heavy tamping) involves raising a large mass to great height (with a crane), and then dropping it, producing both surface impact and vibrational compaction. The depth to which this can be effective is principally a function of the weight that can be raised, and the height from which it can be dropped. Good results can usually be achieved to depths of up to about 6 to 8m. with “conventional” equipment, and special purpose equipment has been built to extend these depths somewhat for individual, large projects. Dynamic consolidation is generally less expensive (per treated volume) than vibrodensification, but cannot reach to the same depths and is progressively less effective as depth increases. Other issues, including treatable soil types and post-treatment verification (including ageing effects) are largely as discussed previously for vibrodensification.

Compaction piles provide improvement by three mechanisms; (1) by densification due to driving installation, (2) by increasing lateral stresses, and (3) by providing structural reinforcing elements. This method is only rarely used, however, due to its cost. It is generally employed in unusual situations where other methods cannot reliably be implemented.

Blasting can be used to achieve deep densification of potentially liquefiable soils. This method, however, tends to produce less uniform densification than vibrodensification, and generally cannot reliably produce densities as high as those that can be obtained with high energy vibrodensification methods that effectively transmit high vibrational energy to

soils at depth (e.g. Vibroflotation, etc.) Blasting also raises environmental concerns, issues regarding propagation of vibrations across neighboring sites, and issues regarding noise and safety.

Compaction grouting is the last of the “in-situ ground densification” methods listed in Table 3, and is also the first of three “grouting” methods listed in this table. Compaction grouting involves injection of very stiff (low slump) cement grout into the ground at very high pressure, ideally forming “bulbs” of grout and displacing the surrounding soils. Compaction grouting works both by densifying soils, and by increasing in-situ effective lateral stresses. The degree of densification that can be achieved by the monotonic (non-cyclic) loading imposed by the growing grout mass is dilationally limited, however, and recent research suggests that the increased lateral stresses can relax over time. An additional drawback is the difficulty in verifying improvement by means of penetration testing. Compaction grouting performed well at one site in San Francisco during the 1989 Loma Prieta Earthquake, but the site was subjected to only moderate levels of shaking ( $a_{max} \sim 0.2g$ , and a relatively short duration of shaking). This method remains unproven at higher levels of shaking.

Permeation grouting involves injection of a grouting agent in a fluid form into the void spaces between the soil grains. A limitation of this method is the inability of even the most finely ground cement grouts to reliably penetrate into the voids of soils with greater than about 6 to 10% fines. As this can include silty fines, this leaves most silty soils potentially vulnerable to liquefaction. This is also problematic in sandy and silty soil deposits of variable fines content, a common situation. Chemical grouts are available that can more reliably penetrate into finer soils, but these are increasingly problematic with regard to environmental and regulatory issues. Another significant drawback with permeation grouting is the inability to know, with certainty, just where the grout has actually gone. This is exacerbated by the inability to “check” conditions after treatment, except by means of expensive borings, as the hardened grout impedes penetration of CPT. Finally, cost is usually very high.

Jet grouting is an attempt to achieve grout penetration by jetting at very high pressure from a rotating probe, as the probe is withdrawn. Ideally, this produces a cylindrical column of treated soil (or soil cement). Penetration of the jet varies with soil density and character, however, so that the diameter of the treated column can be uncontrollably variable. Coarse particles (gravelly and coarser) can fully deflect the jet, leaving untreated slivers in the treated column. As with permeation grouting, post-treatment “checking” is rendered difficult and expensive by the hardened treated column. This method is also expensive, and it is not economical to attempt to treat the full volume of liquefiable soil. Accordingly, treatment of overlapping columns is employed, as described below for deep soil mixing. Overall, jet grouting can be an uncertain process in variable cohesionless soils, and has been

supplanted to some extent by the more certain process of deep mixing for liquefaction applications.

Deep mixing involves the use of large augers both to introduce cement grout and to mix it with the soil, producing treated soil cement columns. This is essentially a brute force method, and it has a significant advantage over both permeation and jet grouting inasmuch as the injection and mixing process provides reliable treatment of a known volume of soil. The problem with deep mixing is that it is not economical to treat the full liquefiable soil volume. Accordingly, rows of slightly overlapping treated columns are used to create “walls”, and these are arranged in a cellular pattern (in plan), surrounding “cells” of untreated soil. The soils within the cells can still liquefy, however, especially when the “treatment ratio” (the ratio between treated soil volume, and the untreated volume within the cells) is low. Soils within the cells can also settle, producing differential settlements. This can, clearly, be an effective method, and performance was good at one site during the recent 1995 Kobe Earthquake. It is not known with any assurance, however, exactly what treatment ratios are required for various situations, and as the cost of treatment is relatively high, selection of treatment ratios has a tremendous impact on overall cost.

Drains are a very interesting and challenging method for mitigation of liquefaction hazard. An important potential drawback of this method is that it poses a “brittle” solution; it is effective only if it successfully promotes sufficiently rapid dissipation of pore pressures as to prevent the occurrence of liquefaction. If pore pressure dissipation is not sufficiently rapid during the relatively few critical seconds of the earthquake, however, this method does relatively little to improve post-liquefaction performance. An additional drawback is that, although it may prevent liquefaction, this method only reduces (but does not eliminate) settlements due to cyclic densification and reconsolidation after partial cyclic pore pressure generation.

A major difficulty in the use of drains is the need to assess the in-situ permeability of the soils to be drained. It is usually difficult to reliably assess the in-situ permeability of soils with an assured accuracy of better than about plus and minus one to two orders of magnitude, and this type of uncertainty can have a tremendous effect on the required spacing of drains. This is routinely exacerbated by the intrinsic in-situ variability in character (e.g.: fines content, etc.) of liquefiable soil deposits. It should also be noted that concerns regarding potential “plugging” of drains, either by formation of an external “skin” of transported fines, or by infiltration of transported fines into soil drains, is a risk that is difficult to quantify. When drains are installed by vibro-probes, without external filters, significant mixing of the coarse (and ostensibly free draining) drain soils and the (finer) surrounding soils routinely occurs, and this greatly reduces the drains’ ability to rapidly pass large volumes of water over the critical few seconds of an earthquake.

Drains, alone, can represent a difficult and uncertain mitigation approach. Many of the drain installation techniques employed also provide in-situ vibrodensification, however, and this can be a very attractive combination. As discussed previously, in-situ vibrodensification can be an effective mitigation method, and can be checked to verify post-treatment conditions. When coupled with drains, the drains can be useful in retarding the formation of “loose” zones and/or water blisters at the interfaces between layers of differing vertical permeability.

Surcharge pre-loading (Method III(e) in Table 3) induces increased vertical and horizontal effective stresses. When the surcharge is then removed, the resulting overconsolidation leaves the soil somewhat more resistant to triggering or initiation of liquefaction. The degree of increased liquefaction resistance that can be achieved is only moderate, however, and this is not generally an effective method in regions of high seismicity.

Structural fills can be used to increase the thickness of a non-liquefiable “crust” overlying potentially liquefiable soils (see Figures 26(c) and 29). These can be further improved by inclusion of horizontal layers of high-strength and ductile reinforcing mats, to minimize differential movements at the edges of “blocks” of intact crust and/or structural fill (see Figure 26(c)).

Structural fills can also be used to buttress free faces towards which lateral spreading otherwise might occur, and this leads naturally to the suite of methods in Group IV of Table 3. These methods involve creating secure containment of “edges” or free faces towards which liquefaction-induced lateral spreading might otherwise occur. The key here, of course, is to ensure that the containment system itself does not fail during the earthquake. These methods serve primarily to prevent “large” lateral spreading deformations; they are often less effective at reducing localized differential lateral and vertical movements and/or bearing settlements, so the acceptability of expected localized deformations after remediation must be checked.

The next two groups of mitigation methods in Table 3 are “structural” methods, and the first of these is the use of deep foundations (piles or piers). Piles or piers, safely bearing at depths below the occurrence of liquefaction (or significant cyclic softening due to partial liquefaction), can provide reliable vertical support and so can reduce or eliminate the risk of unacceptable liquefaction-induced settlements. Pile or pier foundations do not, however, necessarily prevent damages that may occur as a result of differential lateral structural displacements, so piles and/or piers must be coupled with sufficient lateral structural connectivity at the foundation as to safely resist unacceptable differential lateral displacements.

An additional concern, which prior to this past decade had been routinely neglected, is the need to ensure that the piles or piers themselves are not unacceptably damaged during seismic excitation. Numerous field cases of damage to piles during

earthquakes, dating back as far as the 1964 earthquakes in Alaska and Niigata (Japan), and continuing through the recent Kobe (Japan) and Chi Chi (Taiwan) Earthquakes, continue to emphasize the importance of this topic. Significant research efforts over the past 15 years have led to the development of a range of analytical methods for this problem, ranging from fully nonlinear, time domain, fully integrated soil/pile/superstructure interaction analyses to considerably simpler analyses based on separate assessment of expected site response and resultant pile (or pier) loadings (e.g.: Pestana, 2001). These types of methods, complemented with appropriate conservatism, can provide a suitable basis for analysis of this issue, and for the design and detailing of piles (or piers) and pile/cap connections.

The second group of “structural” mitigation methods in Table 3 involves the use of very stiff, reinforced shallow foundations to resist differential lateral and vertical displacements. Japanese practice has increasingly employed both grade beams and continuous reinforced foundations for low to moderate height structures, and performance of these types of systems in earthquakes has been good. The strength and stiffness of both grade beams and reinforced continuous foundations used in Japan for this purpose are higher than those often used in U.S. practice, however, and standards for design of these are lacking in the U.S., so that engineering judgement is required here.

Stiff, shallow foundations can be designed to adequately resist unacceptable flexure and resultant “wrecking” of the structure, but it should be noted that differential settlements can still result in rotational “tilting” of the structure. A number of methods have been developed to re-level such structures after earthquake-induced settlements, including careful micro-underexcavation (extraction of soil by horizontal borings), and successful re-leveling of a pair of large (12-story) reinforced concrete apartment buildings in Nantou, Taiwan after the 1999 Chi-Chi Earthquake suggests that these methods are more adaptable than had previously been expected.

## 7.2 Assessment of Mitigation:

It is important to assess the expected performance of the mitigated situation. This involves returning to the top of the framework illustrated in Figure 1, and again progressing through the various steps to assess the expected performance of the mitigated site and/or system, and the adequacy of this expected performance. It is no longer acceptable practice to simply implement mitigation; the adequacy of the mitigation must also be evaluated.

## 8.0 SUMMARY AND CONCLUSIONS

There have been major advances in seismic soil liquefaction engineering over the past decade. These advances have been spurred in no small part by lessons and data provided by earthquakes that have occurred over the past 15 years, as well

as by the research efforts and professional will borne of these events. The advances achieved have, importantly, affected practice as well as research, and soil liquefaction engineering has now grown into a semi-mature field in its own right.

As important and heartening as the recent advances in this field are, however, more needs to be done. Major recent, and ongoing, advances are significantly improving our ability to predict the probability of “triggering” or initiation of soil liquefaction, but major gaps continue to persist with regard to our ability to accurately and reliably assess the likely consequences of liquefaction. This is particularly true for situations in which structural and/or site displacements and deformations are likely to be “small to moderate” ( $\leq 0.75m$ ). Improved analytical and design tools, and improved understanding of what constitutes “acceptable” performance, are urgently needed here.

The rapid rate of progress in liquefaction engineering can be confidently expected to continue in the years ahead. Significant research efforts are currently underway, literally around the world, to address all of these urgent needs. Over the next 3 to 5 years, engineers can expect to see the results of these efforts begin to make their way into practice.

We can also expect a need to provide improved assessments of expected performance in response to the evolving new questions being raised in the name of “performance-based” engineering. Performance-based predictions are not new to geotechnical engineers, but the levels of refinement (in terms of increased accuracy and increased reliability) beginning to be sought are new to the general area of liquefaction engineering, and will continue to pose a new set of challenges.

In summary, the past decade has seen a laudable rate of improvements in practice, and more of the same can be expected over the next 3 to 5 years. Indeed, further advances will be needed to keep pace with the increased demands being generated by the ongoing shift in practice towards increasingly performance-based design.

## ACKNOWLEDGEMENTS

The authors wish to acknowledge the many dedicated and insightful individuals who have collaborated in fomenting many of the advances chronicled in this paper. We are grateful to Prof’s. Armen Der Kiureghian, Khoji Tokimatsu and Jon Stewart as well as Dr. Les Harder for their work on the new SPT-based triggering correlation, and Prof’s Les Youd, Kohji Tokimatsu and Jon Stewart as well as Mr. Daniel Chu for their assistance in development of the new CPT-based correlation. We are also grateful for discussions and sharing of ideas with many researchers; it is often the sharing of ideas, and even debate, that leads to important progress. Finally, we are also grateful for continued support for much of this work through the Pacific Earthquake Engineering Research Center (PEER) Lifelines Research Program, without which much of this would not have been possible.

## REFERENCES

- Ambraseys, N. N. (1988). "Engineering Seismology." *Earthquake Engineering and Structural Dynamics*, Vol. 17, pp. 1-105.
- Andrews, D. C. A. and Martin, G. R. (2000). "Criteria for Liquefaction of Silty Soils." 12<sup>th</sup> World Conference on Earthquake Engineering, Proceedings, Auckland, New Zealand.
- Andrus, R. D. (1994). "In situ characterization of gravelly soils that liquefied in the 1983 Borah Peak Earthquake." Ph.D. Dissertation, University of Texas at Austin.
- Andrus, R.D. and Stokoe, K.H (1997). "Liquefaction Resistance Based on Shear Wave Velocity." Proc., NCEER Workshop on Evaluation of Liquefaction Resistance of Soils, NCEER-97-0022.
- Andrus, R.D. and Stokoe, K.H., (2000). "Liquefaction Resistance of Soils from Shear-Wave Velocity." *Journal of Geotechnical and Geoenvironmental Engineering*, Vol. 126, No. 11, pp. 1015-1025.
- Arango, I. (1996). "Magnitude Scaling Factors for Soil Liquefaction Evaluations." *Journal of Geotechnical Engineering*, Vol. 122, No. 11, pp. 929-936.
- Arulanandan, K. and Symbico, J. (1993). "Post-Liquefaction Settlement of Sands." *Predictive Soil Mechanics: Proceedings of the Wroth Memorial Symposium held at St. Catherine's College, Oxford, July 27-29, Thomas Telford, London*, pp. 94-110.
- Bardet, J.P., Mace, N., Tobita, T., and Hu, J. (1999a). "Large-Scale Modeling of Liquefaction-Induced Ground Deformation Part I: A Four-Parameter MLR Model." Proceedings of the Seventh U.S.-Japan Workshop on Earthquake Resistant Design of Lifeline Facilities and Countermeasures Against Soil Liquefaction, Technical Report No. MCEER-99-0019, Mid-America Center for Earthquake Engineering Research, Buffalo, N.Y.
- Bardet, J.P., Mace, N., Tobita, T., and Hu, J. (1999b). "Large-Scale Modeling of Liquefaction-Induced Ground Deformation Part II: MLR Model Applications and Probabilistic Model." Proceedings of the Seventh U.S.-Japan Workshop on Earthquake Resistant Design of Lifeline Facilities and Countermeasures Against Soil Liquefaction, Technical Report No. MCEER-99-0019, Mid-America Center for Earthquake Engineering Research, Buffalo, N.Y.
- Bartlett, S. F. and Youd, T.L. (1992). "Empirical Analysis of Horizontal Ground Displacement Generated by Liquefaction-Induced Lateral Spread." Technical Report No. NCEER-92-0021, National Center for Earthquake Engineering Research, Buffalo, N.Y.
- Bartlett, S.F. and Youd, T.L. (1995). "Empirical Prediction of Liquefaction-Induced Lateral Spread." *Journal of Geotechnical Engineering*, Vol. 121, No. 4, pp. 316-329.
- Beaty, M. H. and Byrne, P.M. (1998). "An Effective Stress Model for Predicting Liquefaction Behaviour of Sand." *Geotechnical Special Publication No. 75, Proceedings of a Specialty Conference on Geotechnical Earthquake Engineering and Soil Dynamics III*, pp. 766-777.
- Beaty, M. H. (2001). "A Synthesized Approach for Estimating Liquefaction-Induced Displacements of Geotechnical Structures." Ph. D. Thesis. University of British Columbia, Vancouver, Canada.
- Boulanger, R. W. and Seed, R. B. (1995). "Liquefaction of Sand Under Bi-directional Monotonic and Cyclic Loading." *Journal of Geotechnical Engineering*, Vol. 121, No. 12, pp. 870-878.
- Boulanger, R. W. (2003). "High Overburden Stress Effects in Liquefaction Analyses." *Journal of Geotechnical and Geoenvironmental Engineering*, accepted in press.
- Bray, J.D. and Stewart, J.P., coordinators (2000). "Damage Patterns and Foundation performance in Adapazari." Kocaeli, Turkey Earthquake of August 17, 1999 Reconnaissance Report, T.L. Youd, J.P. Bardet, and J.D. Bray, eds., *Earthquake Spectra, Supplement A to Vol. 16*, 163-189.
- Bray, J. D., Sancio, R. B., Durgunoglu, H. T., Onalp, A., Seed, R. B., Stewart, J. P., Youd, T. L., Baturay, M. L., Cetin, K. O., Christensen, C., Karadayilar, T., and Emrem, C. (2001). "Ground Failure In Adapazari, Turkey." Proceedings of Earthquake Geotechnical Engineering Satellite Conference of the XVth International Conference on Soil Mechanics & Geotechnical Engineering, Istanbul, Turkey, August 24-25.
- Bray, J. D., Sancio, R. B., Durgunoglu, T., Onalp, A., Youd, T. L., Stewart, J. P., Seed, R. B., Cetin, K. O., Bol, E., Baturay, M. B., and Christensen, C. (2003). "Subsurface Characterization at Ground Failure Sites in Adapazari, Turkey." *Journal of Geotechnical and Geoenvironmental Engineering*, submitted.
- Cao, L. F., Teh, C. I., and Chang, M. F. (2001). "Undrained Cavity Expansion in Modified Cam Clay I: Theoretical Analysis." *Geotechnique*, Vol. 51, No. 4, pp. 323-334.
- Cetin, K. O. (2000). "Reliability-Based Assessment of Seismic Soil Liquefaction Initiation Hazard." Dissertation in partial fulfillment for the degree of doctor of philosophy, University of California, Berkeley.
- Cetin, K.O. & Seed, R.B. (2000). "Earthquake-Induced Nonlinear Shear Mass Participation Factor (rd)." *Geotechnical Engineering Research Report No. UCB/GT-2000/08*, University of California, Berkeley.

- Cetin, K. O. and Seed, R. B. (2001). "Nonlinear Shear Mass Participation Factor ( $R_d$ ) For Cyclic Shear Stress Ratio Evaluation." Research Report No. UCB/GT-2000/08, University of California, Berkeley.
- Cetin, K.O., Der Kiureghian, A., & Seed, R.B. (2002). "Probabilistic Models for the Initiation of Seismic Soil Liquefaction." *Structural Safety*, Vol. 24, pp. 67-82.
- Chang, W. S., Bray, J. D., Gookin, W. B., and Riemer, M. F. (1997). "Seismic Response Of Deep Stiff Soil Deposits in the Los Angeles, California Area During The 1994 Northridge, Earthquake." Geotechnical Research Report No. UCB/GT/97-01, University of California, Berkeley.
- Evans, M. D. (1987). "Undrained Cyclic Triaxial Testing of Gravels : the Effect of Membrane Compliance." Ph.D. Thesis, University of California, Berkeley.
- Finn, W. D. L., Ledbetter, R. H., and Beratan, L. L. (1986). "Seismic Soil-Structure Interaction: Analysis and Centrifuge Model Studies." *Nuclear Engineering and Design*, Vol. 94, No. 1, pp. 53-66.
- Finn, W. D. L., Ledbetter, R. H., and Wu, G. (1994). "Liquefaction in Silty Soils: Design and Analysis." *Ground Failures under Seismic Conditions*, Geotechnical Special Publication 44, ASCE, New York, pp. 51-76.
- Finn, W. D. L. (1998) "Seismic Safety of Embankment Dams Development in Research and Practice 1988-1998." Geotechnical Special Publication No. 75, Proceedings of a Specialty Conference on Geotechnical Earthquake Engineering and Soil Dynamics III, pp. 812-853.
- France, J. W., Adams, T., Wilson, J., and Gillette, D. (2000). "Soil Dynamics and Liquefaction", Geotechnical Special Publication No. 107, ASCE.
- Geyskens, P., Der Kiureghian, A., Monteiro, P. (1993), "Bayesian Updating of Model Parameters", *Structural Engineering Mechanics and Materials Report No. UCB/SEMM-93/06*, University of California at Berkeley.
- Hamada, M., Yasuda, S., Isoyama, R., and Emoto, K. (1986). "Study On Liquefaction Induced Permanent Ground Displacements", Report of the Association for the Development of Earthquake Prediction in Japan, Tokyo Japan.
- Hamada, M., O'Rourke, T. D., and Yoshida, N. (1994). "Liquefaction-Induced Large Ground Displacement." Performance of Ground and Soil Structures during Earthquakes: Thirteenth International Conference on Soil Mechanics and Foundation Engineering, New Delhi, Proceedings, Japanese Society of Soil Mechanics and Foundation Engineering, Tokyo, p. 93-108.
- Harder, L. F. Jr. (1977). "Liquefaction of Sand under Irregular Loading Conditions." M.S. Thesis, University of California, Davis.
- Harder, L. F. Jr. (1988). "Use of Penetration Tests to Determine the Cyclic Loading Resistance of Gravelly Soils During Earthquake Shaking." Ph.D. Thesis, University of California, Berkeley.
- Harder, L. F. Jr. (1997). "Application of the Becker Penetration Test for Evaluating the Liquefaction Potential of Gravelly Soils." Proc., NCEER Workshop on Evaluation of Liquefaction Resistance of Soils, NCEER-97-0022.
- Harder, L. F. Jr. and Boulanger, R. (1997). "Application of  $K_\sigma$  and  $K_\alpha$  Correction Factors." Proc., NCEER Workshop on Evaluation of Liquefaction Resistance of Soils, NCEER-97-0022.
- Hausmann, M. R. (1990). *Engineering Principals of Ground Modification*, McGraw Hill, pp. 632.
- Hazen, A. (1918). "A Study of the Slip in the Calaveras Dam." *Engineering News Record*, Vol. 81, No. 6, pp. 1158-1164.
- Hynes, M. E. (1988). "Pore Pressure Generation Characteristics of Gravel under Undrained Loading." Ph.D. Thesis, University of California, Berkeley.
- Idriss, I. M., Sun, J. I., (1992). "Users Manual for SHAKE91, A Computer Program for Conducting Equivalent Linear Seismic Response Analyses of Horizontally Layered Soil Deposits, Program Modified Based on the Original SHAKE Program Published in December 1972, by Schnabel, Lysmer and Seed, August.
- Idriss, I. M. (2000). "Personal Communication"
- Idriss, I.M. (2002). Notes from CDMG-sponsored professional continuing education short-course on "Evaluation and Mitigation of Seismic Soil Liquefaction and Seismic Slope Instability and Slope Deformation Hazard." Univ. of Calif. Extension, Berkeley, Calif., August 8 – 10.
- Ishihara, K. (1985). "Stability Of Natural Deposits During Earthquakes." 11th International Conference on Soil Mechanics and Foundation Engineering, Proceedings, San Francisco, Vol. 1, pp. 321-376.
- Ishimara, K. and Yoshimine, M. (1992). "Evaluation of Settlements in Sand Deposits Following Liquefaction During Earthquakes." *Soils and Foundations*, Vol. 32, No. 1, March, pp. 173-188.
- Ishihara, K. (1993). "Liquefaction And Flow Failure During Earthquakes: Thirty-Third Rankine Lecture." *Geotechnique*, Vol. 43, No. 3, pp. 351-415.

Itasca Consulting Group, Inc., (2000) "FLAC Version 4.0-Fast Lagrangian Analysis of Continua- User's Manual."

Jong, H.L. and Seed, R. B. (1988). "A Critical Investigation of Factors Affecting Seismic Pore Pressure Generation and Post-Liquefaction Flow Behavior of Saturated Soils." Geotechnical Engineering Research Report No. SU/GT/88-01, Stanford University.

Juang, C.H., Yuan, H., Lee, D.-H., and Lin, P.-S. (2003). "Simplified Cone Penetration Test-based Method for Evaluating Liquefaction Resistance of Soils." Journal of Geotechnical and Geoenvironmental Engineering, Vol. 129, No. 1, pp. 66-80.

Kammerer, A., Pestana, J., and Seed, R. (2002). "Undrained Response of 0/30 Sand Under Multidirectional Cyclic Simple Shear Loading Conditions." Geotechnical Engineering Research Report No. UCB/GT/02-01, University of California, Berkeley, July, 2002.

Kishida, H. (1966), "Damage to Reinforced Concrete Buildings in Niigata City with Special Reference to Foundation Engineering", Soils and Foundations, Vol. VII, No. 1.

Koizumi, Y (1966). "Change in Density of Sand Subsoil caused by the Niigata Earthquake", Soils and Foundations, Vol. VIII, No. 2, pp. 38-44.

Ladanyi, B. and Johnston, G. H. (1974). "Behavior of Circular Footings and Plate Anchors Embedded in Permafrost." Canadian Geotechnical Journal, 11, 531-553.

Liao, S. S. C., and Whitman, R. V. (1986). "Overburden Correction Factor for SPT in Sand." Journal of Geotechnical Engineering, Vol. 112, No. 3, March 1986, pp. 373-377.

Liao, S. S. C., Veneziano, D., and Whitman, R.V. (1988). "Regression Models for Evaluating Liquefaction Probability." Journal of Geotechnical Engineering, Vol. 114, No. 4, pp. 389-409.

Liao, S. S. C., and Lum, K. Y. (1998). "Statistical Analysis and Application of the Magnitude Scaling Factor in Liquefaction Analysis." Geotechnical Earthquake Engineering and Soil Dynamics III, Vol. 1, 410-421.

Martin, G.R. and Lew, M., eds. (1999) "Recommended Procedures for Implementation of DMG Special Publication 117: Guidelines for Analyzing and Mitigating Liquefaction Hazards in California," Southern California Earthquake Center, Univ. of Southern Calif., March.

Mitchell, J. K., Baxter, C. D. P., and Munson, T. C. (1995). "Performance of Improved Ground during Earthquakes." Soil Improvement for Earthquake Hazard Mitigation, ASCE, New York, 1-36.

Moss, R.E.S. (2003). "CPT-Based Probabilistic Assessment of Seismic Soil Liquefaction Initiation." Dissertation in partial fulfillment of the requirements for the degree of Doctor of Philosophy, University of California, Berkeley, in preparation.

Muraleetharan, K.K., Seed, R.B., Kabilamany, K. (1993). "Centrifuge Study of Volume Changes and Dynamic Stability of Earth Dams." Journal of Geotechnical Engineering, Vol. 119, No. 11, pp. 1717-1731.

NCEER (1997). "Proceedings of the NCEER Workshop on Evaluation of Liquefaction Resistance of Soils." Edited by Youd, T. L., Idriss, I. M., Technical Report No. NCEER-97-0022, December 31, 1997.

Ohsaki, Y. (1966). "Niigata Earthquakes, 1964, Building Damage and Soil Conditions", Soils and Foundations, Vol. 6, No. 2, pp. 14-37.

Olivia Chen Consultants, Inc. (2003). "Report on the Seismic Stability of Calaveras Dam", report prepared for the San Francisco Public Utilities Commission, Utilities Engineering Bureau.

Olsen, R. S. and Mitchell, J. K. (1995). "CPT Stress Normalization and Prediction of Soil Classification." International Symposium on Cone Penetration Testing, CPT 95 Linköping, Sweden, pp. 257-262.

Poulos, S. J., Castro, G., and France, J. W. (1985). "Liquefaction Evaluation Procedure." Journal of Geotechnical Engineering, Vol. 111, No. 6, pp. 772-792.

Rauch, A.F. and Martin II, J.R. (2000). "EPOLLS Model for Predicting Average Displacements on Lateral Spreads." Journal of Geotechnical and Geoenvironmental Engineering, Vol. 126, No. 4, pp. 360-371.

Rauch, A.F. and Martin II, J.R. (2001). "Prediction the Maximum and Distribution of Displacements on Liquefaction-Induced Lateral Spreads." Proceedings: Fourth International Conference on Recent Advances in Geotechnical Earthquake Engineering and Soil Dynamics, San Diego, California.

Riemer, M. F. (1992). "The Effects of Testing Conditions on the Constitutive Behavior of Loose, Saturated Sands under Monotonic Loading." Ph.D. Thesis, University of California, Berkeley.

Riemer, M. F., Seed, R. B., and Sadek, S. (1993). "The SRS/RFT Soil Evaluation Testing Program." University of California, Berkeley Geotechnical Report No. UCB/GT-93/01.

Riemer, M.F., and Seed, R.B. (1997). "Factors Affecting Apparent Position of Steady-State Line", Journal of Geotechnical and Geoenvironmental Engineering, Vol 123, No. 3, pp. 281-288.

- Robertson, P. K. and Wride, C. E. (1997). "Cyclic Liquefaction and its Evaluation Based on the SPT and CPT." NCEER-97-0022, Proceedings of the NCEER Workshop on Evaluation of Liquefaction Resistance of Soils.
- Robertson, P. K. and Wride, C. E. (1998). "Evaluating Cyclic Liquefaction Potential Using The Cone Penetration Test." Canadian Geotechnical Journal, Vol. 35, No. 3, pp. 442-459.
- Salgado, R. and Randolph, M. F. (2001). "Analysis of Cavity Expansion in Sand." International Journal of Geomechanics, Vol. 1, No. 2, pp. 175-192.
- Sancio, R. B., Bray, J. D., Stewart, J. P., Youd, T. L., Durgunoglu, H. T., Onalp, A., Seed, R. B., Christensen, C., Baturay, M. B., and Karadayilar, T. (2002). "Correlation between ground failure and soil condition in Adapazari, Turkey." Soil Dynamics and Earthquake Engineering, 22, 1093-1102.
- Sancio, R. B. (2003). "Ground Failure and Building Performance in Adapazari, Turkey", Ph.D. Dissertation (in progress), supervised by Prof. J.D. Bray, University of California, Berkeley.
- Sancio, R. B., Bray, J. D., Riemer, M. F., and Durgunoglu, H. T. (2003). "An Assessment of the Liquefaction Susceptibility of Adapazari Silt." Paper 172, Pacific Conference on Earthquake Engineering, Proceedings, New Zealand
- Seed, H. B. and Idriss, I. M. (1971). "Simplified Procedure for Evaluating Soil Liquefaction Potential", Journal of the Soil Mechanics and Foundations Division, ASCE, Vol. 97, No SM9, Proc. Paper 8371, September 1971, pp. 1249-1273.
- Seed, H.B. (1979). "Considerations in the earthquake-resistant design of earth and rockfill dams", Geotechnique, Vol. XXIX, No. 3, pp. 213-263.
- Seed, H.B. and Idriss, I.M. (1982). "Ground motion and soil liquefaction during earthquakes", Monograph, Earthquake Engineering Research Institute, Oakland, Ca.
- Seed, H. B., Tokimatsu, K., Harder, L. F., Chung, R. M. (1984). "The Influence of SPT Procedures in Soil Liquefaction Resistance Evaluations", Earthquake Engineering Research Center Report No. UCB/EERC-84/15, University of California at Berkeley, October, 1984.
- Seed, H. B., Tokimatsu, K., Harder, L. F., and Chung, R. M. (1985). "Influence of SPT Procedures in soil liquefaction resistance evaluations." Journal of Geotechnical Engineering, ASCE, 111(12), 1425-1445.
- Seed, H. B., Seed, R. B., Harder, L. F., and Jong, H. L. (1988). "Re-evaluation of the Slide in the Lower San Fernando dam in the 1971 San Fernando earthquake", Earthquake Engineering Research Center Report No. UCB/EERC-88/04, University of California, Berkeley.
- Seed, R. B. and Harder, L. F. (1990). "SPT-Based Analysis Of Cyclic Pore Pressure Generation And Undrained Residual Strength." H.B. Seed Memorial Symposium, Berkeley, Ca., BiTech Publishing, Ltd., v. 2, p. 351-376.
- Seed, R. B., Chang, S. W., Dickenson, S. E., and Bray, J. D. (1997). "Site-Dependent Seismic Response Including Recent Strong Motion Data." Proc., Special Session on Earthquake Geotechnical Engineering, XIV International Conf. On Soil Mechanics and Foundation Engineering, Hamburg, Germany, A. A. Balkema Publ., Sept. 6-12, pp. 125-134.
- Seed, R. B., Cetin, K. O., Moss, R. E S., Kammerer, A. M., Wu, J., Pestana, J. M., and Riemer, M. F. (2001). "Recent Advances in Soil Liquefaction Engineering and Seismic Site Response Evaluation." 4th Int. Conf. Recent Advances in Geotechnical Earthquake Engineering and Soil Dynamics, San Diego, California, March.
- Seed, R. B., Cetin, K. O., Der Kiureghian, A., Tokimatsu, K., Harder, L. F. Jr., Kayen, R. E., and Moss, R. E. S. (2002). "SPT-Based Probabilistic and Deterministic Assessment of Seismic Soil Liquefaction Potential." Journal of Geotechnical and Geoenvironmental Engineering, accepted, in-press.
- Shamoto, Y., Zhang, J.-M., and Tokimatsu, K. (1998). "Methods for evaluating residual post-liquefaction ground settlement and horizontal displacement." Soils and Foundations, Special Issue, 69-83.
- Shibata, T. and Teparaksa, W. (1988). "Evaluation of Liquefaction Potentials of Soils using Cone Penetration Tests." Soils and Foundations, Vol. 28, No. 2, pp. 49-60.
- Stark, T. D. and Mesri, G. (1992). "Undrained Shear Strength of Liquefied Sands For Stability Analysis." Journal of Geotechnical Engineering, ASCE, 118(11), 1727-1747.
- Suzuki, Y., Tokimatsu, K., Koyamada, K., Taya, Y., and Kubota, Y. (1995). "Field Correlation of Soil Liquefaction Based on CPT Data." International Symposium on Cone Penetration Testing, CPT 95 Linkoping, Sweden.
- Sy, A. and Campanella, R. G. (1994). "Becker and Standard Penetration Tests (BPT-SPT) Correlations with Consideration of Casing Friction", Canadian Geotechnical Journal, Vol. 31, No. 3, pp. 343-356.
- Sy, A. (1997). "Recent Developments in the Becker Penetration Test; 1986-1996", 20<sup>th</sup> Canadian Geotechnical Colloquium, Richmond, Canada, pp. 952-973.
- Tokimatsu, K., and Seed, H. B. (1987). "Evaluation of Settlements in Sands due to Earthquake Shaking." Journal of Geotechnical Engineering, Vol. 113, No. 8, pp. 861-878.
- Toprak, S., Holzer, T. L., Bennett, M. J., Tinsley, J. C. (1999). "CPT- and SPT-based Probabilistic Assessment of Liquefaction Potential, Proceedings of Seventh U.S.-Japan

Workshop on Earthquake Resistant Design of Lifeline Facilities and Countermeasures Against Liquefaction.

Vaid, Y.P., Chung, E.K.F., and Kuerbis, R.H. (1990). "Stress path and steady state." *Canadian Geotechnical Journal*, 27, 1-7.

Von Thun, J. L. (1986). "Analysis of Dynamic Compaction Foundation Treatment Requirements, Stage I, Jackson Lake Dam", Technical Memo No. TM-JL-230-26, Bureau of Reclamation, Engineering and Research Center, Embankment Dams Branch.

Vreugdenhil, R., Davis, R., and Berrill, J. R. (1994). "Interpretation of Cone Penetration Results in Multilayered Soils." *International Journal for Numerical and Analytical Methods in Geomechanics*, 18, 585-599.

Wang, W. (1979.) "Some Findings in Soil Liquefaction", Research Report, Water Conservancy and Hydroelectric Power Scientific Research Institute, Beijing, August.

Wu, J. (2003). "Liquefaction Triggering and Post Liquefaction Deformations of Monterey 0/30 Sand Under Uni-Directional Cyclic Simple Shear Loading." Dissertation in partial fulfillment for the degree of doctor of philosophy, University of California, Berkeley.

Yoshimi, Y., Tokimatsu, K., Ohara, J. (1994). "In-situ Liquefaction Resistance of Clean Sands Over a Wide Density Range", *Geotechnique*, Vol. 44, No. 3, pp. 479-494.

Youd, T. L., Idriss, I. M., Andrus, R. D., Arango, I., Castro, G., Christian, J. T., Dobry, R., Finn, W. D. L., Harder, L. F. Jr., Hynes, M. E., Ishihara, K., Koester, J. P., Liao, S. S. C., Marcuson, W. F. III., Martin, G. R., Mitchell, J. K., Moriwaki,

Y., Power, M. S., Robertson, P. K., Seed, R. B., and Stokoe, K. H., II. (1997). Summary Paper, Proc., NCEER Workshop on Evaluation of Liquefaction Resistance of Soils, NCEER-97-0022.

Youd, T. L., Noble, S. K. (1997). "Liquefaction Criteria Based on Statistical and Probabilistic Analyses", Proceedings of the NCEER Workshop on Evaluation of Liquefaction Resistance of Soils, December 31, 1997, pp. 201-205.

Youd, T. L. (2000). Personal Communication.

Youd, T.L., I. M. Idriss, Ronald D. Andrus, Ignacio Arango, Gonzalo Castro, John T. Christian, Richardo Dobry, W. D. Liam Finn, Leslie F. Harder Jr., Mary Ellen Hynes, Kenji Ishihara, Joseph P. Koester, Sam S. C. Liao, William F. Marcuson III, Geoffrey R. Martin, James K. Mitchell, Yoshiharu Moriwaki, Maurice S. Power, Peter K. Robertson, Raymond B. Seed, and Kenneth H. Stokoe II. (2001). "Liquefaction Resistance of Soils: Summary Report from the 1996 NCEER and 1998 NCEER/NSF Workshops on Evaluation of Liquefaction Resistance of Soils." *Journal of Geotechnical and Geoenvironmental Engineering*, 124(10).

Youd et al. (2001). Personal Communication.

Youd, T. L., Hansen, C. M., and Bartlett, S. F. (2002). "Revised Multilinear Regression Equations for Prediction of Lateral Spread Displacement", *Journal of Geotechnical and Geoenvironmental Engineering*, Vol. 128, No. 12, pp. 1007-1017.

Yu, H. S. (2000). "Cavity Expansion Methods in Geomechanics." Kluwer Academic Publishers.